To my wife Janet

Contents

COLLISIONAL PRODUCTION AND LOSS OF 1- TO 42-keV/NUCLEON $X^1\Sigma_g^+$ AND $c^3\Pi_u$ HYDROGEN MOLECULES, AND APPLICATION TO CONTROLLED NUCLEAR FUSION

Thomas Joseph Morgan

(Ph.D. Thesis)

Lawrence Berkeley Laboratory
University of California
Berkeley, California 94720

September 1971

ABSTRACT

As part of a study to devise new and more efficient schemes for injecting fast neutral particles into plasma fusion devices, we have investigated collisions which result in the formation and destruction of the $(1s\sigma^2)X^1\Sigma_g^+$ ground state $\left[1 \leq E \text{ (keV/nucleon)} \leq 42\right]$ and the $(1s\sigma 2p\pi)c^3\Pi_u$ long-lived electronically excited state $\left[5 \leq E \text{ (keV/nucleon)} \leq 42\right]$ of molecular hydrogen. The $c^3\Pi_u$ molecules were formed by electron capture by 5- to 42-keV/nucleon H_2^+ ions in Mg vapor.

The molecules and atoms were detected by particle-counting techniques using CsI(Tl) scintillation crystals mounted on photomultipliers, with the resulting signal being amplified and shaped, pulse-height analyzed, and scaled.

H_2 molecules produced by electron capture by H_2^+ ions in H_2 or N_2 gases yield, upon analysis of the attenuation of the H_2 molecules transmitted through an H_2 gas target versus target thickness, a single total-loss cross section, σ_t, $(H_2 \rightarrow H_2^+,$

$H + H$, $H + H^+$, $H^+ + H^+$) attributed to the $X^1\Sigma_g^+$ state. When the H_2 molecules are produced in Mg vapor, the analysis of the attenuation curve yields the same cross section attributed to the $X^1\Sigma_g^+$ state plus a larger cross section, σ_t^*, attributed to the $c^3\Pi_u$ state.

Similarly, H_2 molecules produced by electron capture by H_2^+ ions in H_2 or N_2 gases yield an ionization cross section, $\sigma_{H_2^+}$, ($H_2 \rightarrow H_2^+$) attributed to the $X^1\Sigma_g^+$ state. When the H_2 molecules are produced in Mg vapor, the same technique yields a larger composite cross section from which the ionization cross section of the $c^3\Pi_u$ state, $\sigma^*_{H_2^+}$, can be determined. From an analysis of the attenuation curves we also obtain the fraction, f, of the H_2 molecules that are in the $c^3\Pi_u$ state.

The fraction, $\mathcal{F}^*$, of the incident H_2^+ beam that can be converted to $c^3\Pi_u$ molecules in collisions with Mg vapor has also been determined by combining the measurements of f with measurements on the yields of H_2 without regard to the population of the states of the molecule.

Values for $\sigma_{H_2^+}$, $\sigma^*_{H_2^+}$, σ_t, σ_t^*, f_M (the maximum value of f), and $\mathcal{F}^*_M$ (the maximum value of $\mathcal{F}^*$), at three representative energies are given in the table below. The cross sections are in units of 10^{-16} cm^2.

	11.2 keV/nucleon	20 keV/nucleon	30 keV/nucleon
$\sigma_{H_2^+}$	1.37 ±0.13	1.70 ±0.18	2.10 ±0.20
$\sigma^*_{H_2^+}$	6.20 $^{+1.2}_{-1.1}$ [a]	6.50 $^{+1.2}_{-1.5}$	4.80 ±1.2
σ_t	3.10 ±0.3	3.58 ±0.3	3.55 ±0.3
σ^*_t	14.0 ±2.5	13.5 $^{+2.2}_{-2.6}$	9.00 ±2.2
f_M	0.36 ±0.06	0.28 $^{+0.06}_{-0.05}$	0.23 $^{+0.06}_{-0.05}$
$\mathcal{F}^*_M$	0.065±0.014	0.018±0.004	

a = 12.2 keV/nucleon

A search was made for $c^3\Pi_u$ H_2 formation from H_3^+ collisions in Mg vapor and for H_2^- negative-ion formation from H_2^+ collisions in Mg vapor. Neither process was observed to occur. Based on the H_2^- search we are able to assign an upper bound of 10^{-21} cm^2/atom to the cross section for couble electron capture which results in an H_2^- ion with a lifetime longer than ~ 10^{-7} sec. When the results were compared at equal velocities, the use of H_2^+, D_2^+, or HD^+ showed no observable differences.

The $c^3\Pi_u$ excited state population results are used to calculate the efficiency for injecting H_2 molecular beams into a controlled nuclear fusion neutral injection experiment. The results of this calculation are compared with H atom beam calculations of total trapping efficiencies and with H atom beam cascade effects. From these calculations asymmetric plasma trapping of the H atom beam at intermediate densities is analytically demonstrated. For equally intense neutral beams (i.e., projectiles/sec), the total

trapping of the molecular beam (containing $c^3\Pi_u$ H_2 molecules) is shown to be from 2 to 5 times larger than the total trapping of the atomic beam for plasma densities greater than 10^{11} cm^{-3}, with no significant asymmetric trapping occurring. The total trapping for both H and H_2 beams is shown to be insensitive to changes in the electron temperature of the plasma from 1.0 to 1000 eV. From these calculations we conclude that a H_2 beam containing $c^3\Pi_u$ excited molecules is desirable for injection into present day neutral injection fusion devices for plasma densities greater than $\sim 10^{11}$ cm^{-3} and for injection energies less than $\sim$ 20 keV/ nucleon.

Notation Frequently Used in Main Text

$c^3\Pi_u$	n = 2 long-lived electronically excited state of H_2
$X^1\Sigma_g^+$	Stable ground state of H_2
+, -	The symmetry of the electronic eigenfunction with respect to a reflection of the electrons through a plane passing through the two nuclei
B	Magnetic field
CSI (Tℓ)	Cesium Iodide crystal dopped with Thallium
e	Fundamental charge
E	Energy
$f(\pi_n)$	Fraction of the H_2 beam incident on the H_2 target that is in the $c^3\Pi_u$ state due to passage of H_2^+ ions through a neutralizer of thickness π_n
$F(\pi_t)$	$X^1\Sigma_g^+$ H_2 fraction in the H_2 beam after passage through an H_2 target of thickness π_t $(F(0) = 1-f)$
$F^*(\pi_t)$	$c^3\Pi_u$ H_2 fraction in the H_2 beam after passage through an H_2 target of thickness π_t $(F^*(0) = f)$
$F^+(\pi_t)$	H_2^+ fraction in the H_2 beam after passage through an H_2 target of thickness π_t $(F^+(0) = 0)$
$\mathcal{F}(\pi_n)$	Fraction of H_2^+ ions converted to H_2 molecules in a neutralizer of thickness π_n
$\mathcal{F}^*(\pi_n)$	Fraction of H_2^+ ions converted to $c^3\Pi_u$ H_2 molecules in a neutralizer of thickness π_n

$\mathcal{F}_M, \mathcal{F}^*_M, f_M$	The maximum values of $\mathcal{F}, \mathcal{F}^*$, and f
g	Gerade (even) the symmetry of the electronic eigenfunction with respect to reflection of the electrons through the origin
Method I	Beam measurement by use of particle counting techniques
Method II	Beam measurement by use of a Faraday cup
n	Principal quantum number
u	Ungerade (odd) the symmetry of the electronic eigenfunction with respect to reflection of the electrons through the origin
v	Velocity or vibrational level
σ_t	Total loss cross section of the $X^1\Sigma_g^+$ state of H_2 in collision with H_2 gas
σ_t^*	Total loss cross section of the $c^3\Pi_u$ state of H_2 in collision with H_2 gas
σ_k	The cross section for the conversion $X^1\Sigma_g^+$ $H_2 \rightarrow k$ due to $X^1\Sigma_g^+$ H_2 molecules in collision with H_2 gas
σ_k^*	The cross section for the conversion $c^3\Pi_u$ $H_2 \rightarrow k$ due to $c^3\Pi_u$ H_2 molecules in collision with H_2 gas
Σ, Π, ...	Total angular momentum of molecule in the direction of the internuclear axis
π_n	Neutralizer thickness (atoms or molecules/cm^2) [$\pi = n\chi$ where n ≡ density, χ ≡ interaction length]
π_t	Target thickness (molecules/cm^2)

I. INTRODUCTION

In recent years a large amount of experimental work has been devoted to measuring excited-state populations of energetic atomic hydrogen and helium beams, and their destruction and formation cross sections. Conspicuously missing is a corresponding knowledge of energetic molecular hydrogen beams.

The tremendous surge of interest in controlled thermonuclear research (CTR) has generated a need for knowledge of the formation and destruction of H, He, and H_2 beams. Presently, one phase of the neutral injection program of the CTR effort is interested in making beams of excited-state neutral projectiles whose electronic excitation energy is greater than the ground state but well below the ionization limit (this topic is discussed below).

In response to these needs the present work presents results of an experimental investigation on the collisional formation and destruction of energetic H_2 beams containing large amounts of H_2 molecules in the $c^3\Pi_u$ long lived electronically excited state.

Within certain impact velocity ranges, the more electronic excitation energy possessed by a fast projectile colliding with a gaseous target, the greater the electron loss cross section of the projectile.

Therefore, careful observation and analysis of the collision products of neutral fast beams could lead to the determination of the excited state population in the beam and the collision cross sections of the excited-state component.

Barnett and Stier,[1] and Allison,[2] while investigating the

electron-loss of He atoms in collision with various gases, both noted the dependence of the attenuation of the He beam on the pressure of the gas used to neutralize the incident He^+ ions. Subsequently, Wittkower et al.[3] showed the attenuation to be dependent also on the type of neutralizing gas used. These effects were attributed to the presence of metastable atoms in the beam. Figure 1 illustrates the observations of Barnett and Stier of the dependence of the measured cross section on the pressure of the neutralizing gas.

Gilbody et al.[4] first performed a systematic investigation of these effects and introduced a beam-attenuation technique for the study of fast metastable He atoms in collisions involving electron loss. Since then a large amount of experimental work has been performed using this technique[5-8] and related methods[9-13] to obtain information on the properties of the metastable and ground states of keV-energy He atoms in collisions with gaseous targets.

The optical technique, based on observations of the spontaneous or induced radiative emission of excited states, has been used extensively to measure populations and cross sections of keV-energy atomic hydrogen for principal quantum numbers $2 \leq n \leq 6$.[14-22] This technique has also been used to study electron capture into excited states of fast helium for $3 \leq n \leq 6$.[23,24]

Electric-gap techniques, based on field ionization of highly excited states, have yielded a substantial amount of information on the highly excited states ($n \geq 9$) of atomic hydrogen.[25-31]

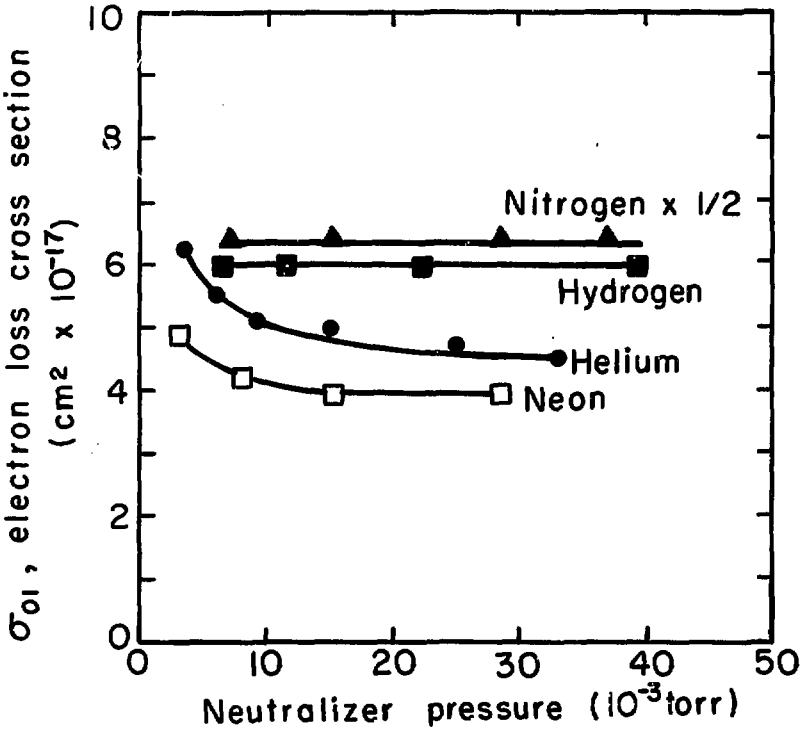

Fig. 1. The variation, with N_2 neutralizer pressure, in the measured electron loss cross section for H, He, Ne, and N in collision with H_2 gas (from Ref. 1).

A limited amount of work on high electronically excited states ($n \geq 9$) of molecular hydrogen, called Rydberg states, has also been carried out by this method.[25,30,31]

The present work extends the field of measurement of keV-energy heavy-particle collisions involving excited states to the $n = 2$ united atom equivalent state of molecular hydrogen. In particular this work quantitatively analyzes the collisional formation and loss of $(1s\sigma^2)X^1\Sigma_g^+$ ground state and $(1s\sigma 2p\pi)c^3\Pi_u$ long-lived electronically excited state of energetic molecular hydrogen. The energy range of the present work is from 1 to 42 keV/nucleon.

The experimental technique used for the analysis of the hydrogen molecules is the beam-attenuation technique similar to that introduced by Gilbody et al.[4] for metastable He atoms. Accurate absolute measurements by this method can be obtained only if there exists in a beam of fast projectiles sufficient excited particles, with long enough lifetimes and large enough cross sections, to insure observable changes in the collisional attenuation of the beam when compared with a beam prepared almost exclusively of ground state atoms or molecules. The applicability of this technique to the present measurements rather than the electric gap or optical technique is discussed in Appendix A.

There has been a substantial amount of theoretical work, in conjunction with recent experimental progress, devoted to the determination of fast excited-state collisional information. A survey of the pertinent theoretical efforts can be found in

Appendix B.

Suffice it to say at this point that due to the structural complexity of the H_2 molecule there exist no theoretical calculations to compare with present results. However, Hiskes'[32] predictions of $c^3\Pi_u$ H_2 populations, based on calculations for H^+ electron capture into excited states of atomic hydrogen, show remarkably good agreement with the present measurements.

The study of fast heavy-particle excited-state collisional phenomena, besides being necessary for the proper interpretation of experiments, is of fundamental interest for the understanding of atomic and molecular processes. Recently, studies of this type have found direct application to thermonuclear fusion experiments employing neutral injection for the creation and buildup of a plasma. The present state of the art of neutral injection into mirror machines suggests the following sequence of events (the density and quantum level values are qualitative only and are given simply as a model to illustrate the main ideas); the neutral beam that is injected is composed of ground state and excited atomic hydrogen produced by charge exchange of protons in a gaseous target.

Firstly, the plasma buildup takes place by means of Lorentz ionization[33] of the highly excited states of atomic hydrogen, i.e., ionization by the $e\vec{v} \times \vec{B}$ force exterted on the proton-electron system because the atom is moving with velocity $\vec{v}$ through a magnetic field $\vec{B}$. Typical levels which are Lorentz-ionized in contemporary experiments using ~ 20 keV atomic hydrogen injection

are levels with principal quantum number $n > 9$. When a high enough density of ions has been achieved (10^{10} cm^{-3}) in the magnetic confinement region by Lorentz ionization, collisional trapping becomes important because of successive excitation collisions of the intermediately excited states to less bound states which are capable of being Lorentz-ionized.[34] This process is generally referred to as an inverted cascade. Levels which generally contribute appreciably to this inverted cascade process are $6 \leq n \leq 8$. The excited levels $n < 6$ cannot contribute to this process since their lifetimes are shorter than the transit time in the apparatus and they will therefore radiatively decay while in flight to the $n = 1$ level. The metastable $n = 2$ level is easily quenched in the fringe magnetic field of the confinement device so that inside the device the excited levels $2 \leq n \leq 5$ are not present in the beam. The $n = 1$ level, due to its small collisional excitation and ionization cross sections, does not at this stage of the plasma buildup (10^{10} cm^{-3}) contribute significantly.

Now, as first suggested by Hiskes,[32] when the plasma reaches a density of approximately 10^{11} cm^{-3}, it will become collisionally opaque to the inverted cascade process, i.e., the available excited levels for this process will have depleted themselves in the outer portion of the trapped plasma and will not penetrate to the interior. Therefore at this density an inverted cascade is no longer an effective trapping mechanism in the center of the plasma. Furthermore, collisional trapping of the ground state is still not efficient enough to contribute significantly to the

plasma buildup. Injection of $c^3\Pi_u$ H_2 beams at this stage of the buildup will provide penetration of an excited state to the interior of the plasma since (1) the $c^3\Pi_u$ state will not quench in the confinement magnetic field,[35] (2) it is sufficiently long lived to travel the length of the apparatus (see Sec. II, B), and (3) at this density the $c^3\Pi_u$ state cannot be effectively cascaded upward in the outer portion of the plasma (that is, at this density the lifetime of the n = 3 state is shorter than the mean free path so that a collisional excitation from n = 2 to n = 3 results in a radiative de-excitation before the n = 3 state can be collisionally excited). The penetration of this state will allow efficient collisional trapping in the interior of the plasma since its cross sections for these processes are expected to be up to factors of 10 or more larger than the n = 1 level of atomic hydrogen.[32] Without the use of a $c^3\Pi_u$ H_2 beam, the plasma is expected to accumulate mostly on the periphery of the trapped plasma for densities greater than 10^{11} cm^{-3} and less than 10^{13} cm^{-3}, thus voiding the center region and causing a highly asymmetric plasma buildup.

The major point of concern in assessing the usefulness of this $c^3\Pi_u$ process for neutral injection is how well this level can be populated in neutral H_2 beams. The present work measures this quantity and concludes that $c^3\Pi_u$ processes can be useful at energies below ~ 20 keV/nucleon.

In Sec. VI we apply the results of the present work to calculate the efficiency for trapping H_2 beams and compare the

results with trapping efficiencies of H beams.

II. THE HYDROGEN MOLECULE

A. Molecular Electronic States and Notation

The structure of the hydrogen molecule has been extensively studied both theoretically and experimentally (Herzberg[36] has tabulated a large number of references on this topic up to 1950, and the present section contains a large number of references since 1950). Figure 2 shows the potential energy curves for the electronic states of H_2 and H_2^+ that are of interest in this work.

The electronic state designation, i.e., $X\,^1\Sigma_g^+$, etc., is the well established short reference designation in which the electronic configuration is not indicated.[37] In this nomenclature the ground state is referred to as X, the excited states of the same electron spin multiplicity (indicated by the superscript 1 in the above example) as A, B, C, ··· and those of different multiplicity as a, b, c, ···. The alphabetical order usually corresponds to increasing excitation energy above the ground state, but, unfortunately, H_2 is an exception to this rule due to well established earlier designations. In the case of Fig. 2 all H_2 states not shown have larger excitation energy than those that are shown. The symbols Σ, Π, ··· correspond to the values 0, 1, ··· of the component of the electronic orbital angular momentum vector along the internuclear axis. The subscripts g (even) and u (odd) refer to the symmetry of the electronic eigenfunctions with respect to a reflection of the electrons through the center of the molecule. The + and - superscripts refer to

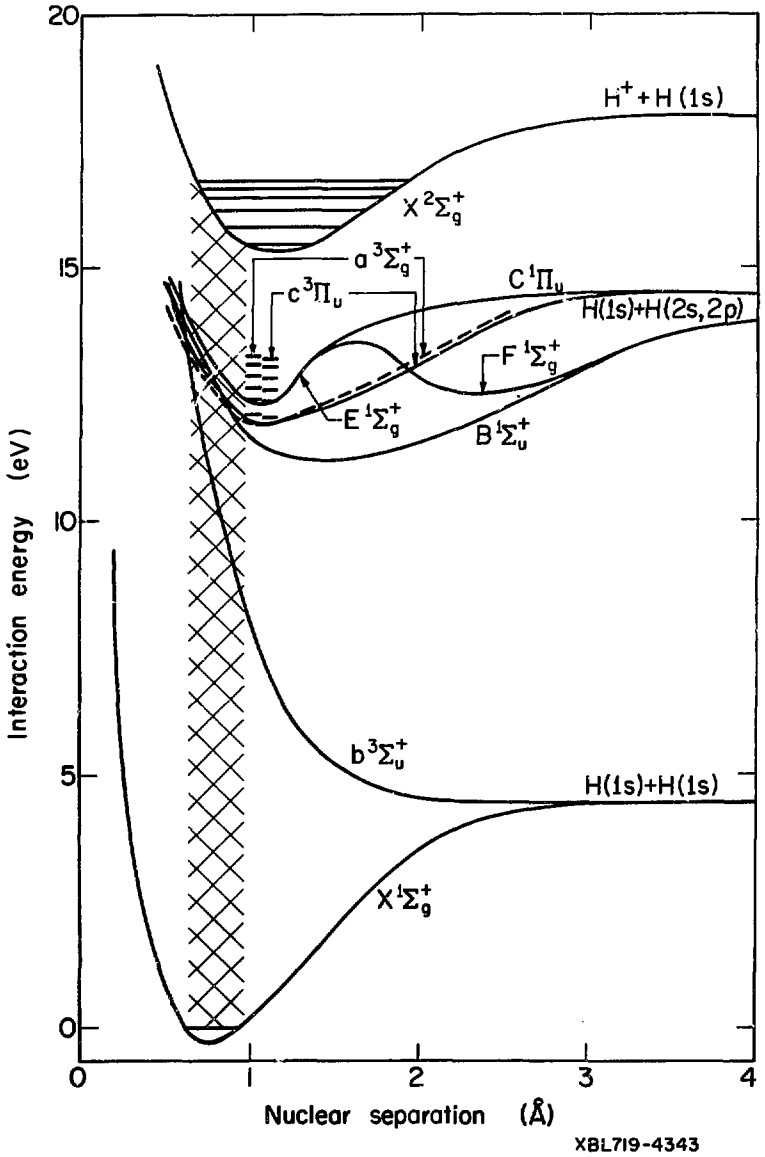

Fig. 2. Potential energy diagram of H_2 and H_2^+ showing several excited states of H_2. The hatched area is the Franck-Condon classical region of transition from the ground state of ($v = 0$) H_2 to the ground state of H_2^+. Several vibrational levels are indicated by dashes. The potential energy curves shown are based on calculations cited throughout this section.

whether the electronic eigenfunction changes sign (-) or remains unchanged (+) while the electrons are reflected through a plane passing through the two nuclei. The atomic symbols on the right hand side of Fig. 2 designate the state of the molecule for infinite internuclear separation.

The molecule contains two independent emission spectra: a triplet spectrum due to the two electron spins of the molecule being unpaired, and a singlet spectrum due to electronic states with paired electron spins. Spontaneous radiative transitions between these two term schemes is strictly forbidden by the selection rule on the total electron spin momenta of the molecule, i.e., $\Delta S \neq 0$. Appendix C discusses and lists the pertinent selection rules for radiative and nonradiative transitions in diatomic molecules. An elaborate treatment of transitions in diatomic molecules is given by Herzberg.[38] Also, a concise and useful summary of selection rules is given by Bates.[39]

B. Excited State Lifetimes

In order to interpret the results of the present experiment an understanding of the electronic states of the H_2 molecule is necessary. The present section presents the results of a survey of the known H_2 spectra in order to find out which excited states have lifetimes greater than 10^{-6} sec. (In typical present day keV-energy collision experiments and in some neutral injection experiments, apparatus lengths are ~ 1 meter with particle velocities of ~ 10^8 cm/sec, giving transit times on the order of 10^{-6} sec.)

For the present discussion we can segment the excited states into three groups: (1) low lying energy states having excitation energies less than ~ 12.5 eV, (2) intermediate excited states ($n < 8$), and (3) highly excited states ($n > 8$).

Firstly, we address ourselves to groups (2) and (3). Since the excited electrons in H and H_2 move in approximately the same potential they will have approximately the same radiative lifetimes. Based on the theoretical work of Hiskes and Tarter,[40] we find that the atomic hydrogen states with $n \gtrsim 8$ [group (3)] have lifetimes which are greater than ~ 10^{-6} sec. For group (2) it can be shown that these intermediate states decay in times shorter than ~ 10^{-6} sec to lower states,[40] and further, that no anomalies resulting in longer than normal lifetimes are expected.[36]

We now turn our attention to group (1) (the H_2 excited states shown in Fig. 2 comprise this group). Lichten,[41] in 1960, first verified the existence of metastable molecular hydrogen by use of the atomic-beam magnetic-resonance technique. Specifically, he found that the lowest vibrational level ($v = 0$) of the $c^3\Pi_u$ state of H_2 is metastable, i.e., does not radiatively decay by electric dipole transitions (see Appendix C). Recently, Brooks et al.[42] have found experimental evidence which leads them to conclude that there is at least one more long-lived level of the $c^3\Pi_u$ state other than the $v = 0$ level. They conclude that the level is most likely, but not conclusively, the $v = 1$ level. Since 1960 a large amount of work has been performed on the $c^3\Pi_u$ state.[43-53] The Kronig selection rules for an allowed radiative transition

in a diatomic molecular system (see Appendix C) show that the $c^3\Pi_u$ ($v = 0$) level, although not able to decay via electric dipole transitions, can radiatively decay by magnetic dipole, electric quadrupole, or higher moment emissions to the $b^3\Sigma_u^+$ state (the $b^3\Sigma_u^+$ state is repulsive and dissociates into two ground state H atoms in $\sim 10^{-14}$ sec [41]). The radiative lifetime for these transitions has been estimated by Freis and Hiskes[35] for H_2 to be 10^{-3} sec and recently Johnson[53] has obtained experimental values of $\sim 10^{-3}$ sec for H_2, D_2, and HD. Freis and Hiskes[35] have also calculated the electric dipole radiative lifetime for the $v > 0$ $c^3\Pi_u$ levels decaying to the only allowable final state, the $a^3\Sigma_g^+$ state (this state has been observed to decay to the $b^3\Sigma_u^+$ state in $\sim 10^{-8}$ sec[54]). Their calculated lifetimes are $\gtrsim 10^{-4}$ sec for all vibrational levels.

Up until now we have been dealing exclusively with the radiative properties of the $c^3\Pi_u$ state. We now turn our attention to predissociation, the nonradiative transition process in diatomic molecules.[55] The mechanics of the process are discussed in Appendix C; here we restrict ourselves to the results of work on this process as a loss mechanism for the $c^3\Pi_u$ state.

The $c^3\Pi_u$ state is susceptible to perturbations from the repulsive $b^3\Sigma_u^+$ state when the potential energy functions of these states come close enough together so that an overlapping of wave functions exists and causes a nonzero matrix element for predissociation. There are two types of predissociation of the $c^3\Pi_u$ state: allowed, induced by rotational electronic perturba-

tions;[56,57] and forbidden, induced by spin-orbit and spin-spin couplings.[44,47] The selection rules governing predissociation are listed in Appendix C, and indicate that, although there are many states close to the $c^3\Pi_u$ state, predissociation can take place only via the $b^3\Sigma_u^+$ state.

As has been pointed out by Kronig,[58] under very strong coupling conditions, allowed predissociation lifetimes could be as short as 10^{-11} sec. Lichten,[45] in order to explain his experimental observations, has concluded that for the $c^3\Pi_u$ state allowed predissociation lifetimes are $\sim 10^{-9}$ sec. Hiskes has considered this question and concluded that the coupling in this case should be rather weak and suggests the lifetime to be considerably longer than 10^{-9} sec.[59] Herzberg,[49] based on experiments dealing with the absorption spectrum in the visible region of H_2 excited by a flash discharge, has estimated an upper bound of $\tau = 0.3$ μsec on the lifetime for allowed predissociation of the $v = 2$ level of $c^3\Pi_u$. Also, due to the change in proximity of the $b^3\Sigma_u^+$ and $c^3\Pi_u$ potential energy states with changes in internuclear separation, we expect the predissociation lifetime to decrease with increasing vibrational excitation of the $c^3\Pi_u$ state (see Fig. 2). Hertzberg[49] has experimentally verified this behavior. Therefore, based on this available information, we bound the allowed predissociation lifetime as follows:

$$\text{nanoseconds} \lesssim \tau \lesssim \text{tenths of microseconds.}$$

A survey of the selection rules for allowed predissociation

(see Appendix C) shows that half of the $c^3\Pi_u$ levels are susceptable to this loss mechanism. Finally, Bottcher[52] and Chiu[47] have performed theoretical calculations on the forbidden predissociation lifetimes and concluded that they are of the order of 10^{-3} sec, while Lichten has experimentally measured lifetimes ranging from 0.1 to 0.5 x 10^{-3} sec.[45] Hence, we conclude that all the levels of the $c^3\Pi_u$ state have radiative lifetimes longer than $\sim 10^{-6}$ sec, but they most likely do undergo allowed predissociation within this time.

We now turn our attention to the remaining low lying excited states of H_2 (see Fig. 2). The $a^3\Sigma_g^+$ state has been observed to decay to the $b^3\Sigma_u^+$ state in $\sim 10^{-8}$ sec.[54] Also, the $B^1\Sigma_u^+$ and the $C^1\Pi_u$ states have both been shown to decay by allowed transitions in 8 ± 2 x 10^{-10} sec and 6 ± 2 x 10^{-10} sec, respectively.[60] This is not the case, however, for the $^1\Sigma_g^+$ state. Davidson[61] has studied this state and computed the potential curve. He finds the potential function to contain two minima: the $E^1\Sigma_g^+$ state at R = 1.0 Å, and the $F^1\Sigma_g^+$ state at R = 2.27 Å. Wolniewicz[62] has calculated the transition probabilities for the $F^1\Sigma_g^+ - B^1\Sigma_u^+$ transition. Since the $F^1\Sigma_g^+$ state has a much larger internuclear equilibrium separation than all other stable H_2 states (see Fig. 2), we expect the transition probabilities to be small. Wolniewicz finds approximately half the transitions of the F-B band to have lifetimes greater than 10^{-5} sec. For comparable transitions of the E-B band we conclude, based on Wolniewicz's

calculation of the band strengths, that the lifetimes are $< 10^{-8}$ sec.

In summary, we have discussed the excited states of H_2 and conclude that the $c^3\Pi_u$ and $F^1\Sigma_g^+$ states and the $n \gtrsim 8$ states have lifetimes long enough to allow them to traverse typical apparatus lengths and must be considered in the interpretation of experimental results. (It is shown in Appendix D that the only state than can be significantly populated in the present experiment is the $c^3\Pi_u$ state.)

III. EXPERIMENTAL APPROACH AND APPARATUS

A. Approach

The experimental approach to the analysis of the H_2 molecules is by beam attenuation techniques. The energetic H_2 molecules were produced by electron capture when a momentum analyzed beam of H_2^+ ions traversed a neutralizing cell of Mg vapor, or H_2 or N_2 gas. The reasons for the choice of neutralizers and the desirability of Mg vapor as a charge exchange medium for the formation of excited hydrogen atoms and molecules is the topic of Appendix E. We have made measurements with incident H_2^+, D_2^+, and HD^+ ion beams. When the results are compared at the same velocity, they are the same within the experimental uncertainties; hence, in the remainder of this work we treat all projectiles as if they were H_2^+ ions or H_2 molecules. Figure 3 shows the experimental arrangement. Since we are investigating the H_2 molecule, the charged particles emergent from the neutralizer cell were swept out of the beam with an electric field and the H_2^+ component, detected with a Faraday cup, was used to provide a monitor of the beam intensity. The H_2 beam now leaves the portion of the experiment used for its production and enters the analysis section.

As mentioned earlier, the analysis of the H_2 beam is performed by beam attenuation. To this end the neutral beam, consisting of ground-state and excited H and H_2, traverses a target cell containing H_2 gas. We assume that the H_2 molecules are in either the $X^1\Sigma_g^+$ ground state or in the $c^3\Pi_u$ excited state. The justification for this assumption can be found in Appendix D.

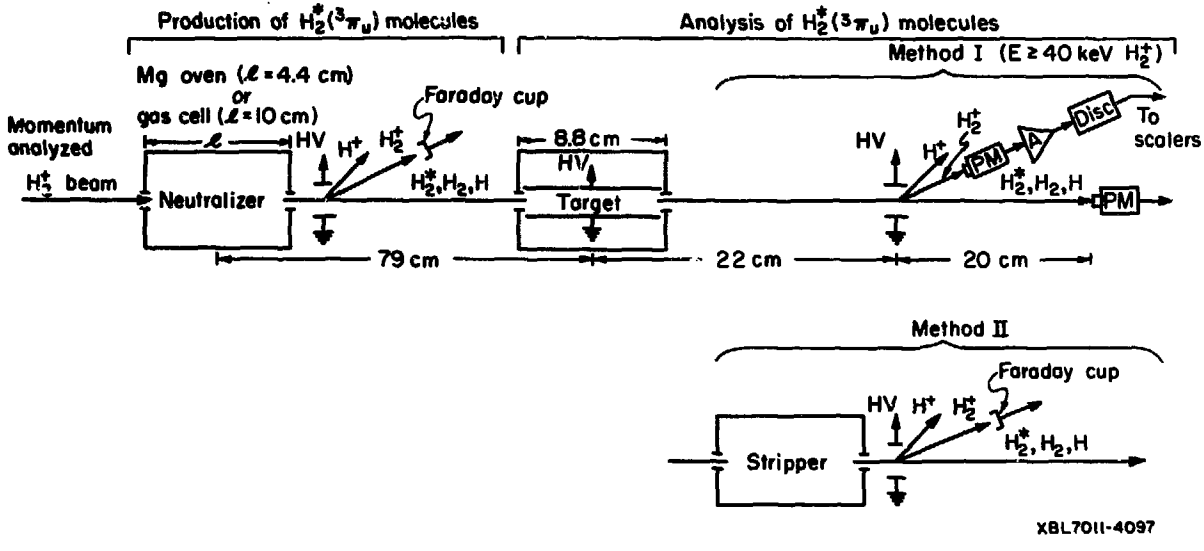

Fig. 3. Diagram of the experimental arrangement.

Since the collision cross sections of these two states are different, they attenuate differently upon traversing the target cell. By observing the emerging particles as a function of H_2 gas thickness in the target cell we are able to deduce the total attenuation and ionization cross sections for the $c^3\Pi_u$ and $X^1\Sigma_g^+$ states as well as the population of these states in the beam. By varying the neutralizer conditions, i.e., type of neutralizer used (Mg, H_2, or N_2) and its thickness (atoms or molecules/cm^2), we are able to maximize the excited state population or reduce it to an insignificant amount.

In order to increase the energy range of the measurements, two methods were used for particle detection. For Method I (see Fig. 3) we employed particle-counting techniques. The particles were detected by CsI(Tl) crystals mounted on photomultipliers. Method I was limited to energies greater than about 10 keV/nucleon; below this energy it is difficult to resolve the pulse height distribution of the atomic portion of the beam from the molecular portion. For Method II a third gas cell (see Fig. 3) held at a constant pressure was used to strip the fast molecules emerging from the target of an electron, and the resulting H_2^+ current was measured with a Faraday cup. This method yields less information than Method I but is applicable to attenuation cross-section measurements below 10 keV/nucleon. Using this method we have extended the attenuation cross section measurements to 1 keV/nucleon.

B. Apparatus

1. The Ion Source and Electrostatic Accelerator

The ion source and accelerator used in the present work have been described in detail elsewhere.[3] Here we will mention only the main features of the apparatus, noting any changes necessary for the present application.

The source was a typical PIG discharge which could also be operated as an electron-gun source. The electron gun was a 0.256-mm-diam tungsten filament operating at a current of from 4 to 6 A. The source area was surrounded by an electromagnet which was used to produce an electron-confining axial magnetic field of from 0 to 400 gauss in the source.[63] The ions were extracted through a 0.916-mm hole in the cathode, after which they passed through an accel-decel potential focusing lens (einzel lens) and were accelerated by use of four rings to which a total of from 1 to 90 kV was applied. The desired ions were then selected by a 90-deg analyzing magnet which was monitored by a Hall probe and traveled 120 cm through a drift tube where they entered the experimental region. Just in front of the experimental region is an electromagnet that is used to produce a transverse magnetic field in order to sweep the primary H_2^+ ions out of the beam path but still allow the H_2 molecules, produced by electron capture by H_2^+ in the drift tube, to pass. This contribution is detected and subtracted as background. Under typical single collision conditions in the neutralizer the background neutral production was $\lesssim 10\%$. The beam, before the experimental

region, is collimated by a 0.636-cm-diam aperture before the bending magnet and by a 0.396-cm-diam aperture after it.

The accelerator voltage was measured by a high-impedance divider calibrated to ~ 1%. The uncertainty in the absolute value of the energy of the particles is estimated to be ~ 3%, except for energies less than 2 keV/nucleon where it is estimated to be ~ 5%. This is based on the analysis of the deviation from linearity of a plot of the voltage necessary to deflect the particles versus the measured value of the energy. The lower energy limit was determined by the performance of the detection system and the upper limit by our accelerator.

Typical operating characteristics are listed in Table I. Acclerator and drift tube base pressures measured by ion gauges were 1×10^{-6} and 5×10^{-6} torr, respectively. These pressures are maintained by a 6-in. and a 2-in. diffusion pump.

2. The Mg Oven Neutralizer

The Mg vapor oven which served as the neutralizer cell is shown in Fig. 4. The beam entrance and exit collimators were 0.508 and 1.27 mm, respectively. The effective length of the stainless steel oven was taken to be 4.4 cm. This length was measured from the entrance collimator to the exit collimator. An operating temperature of 665°K produced a Mg vapor thickness of 1.75×10^{14} atoms/cm^2. Typical range of operation was from 616 to 783°K.

Before data were taken, the oven was outgassed at a temperature higher than the temperature needed to produce the thickest

Table I. Typical accelerator operating parameters.

Characteristic	PIG mode	EG mode
Accelerator pressure (ion gauge)	4.5×10^{-5} torr	9×10^{-6} torr
Drift tube pressure (ion gauge)	1.3×10^{-5} torr	8×10^{-6} torr
PIG anode bias	0.5 to 2.0 kV	---
Electron gun filament bias (EG)	---	10 to 60 V
Extractor voltage	-1 to -3 kV	-3 to -5 kV

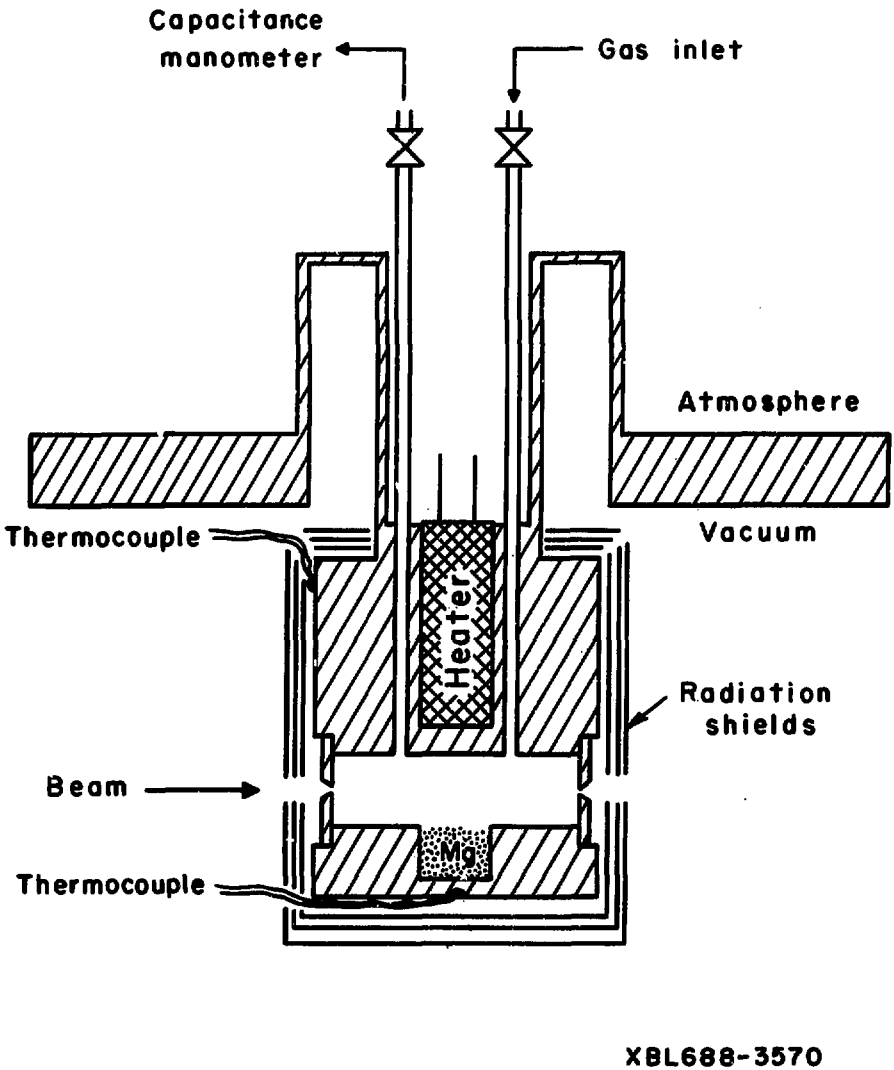

Fig. 4. The magnesium vapor cell.

Mg vapor neutralizer of interest. This was done to insure: (1) the purity of the vapor, and (2) the proper interpretation of the vapor pressure. The temperature of the oven, which must be known in order to determine the Mg vapor pressure, was determined with two chromel-alumel thermocouples, with a zero-degree centigrade reference junction, connected to a potentiometer. To minimize radiative loss from the thermocouples, which would cause a low temperature reading relative to the temperature inside the oven, the cell was surrounded by three layers of 0.25-mm-thick dimpled stainless steel. The calibration of the device was performed by Berkner et al.[64] who originally used the oven as a collision cell for the measurement of electron transfer cross sections of H and H^+ in Mg vapor. Data necessary for the calculations of the vapor pressure are due to Hultgren et al.[65] There exists the possibility of a ±10% standard error in this Mg vapor pressure data.[16]

The possibility of quenching of the $c^3\Pi_u$ state by thermal photons or electrons produced in the oven has not been investigated experimentally. But since oven temperatures were always less than 800°K, we expect no significant photo-absorption[66] or electron emission (the work function for the stainless steel walls of the oven is ~ 4 eV).

3. <u>The Neutral Beam Monitor</u>

The emergent H_2^+ component from the neutralizer was deflected 20 deg into a Faraday cup by a set of plates, one of which had a positive high voltage applied to it. The signal from the cup

was sent to an electrometer whose output was fed to an integrator. This accumulated charge, which is proportional (for a given neutralizer thickness) to the number of neutrals incident on the target cell, was used to monitor the neutral beam by gating off the scalers or integrating electrometer when some appropriate preset charge level was reached.

Since the beam entering the target cell is 35 cm from the monitor Faraday cup, strict alignment was necessary in order to insure correlation between the detected particles and the monitor which are 85 cm apart. Alignment was performed visually with the aid of a telescope. Previous to taking data, the beam was tuned and maximized by observing the count rate due to the neutral particles. This count rate was then compared, as a function of the tuning parameters, with the electrometer output of the monitor Faraday cup. If the two signals were correlated reasonably well, i.e., exhibited the same rise in signal, signal plateau, and decrease in signal intensity as a function of the tuning parameters to within the uncertainty of visual meter observation, data was acquired; if not, the beam was retuned and occasionally realignment was necessary. The position of the beam was observed visually by replacing the Faraday cup with a phosphor-coated glass plate. It was evidently significantly smaller than the Faraday cup diameter (2.54 cm). Permanent magnets were used to suppress secondary electrons from the cup.

4. The Target Cell

The neutral beam traveled 72 cm from the oven exit to the

target gas cell entrance (see Fig. 3). Figure 5 shows the target cell. The beam entrance and exit collimators were 3.30 and 4.31 mm, respectively. The effective length of the cell was 8.8 cm. This length was measured from the midpoint of the tubular entrance collimator to the midpoint of the tubular exit collimator (changes in the target gas thickness owing to gas in the surrounding tank of the target cell were inconsequential at all target pressures). The target cell is equipped with a pair of metal rods, ~ 0.5 cm apart, parallel to the beam line, which extend over the entire length of the cell. While measuring the H_2 attenuation, a voltage of 4 kV was applied to one of the rods in order to produce an electric field which insured that the exiting H_2 beam was due only to attenuation, without the contribution of two-step processes, i.e., $H_2 \rightarrow H_2^+ \rightarrow H_2$. While measuring the ionization cross section the voltage was not present so that the H_2^+ component was allowed to leave the target cell and be detected. The pressure in the cell was measured by a Barocel capacitance manometer which had been calibrated numerous times over a period of several years by a McLeod gauge and an oil manometer.

5. Particle Detection

a. Method I: Single Particle Counting

After traveling 18 cm from the target cell exit the H_2^+ component of the beam was bent 20 deg by a set of electrostatic deflection plates and traveled 24 cm where it was incident on a 2.54-cm-diam CsI(Tl) scintillation crystal which was mounted on an Amperex 10-stage XP-1010 photomultiplier tube (see Fig. 3).

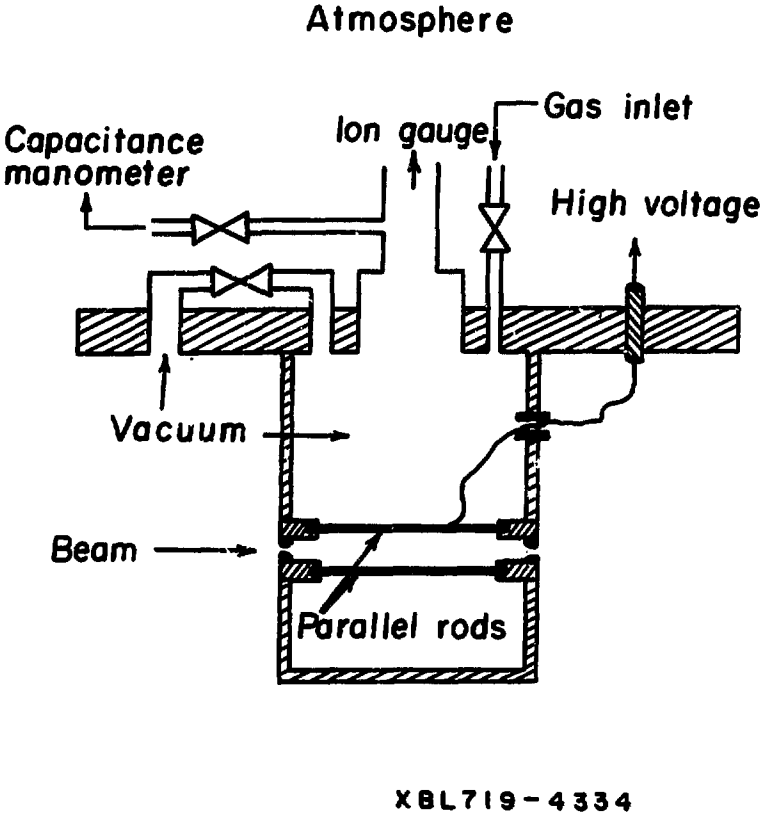

Fig. 5. The target gas cell.

Also, the neutral beam traveled 20 cm after the deflector plates and intercepted a similar arrangement. The photomultipler tubes were not cooled since upon cooling no significant increase in energy resolution was observed.

For this method, the ion source was operated in the electron-gun mode in order to obtain low intensity countable beams. Typical counting rates were from 1 to 4 x 10^3 counts/sec.

Considerable effort was taken to optimize the energy resolution of the detectors. The scintillation crystals used varied from 13 mm to less than 1 mm in thickness. (It has been found by Martinez[67] that the optimum thickness for CsI(Tl) crystal resolution of ^{210}Po alpha particles is 0.38 mm.) The resolution decreases slowly with increasing thickness, changing by less than 10% from 0.38 to 8 mm. When possible the crystal edges were bevelled at ~ 45 deg to increase light-collection efficiency as first noted by Riviere and Sweetman.[68] The crystal was highly polished to insure near-uniform scintillation response to all incident particles of the same energy. A mixture of MgO and isopropyl alcohol was used as an abrasive for polishing, and the crystal was mounted on the tube by use of epoxy.

The tube is a box-type dynode structure with a Sb-Cs photocathode.[69] The photomultiplier base, i.e., the voltage divider for the dynodes, had typically a potential difference of 1.8 kV applied across the anode to cathode. The cathode was at ground potential so as not to introduce any undesirable electric fields. The signal, which could be extracted from the sixth dynode or

from the anode, was sent directly to a charge-sensitive preamplifier for impedance matching and to insure better signal-to-noise ratio. The signal then traveled ~ 15 ft of cable to where it was amplified and shaped, discriminated, and finally scaled. A 400-channel pulse-height analyzer was used to set the pulse-height acceptance limits of the discriminators. A typical spectrum of the neutral component of the beam is shown in Fig. 6.

Since the scintillator response, i.e., the number of photons produced per incident energetic particle, is proportional to the amount of energy transmitted to the crystal during the impact of the energetic particle, two atoms, each of energy E/2, whose difference in impact time is considerably shorter than the characteristic decay time of the crystal (~ 0.6×10^{-6} sec), would be interpreted as a single particle of energy ~ E.

In the present experiment, the maximum possible difference in the impact time of the two H atoms produced by dissociation of H_2 in the target cell is ~ 5×10^{-9} sec. The H atoms may, however, be spatially distinguishable by use of a low transparency (~ 1%) copper mesh.

Assuming a random orientation of the H_2 internuclear axis with respect to the beam line and an isotropic H atom angular distribution from dissociation arising from H_2 collisions with a H_2 target, we have calculated for the case which produces the smallest scatter in the present experiment (42 keV/nucleon and ~ 2 eV dissociation energy), that the H atoms at the detector from dissociation in the target are uniformly distributed over

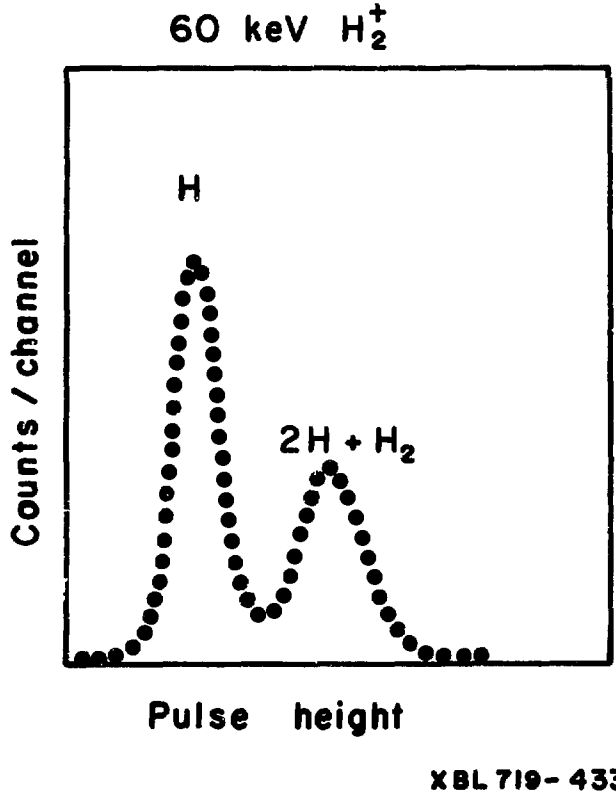

Fig. 6. The pulse height spectra obtained with a CsI(Tl) scintillation crystal for the neutral collision products of a 60-keV H_2^+ beam.

an area of radius 2.2 mm. The mesh grid is composed of square holes of length 6.35×10^{-3} mm with the same wire thickness. Clearly, the grid size is significantly smaller than the majority of the H atom separations.

Therefore, in order to identify the H_2 molecules from the (H + H) signal, the mesh was placed in front of the neutral detector. With the mesh in the beam line the probability of obtaining a full energy pulse from two simultaneous H atoms is $\sim 10^{-4}$, while the probability of obtaining a full-energy pulse from a H_2 molecule is 10^{-2}. This is due to the spatial separation of the H atoms being much larger than the mesh grid size so that the atoms are no longer correlated and transmit through the mesh independently. The transmission was measured by using a H atom beam and was found to vary from day to day by ±4%.

To insure ourselves that the mesh was functioning as we thought, its performance was tested experimentally. The H_2^+ beam was incident on the target cell with the electric field off. For a constant thickness in the cell, and using the charge detector as a monitor, the neutral particles were counted with the mesh out. (The full energy pulses, the half-energy pulses, and the total pulses were counted individually by using three sets of scalers.) Based on the arguments given above, we were able to predict the counts with the mesh in. (The equation used for the predictions is $T = (A' + C')/(A + C)$, where T ≡ the mesh transmission, A ≡ the full energy counts, B ≡ the half energy counts, C ≡ the total counts, and the primes refer to the counts

with the mesh in.) Our predictions for the number of counts in each energy peak agreed to within ±6% with the measured values. Therefore, since the ratio $H_2/(H + H)$ incident on the target cell was typically ~ 0.3 for the attenuation measurements, the assumptions about the effect of the mesh on the beam are correct.

For each species of the beam detected (H_2^+, H^+, H_2, H), two sets of scalers were used in order to correct for random noise. By employing a chopped incident H_2^+ beam at a frequency of 4.0 Hz, modulated by applying voltage to a set of steering deflector plates in the accelerator region, one set of scalers measured the beam plus the noise and the other set measured the beam-off signal (i.e., the noise). Subtraction of the two counts yields the counts produced by the beam. A set of timing scalers was also used to determine the beam-on and -off counting times.

Figure 7 shows the electronic details and logic sequence of the particle detection (Method I). The control unit for the accumulation of data was the integrator-control-gate assembly. With the pulse generators running, data acquisition would begin with the starting of the control-gate generator. The integrator would accumulate a preset amount of charge and then turn off the control gate. The beam modulator output was generally around 1.5 kV, depending on how the beam was tuned. The beam passed into the experimental region when the modulation voltage was on and was deflected with the voltage off.

Figure 8 shows a typical set of timing characteristics. Beam-on counts were accumulated for 124 msec while beam-off

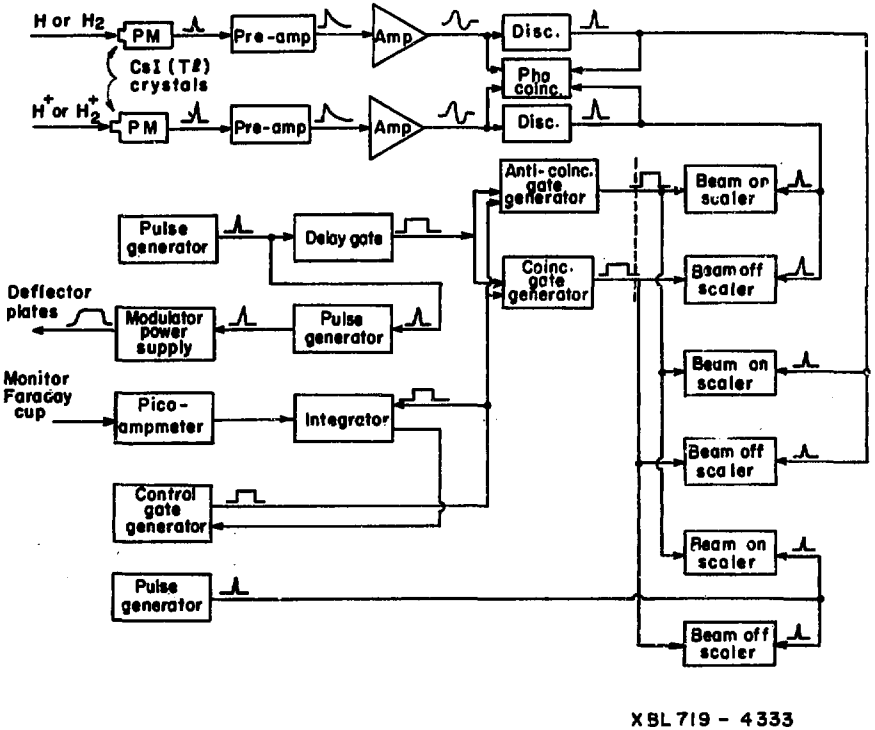

Fig. 7. Block diagram of the electronics and counting logic used in Method 1. _/_ pulse; _⌐¬_, gate.

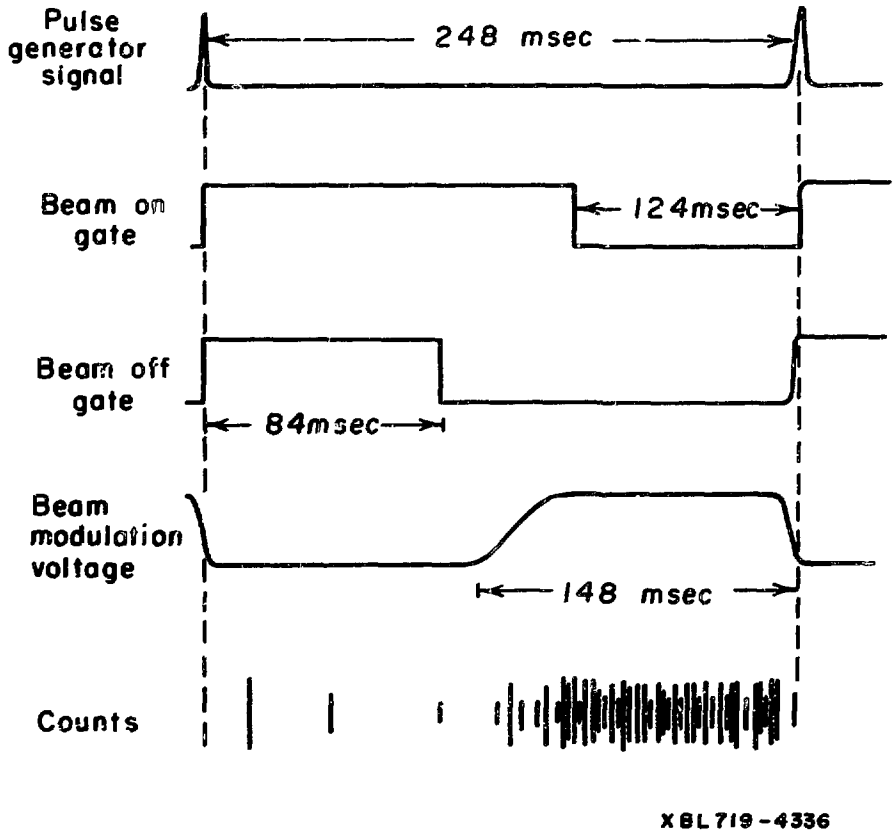

Fig. 8. Timing characteristics of Method I.

counts were accumulated for 84 msec. There were 40 msec when no counts were accumulated. This was to insure no overlapping of signals. The beam-off counters were idle for 16 msec before the voltage was applied to the plates. There was a relatively large rise time of the voltage signal due to the characteristics of the power supply which required a delay of 24 msec before accumulating beam-on data. This was done in order to eliminate any possible interference due to beam steering. Changes in the beam counts could be easily seen on the oscilloscope trace during this rise time.

The discriminators were set by observing, on the pulse-height analyzer CRT display, the coincidence output of the signal before and after the discriminator.

The output of the photomultiplier tube was generally $\lesssim$ 1 mV with a decay time characteristic of the scintillation crystal, i.e., about 0.6 μsec. The preamplifier amplified the pulse by a factor of ~ 10 and shaped the decay time to 50 μsec. The output of the amplifier was ~ 3 V with a width of about 2 μsec and rise and fall times of about 1 μsec.

b. Method II: Faraday Cup

Method II for observing the particles (refer to Fig. 3) allows only for the detection of transmitted H_2 molecules from the target and was used to obtain low-energy ($E \leq 10$ keV/nucleon) total-loss cross sections. Ionization cross sections and excited state populations cannot be obtained by this method.

This method uses a third gas region (the stripper), which

contained H_2 gas held at a constant pressure, to ionize the H_2 molecules transmitted through the target. The resulting H_2^+ beam, exiting from the stripper, which is proportional to the H_2 beam transmitted through the target, was deflected to a Faraday cup. The resulting signal was fed to an electrometer whose output was sent to an integrator. For this method the ion source was operated in the PIG mode in order to obtain high beam intensities, measurable by a Faraday cup. Typical H_2^+ currents measured by the final Faraday cup ranged from 10^{-13} to 10^{-10} A.

IV. THE MEASUREMENTS: ANALYSIS AND PROCEDURE

In this section we will describe the measurements that are performed in the present work. The quantities measured are:

(1) Yields of $H_2(c^3\Pi_u)$ excited molecules from the electron capture by H_2^+ ions in Mg vapor and H_2 gas neutralizers as a function of H_2^+ ion energy and neutralizer thickness π_n, and in N_2 gas at 12.5 keV/nucleon.

(2) Yields of $H_2(c^3\Pi_u)$ excited molecules from the breakup of H_3^+ ions in Mg vapor at 7.5 keV/nucleon.

(3) Yields of the various reactions for H_2^+ ions in collisions with Mg vapor as a function of H_2^+ ion energy and Mg vapor thickness π_n.

(4) Cross sections for the total loss and ionization of $X^1\Sigma_g^+$ and $c^3\Pi_u$ H_2 molecules in collisions with H_2 gas.

A. Determination of (i) Total Loss Cross Section for the $X^1\Sigma_g^+$ and $c^3\Pi_u$ States (σ_t, σ_t^*) and (ii) the $c^3\Pi_u$ Population in the Neutral Beam (f) for $10 \leq E$ (keV/nucleon) ≤ 42 by Method I

The measurement of σ_t, σ_t^*, and f was performed by passing an H_2^+ beam through a neutralizer of Mg vapor, H_2 or N_2 gas, sweeping the charged particles aside, and allowing the neutral beam to traverse the target cell which contained H_2 gas. The emerging H_2 particles were detected by single-particle counting techniques (Method I) discussed in Sec. III, B, 5a.

The collision reactions occurring when energetic H_2 passes

through the H_2 target cell are (the right side of the reaction indicates explicitly only the fast collision products):

$H_2 + H_2 \rightarrow H + H + \cdots$	dissociation ·····	σ_{2H}
$H_2 + H_2 \rightarrow H + H^+ + e + \cdots$	dissociative electron detachment ·····	σ_{HH^+}
$H_2 + H_2 \rightarrow H_2^+ + e + \cdots$	ionization ·····	$\sigma_{H_2^+}$
$H_2 + H_2 \rightarrow H^+ + H^+ + 2e + \cdots$	dissociative double electron detachment ··	σ_{2H^+}
$H_2 + H_2 \rightarrow H_2^- - e + \cdots$	electron capture ·····	$\sigma_{H_2^-}$
$H_2 + H_2 \rightarrow H_2^* + \cdots$	excitation ·····	$\sigma_{H_2^*}$

where H_2^* designates the H_2 molecule in an excited state and σ_k is the cross section for the conversion $H_2 \rightarrow k$. In the event that the incident molecule is already excited, an additional reaction is possible:

$H_2^* + H_2 \rightarrow H_2 + \cdots$	de-excitation ·····	$\sigma^*_{H_2}$

and we define σ_k^* as the cross section for the conversion $H_2^* \rightarrow k$.

Neglecting excitation and de-excitation (the justification for this is the topic of Appendix F), and neglecting negative ion formation (As will be discussed in Sec. V, A, no H_2^- ions were observed and insignificant amounts of H^- ions were observed in the present experiment.) we may write the collision relations for the processes occurring in the target cell for the two classes of

H_2 molecules of interest in the present experiment (see Appendix E). Defining the fractions $F(\pi_t)$, $F^*(\pi_t)$, and $F^+(\pi_t)$ as

$F(\pi_t)$ ≡ the number of ground state $H_2(X^1\Sigma_g^+)$ molecules in beam after traversing a target thickness π_t per H_2 molecule incident on the target cell,

$F^*(\pi_t)$ ≡ the number of excited $H_2(c^3\Pi_u)$ molecules in the beam after traversing a target thickness π_t per H_2 molecule incident on the target cell, and

$F^+(\pi_t)$ ≡ the number of H_2^+ molecules in the beam produced by the ionization of $c^3\Pi_u$ H_2 and $X^1\Sigma_g^+$ H_2 while traversing a target thickness π_t per H_2 molecule incident on the target cell,

we have

$$\frac{d}{d\pi_t} F(\pi_t) = - \sigma_t F(\pi_t) + \sigma_{10} F^+(\pi_t) \qquad (1a)$$

$$\frac{d}{d\pi_t} F^*(\pi_t) = - \sigma_t^* F^*(\pi_t) + \sigma_{10}^* F^+(\pi_t) \qquad (1b)$$

where

π_t ≡ the number of target particles per cm^2, i.e., target thickness($\pi_t = n_t x_t$, where n_t is the number density of target molecules and x_t is the length traversed by the beam through the target),

$\sigma_t = \sigma_{2H} + \sigma_{HH^+} + \sigma_{H_2^+} + \sigma_{2H^+}$, and

σ_{10} is the cross section for the reaction

$$H_2^+ + H_2 \rightarrow H_2(X^1\Sigma_g^+) + e + \cdots \text{ electron capture } \cdots\cdots \sigma_{10}.$$

Analogously,

$$\sigma_t^* = \sigma_{2H}^* + \sigma_{HH^+}^* + \sigma_{H_2^+}^* + \sigma_{2H^+}^*$$

and

$$H_2^+ + H_2 \rightarrow H_2(c^3\Pi_u) - e + \cdots \quad \text{electron capture} \cdots\cdot \quad \sigma_{10}^*.$$

For this measurement an electric field of about 8 kV/cm was applied transverse to the beam within the target cell in order to deflect the fast molecular ions, produced from the ionization of fast H_2, from the beam as they were formed. The measurements were repeated as a function of the applied electric field until there was no change in the results with a further increase in the electric field. Under this condition the F^+ term in the above equations vanish and the solutions readily become

$$F(\pi_t) = \left[1 - f(\pi_n)\right] e^{-\sigma_t \pi_t} \tag{2a}$$

$$F^*(\pi_t) = f(\pi_n) e^{-\sigma_t^* \pi_t} \tag{2b}$$

where

$f(\pi_n) \equiv$ the fraction of the incident H_2 molecules in the $c^3\Pi_u$ state produced by electron capture by H_2^+ ions while traversing a neutralizer of thickness π_n.

The detector system was not capable of distinguishing between the two classes of molecules, therefore we measured the sum of the two classes of H_2 molecules transmitted through the target cell. The attenuation of the sum $y(\pi_t) = F(\pi_t) + F^*(\pi_t)$ was observed by counting the number of H_2 molecules transmitted through the target cell for a constant preset accumulation of charge at the monitor

Faraday cup (see Sec. III, B, 3) for several target thicknesses π_t. Figure 9 shows the quantity $y(\pi_t) = F(\pi_t) + F^*(\pi_t)$ vs target thickness for a 50-keV D_2 beam produced in a Mg neutralizer (thin target, i.e., single collision conditions applied) by electron capture of D_2^+ ions. The solid line is the result of a least squares fit of the data to $y(\pi_t)$ (see Appendix G). The nonlinear portion is due to the presence of $c^3\Pi_u$ H_2 molecules (see Appendix E). As the target is made thicker the attenuation becomes linear, reflecting the loss of essentially all $c^3\Pi_u$ molecules in the target cell and the transmittance of only $X^1\Sigma_g^+$ molecules (this is due to $\sigma_t^* > \sigma_t$). By subtracting the extrapolated portion (curve A) of the linear region of the data from the data we obtain the lower straight line (curve B) which is th $c^3\Pi_u$ H_2 attenuation. The straight lines are represented by the equations

$$\ln F(\pi_t) = -\sigma_t\pi_t + \ln\left[1 - f(\pi_n)\right] \quad \text{(curve A)} \quad (3a)$$

$$\ln F^*(\pi_t) = -\sigma_t^*\pi_t + \ln f(\pi_n) \quad \text{(curve B)}. \quad (3b)$$

The cross sections are therefore easily obtained from the slopes as

$$\sigma_t = -\frac{\Delta \ln F(\pi_t)}{\Delta\pi_t} \quad (4a)$$

$$\sigma_t^* = -\frac{\Delta \ln F^*(\pi_t)}{\Delta\pi_t}. \quad (4b)$$

Also, the intercept of curve B yields the fraction of the beam

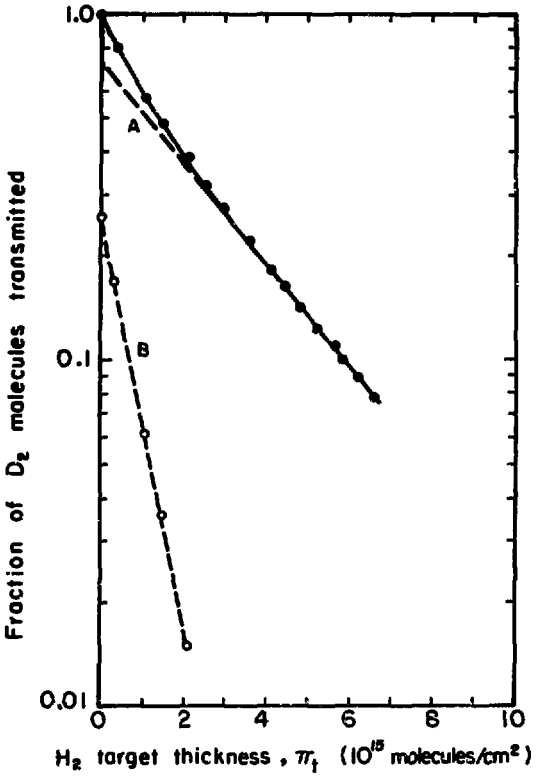

XBL7011-4099

Fig. 9. Observed attenuation of a beam of D_2 molecules in a H_2 target by Method I. The molecules were produced in a Mg neutralizer (thin target) by electron capture of 50-keV D_2^+. The solid line is the result of a least-squares fit of the data to the sum of two exponentials. Curve A is an extrapolation of the thick target asymptote; curve B is the difference between the data and curve A. Solid circles are experimental points; open circles are derived points.

in the $c^3\Pi_u$ state. From Eq. (2b), evaluated at $\pi_t = 0$, we have

$$F^*(0) = f(\pi_n). \tag{5}$$

When the Mg vapor neutralizer thickness was increased to large values ($\pi_n \gtrsim 1 \times 10^{16}$ atoms/cm^2) or when H_2 or N_2 gas was used as a neutralizer, significant nonlinear effects were not observed, i.e., $F^*(0) = 0$. The decrease in the $c^3\Pi_u$ component with increasing Mg vapor neutralizer thickness reflects its larger attenuation-loss cross section. In the case of the H_2 and N_2 gas neutralizers, the lack of nonlinear effects is due to the large competing ground-state electron-capture process (see appendix E).

The determination of σ_t was performed by using a H_2 neutralizer. The cross section was obtained from a least-squares fit of the attenuation data to the equation

$$F(\pi_t) = e^{-\sigma_t \pi_t} \tag{6}$$

since $f(\pi_n) = 0$ in this case [see Eq. (2a)].

The determination of σ_t^* and $f(\pi_n)$ was performed by using a Mg neutralizer. The cross section σ_t^* and the $c^3\Pi_u$ fraction $f(\pi_n)$ were obtained from a least-squares fit of the data to the equation

$$y(\pi_t) = \left[1 - f(\pi_n)\right] e^{-\sigma_t \pi_t} + f(\pi_n)\, e^{-\sigma_t^* \pi_t} \tag{7}$$

with the value of σ_t known from the H_2 neutralizer case. A discussion of the least-squares fit procedure can be found in Appendix G.

The above analysis was also performed on an H_2 beam prepared by H_3^+ dissociation in Mg vapor. The H_2 molecules were formed via the reactions

$$H_3^+ + Mg \rightarrow \begin{cases} H_2 + H - e + \cdots \\ H_2 + H^+ + \cdots . \end{cases}$$

This measurement was performed at 7.5 keV/nucleon for two different Mg vapor thicknesses, 0.9 and 2 x 10^{14} atoms/cm^2. No $c^3\Pi_u$ H_2 molecules were observed.

B. Determination of σ_t and σ_t^* for $1 \leq E$ (keV/nucleon) ≤ 42 by Method II

For this measurement the production, monitoring, and attenuation of the H_2 beam was identical with Method I except we required the use of a third gas cell (the stripper), which contained H_2 gas, for the particle detection (see Fig. 3). The H_2 beam transmitted through the target cell was passed through the stripper where a fraction was ionized ($H_2 \rightarrow H_2^+$). This H_2^+ beam is (for a constant stripper thickness) proportional to the H_2 beam transmitted through the target cell. The H_2^+ current was then deflected to a Faraday cup and integrated for a preset accumulation of charge at the monitor Faraday cup. The collected charge Q can be expressed as (cf. eq. 7)

$$Q(\pi_t) = \alpha_1\left[1 - f(\pi_n)\right]e^{-\sigma_t \pi_t} + \alpha_2 f(\pi_n) e^{-\sigma_t^* \pi_t}, \qquad (8)$$

where α_1 and α_2 are constants for a given stripper thickness and reflect the efficiency of the $H_2(X^1\Sigma_g^+)$ and $H_2(c^3\Pi_u)$ molecules

to produce H_2^+ ions. The measurement was performed by observing the attenuation of $Q(\pi_t)$ for several target cell thicknesses π_t. Figure 10 shows the quantity $Q(\pi_t)$ (in arbitrary units) vs H_2 target thickness for a D_2^+ beam produced in a thin Mg neutralizer (8.5×10^{13} atoms/cm^2) and transmitted through the H_2 target cell. The nonlinearity of the curve in Fig. 10 is larger than the nonlinearity produced by direct observation of the D_2 molecules (Method I) under similar conditions (cf. Fig. 9). This is due to the fact that the cross section for D_2^+ production by $D_2(c^3\Pi_u)$ is larger than by $D_2(X^1\Sigma_g^+)$ (see Sec. V, B, 2), i.e., $\alpha_2 > \alpha_1$. Without a knowledge of α_1 and α_2, we cannot determine $f(\pi_n)$, but we still are able to determine σ_t and σ_t^*. The analysis of the data to yield values for σ_t and σ_t^* was identical with Method I.

C. The Determination of the Ionization Cross Section of the $X^1\Sigma_g^+$ State, $\sigma_{H_2^+}$, and of the $c^3\Pi_u$ State, $\sigma^*_{H_2^+}$

In this section we discuss the measurement of the ionization cross sections ($H_2 \rightarrow H_2^+$) for energetic $X^1\Sigma_g^+$ and $c^3\Pi_u$ molecules in collision with H_2 gas. The molecules were again formed by electron capture by H_2^+ ions in collision with Mg vapor or H_2 or H_2 gas, with the transmitted H_2^+ component, detected with a Faraday cup, providing a monitor of the beam intensity (see Sec. III, B, 3). For this measurement the transverse electric field in the target cell was turned off so that the H_2^+ component in the beam due to the ionization of H_2 could be measured. Detection

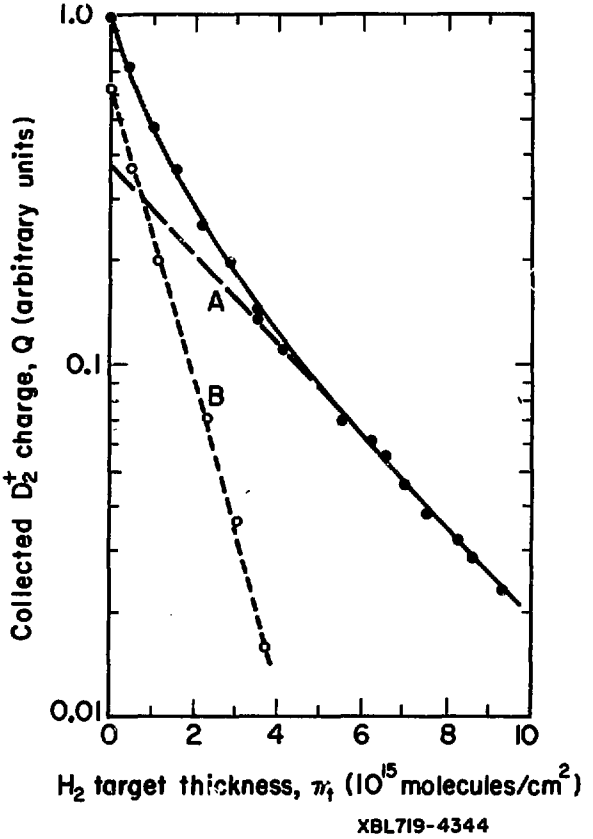

Fig. 10. Observed attenuation of a beam of D_2 molecules in a H_2 target by Method II. The figure is a plot of the collected D_2^+ charge, Q, measured by the Faraday cup after the stripper versus H_2 target gas thickness π_t. The D_2^+ ions were produced by ionization of D_2 in an H_2 target (stripper) ~2×10^{14} molecules/cm^2 thick. The D_2 molecules were produced by electron capture of 62-keV D_2^+ ions in a Mg vapor target(neutralizer) of thickness 8.5×10^{13} atoms/cm^2. Curve A is an extrapolation of the thick target asymptote; curve B is the difference between the data and curve A. Solid circles are experimental points; open circles are derived points.

of the emerging H_2^+ ions and H_2 molecules was performed by single particle counting techniques (Method I).

The collision relation governing the H_2^+ component in the beam due to the ionization of $H_2(X^1\Sigma_g^+)$ and $H_2(c^3\Pi_u)$ in the target cell may be written as (using the definitions presented on p. 39)

$$\frac{d}{d\pi_t} F^+(\pi_t) = \sigma_{H_2^+} F(\pi_t) + \sigma^*_{H_2^+} F^*(\pi_t) - \sigma_\ell F^+(\pi_t) \qquad (9)$$

where

$\sigma_\ell \equiv$ the total loss cross section for H_2^+ ions in collision with H_2 gas.

This equation is based on the assumption that σ_ℓ is the same for H_2^+ ions produced by ionization of either $H_2(X^1\Sigma_g^+)$ or $H_2(c^3\Pi_u)$ molecules.

The determination of $\sigma_{H_2^+}$ and $\sigma^*_{H_2^+}$ was obtained from data taken for $\pi_t < 5.8 \times 10^{13}$ molecules/cm^2. In this case the target is thin for all processes of interest (i.e., $\sigma_{H_2^+} \ll \pi_t^{-1}$, $\sigma^*_{H_2^+} \ll \pi_t^{-1}$, and $\sigma_\ell \ll \pi_t^{-1}$). Under these conditions the following inequality held for all measurements

$$\sigma_\ell F^+(\pi_t) \lesssim \sigma_{H_2^+} F(\pi_t) + \sigma^*_{H_2^+} F^*(\pi_t) \times (3 \times 10^{-2}), \qquad (10)$$

i.e., the ionization cross sections were determined under the condition that the rate of losing the H_2^+ ions was always less than 3% of the rate of producing them.

Also, the value of $F(\pi_t)$ and $F^*(\pi_t)$ did not change by more than ~ 2% and ~ 4% during these measurements, hence we may replace

$F(\pi_t)$ and $F^*(\pi_t)$ by $F(0)$ and $F^*(0)$. Therefore Eq. (9) becomes

$$\frac{d}{d\pi_t} F^+(\pi_t) = \sigma_{H_2^+}\left[1 - f(\pi_n)\right] + \sigma^*_{H_2^+} f(\pi_n) \qquad (11)$$

since $F^*(0) = f(\pi_n)$ and $F^*(0) + F(0) = 1$. The solution to Eq. (11) is

$$F^+(\pi_t) = \left[\sigma_{H_2^+}\left[1 - f(\pi_n)\right] + \sigma^*_{H_2^+} f(\pi_n)\right] \pi_t. \qquad (12)$$

The production of $F^+(\pi_t)$ is observed by counting the number of H_2^+ molecules exiting the target cell for a constant preset accumulation of charge at the monitor Faraday cup for several target thicknesses π_t. Figure 11 shows a plot of $F^+(\pi_t)$ vs. π_t.

When the incoming H_2 beam contained no observable fraction of $c^3\Pi_u$ states [e.g., $f(\pi_n) = 0$ when a H_2, N_2, or thick Mg neutralizer was used] the slope of the linear relation between $F^+(\pi_t)$ and π_t yielded $\sigma_{H_2^+}$ [see Eq. (12) with $f(\pi_n) = 0$], the cross section for the ionization of the ground state (curve B). When the H_2 beam did contain an observable fraction of $c^3\Pi_u$ molecules (thin Mg neutralizer), the same technique yielded the composite cross section $\sigma_{H_2^+}\left[1 - f(\pi_n)\right] + \sigma^*_{H_2^+} f(\pi_n)$ [curve A; see Eq. 12]. Obtaining the value of $f(\pi_n)$ from independent attenuation measurements (see Fig. 9) for the same neutralizer conditions, the cross section for ionization of the $c^3\Pi_u$ state, $\sigma^*_{H_2^+}$, can be determined.

D. The Determination of the Particle Yields Due to Energetic H_2^+ Ions in Collision with Mg Vapor

The present section describes the measurement of the particle

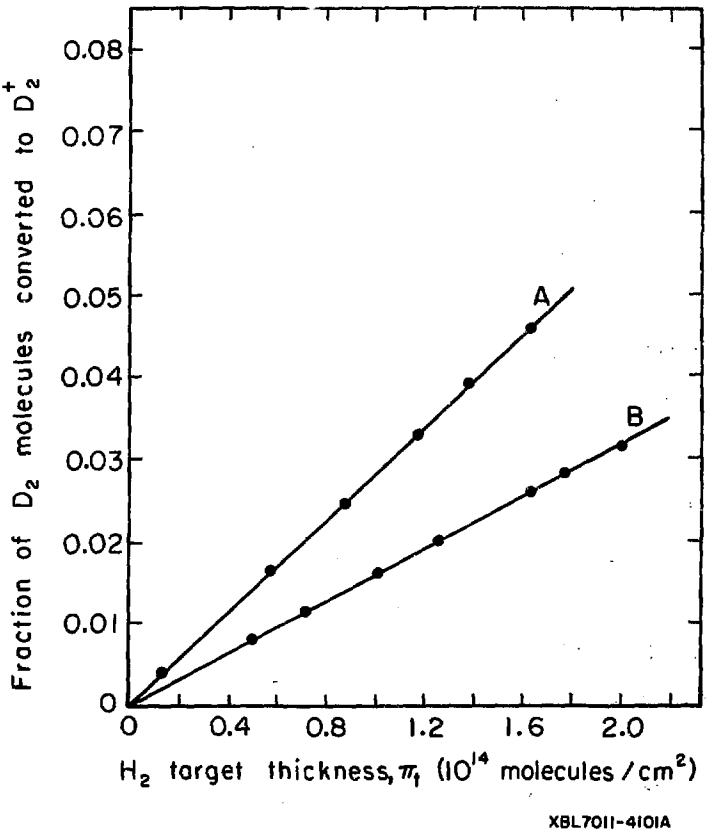

Fig. 11. Production of D_2^+ ions from the ionization of 60-keV D_2 molecules in collision with a H_2 gas target. The D_2 molecules were produced by electron capture of D_2^+ ions in a Mg vapor neutralizer. Line A connects the experimental data using a thin Mg vapor neutralizer ($\pi_n \lesssim 1\times10^{14}$ atoms/cm^2); line B connects the experimental data using a thick Mg vapor neutralizer ($\pi_n \gtrsim 1\times10^{16}$ atoms/cm^2).

yields due to energetic H_2^+ ions in collision with Mg vapor. For this measurement the Mg oven was moved to the target cell position (see Fig. 3). This was done in order to insure complete collection of the breakup products. The exit aperture of the oven was enlarged until, for a constant thickness, there was no observable change in the measured beam components. The final oven collimation was 0.33-mm entrance diameter and 2.8-mm exit diameter. The diameter of the particle detectors (25.4 mm) was larger than the maximum possible beam spreading which is defined by the oven collimation. For this measurement the Mg vapor thickness was varied from 2×10^{14} to 1×10^{16} atoms/cm^2.

The measurements were performed by passing H_2^+ ions through the oven for several Mg vapor thicknesses and counting the exiting H_2^+, H^+, H, and H_2 components of the beam. This enabled us to obtain the yields of the reactions

(1) $H_2^+ + Mg \rightarrow H_2 - e + \cdots$,

(2) $H_2^+ + Mg \rightarrow H + H - e + \cdots$,

(3) $H_2^+ + Mg \rightarrow H + H^+ + \cdots$,

(4) $H_2^+ + Mg \rightarrow H^+ + H^+ + e + \cdots$.

(The H^- yield was measured at 20 keV/nucleon and was inconsequential. We expect the H^- yield to peak at energies less than those used in the present work. For a future experiment we suggest a study of H^- yields at low energies. It is possible that information on the formation of H_2^- ions with lifetimes less than ~ 0.5 μsec could be obtained from a study of this type.)

In order to separate the H_2 and H + H contributions the neutral particles had to be detected once with the mesh in and once with it out (see Sec. III, B, 5a). From these measurements we are able to account for the total beam and calculate the individual beam component fractions.

A search was carried out for the presence of H_2^-. The search was performed by reversing the deflector voltage. The result of the investigation from $7 \leq E$ (keV/nucleon)≤ 20 using the Mg vapor collision cell varying in thickness from 2×10^{14} to 1.0×10^{16} atoms/cm^2 was that no H_2^- ions were observed. The sensitivity of the detection was such that the H_2^- beam-on counter never showed a contribution greater than the statistical uncertainty in the background corrected counts for $\sim 10^9$ H_2^+ primary ions incident on the Mg vapor cell. A discussion of several experimental and theoretical studies of the H_2^- ion is given in Appendix H. Also, in this appendix we indicate the arguments for a search for H_2^- using Mg vapor.

E. Error Analysis

For all experimental results of this work, the assignment of uncertainty is based on the reproducibility of the data occurring in a number of runs taken months apart, on the standard deviation of the least-squares fit of the data, and on systematic experimental errors. The long term reproducibility of the ground state measurements was ±5% with a standard deviation of the least-squares fit of the data of ±3%. This was true in both Methods I and II, although for $E \geq 20$ keV/nucleon the results using the

stripper-Faraday cup combination for detection (Method II) were consistently 9% lower than the results using single particle counting techniques (Method I). A possible explanation for the difference in the results is that the vibrational population distribution of the ions is not the same in the two cases due to the radically different source conditions (see Appendix I).

For the excited state measurements, the long term reproducibility was ±17%, and the standard deviation of the least-squares fit of the data varied from ±5% to ±20%. Counting statistical errors were always less than 4% and in all but a few cases less than 1%. Possible systematic experimental uncertainties resulting from pressure and target length measurements are estimated to total about ±7%.

The effect of collimator interceptions and gas background were determined to be negligible since the fraction of the H_2 beam surviving with no target gas was always >0.998.

To experimentally investigate the possibility of the presence of unknown systematic errors, we measured the well-known total-loss cross section for energetic atomic hydrogen in collision with H_2 gas. Our measurements agree to within ±5% with those of Stier and Barnett.[70] We also measured the single-electron capture cross section for energetic protons passing through H_2 gas. These results agreed to within ±5% with those of McClure.[71]

Other possible sources of error which are determined to be inconsequential in this work are target and source gas contamination and detector signals of unknown origin that are modulated

with the beam. These considerations along with a more detailed discussion of all sources of error and their assessed contribution to the uncertainty of the results may be found in Appendix I.

The estimated absolute uncertainty in the present results ranges from ±18% to ±25% for the excited state cross sections and populations (i.e., those that survive for $t \gtrsim 0.5$ μsec), ±10% for the ground-state cross sections, and ranges from ±10% to ±15% for the particle yield measurements. The confidence level associated with these uncertainties is estimated to be 60% (see Appendix I). The assigned absolute uncertainty for each data point may be found with the tabulated data in Sec. V.

V. RESULTS AND DISCUSSION

A. Beam Populations

1. Yields of Atoms and Molecules from the Breakup of H_2^+ Ions in Mg Vapor

The data plotted in Figs. 12 and 13 show the variation with Mg vapor thickness of the experimental yields of reaction products due to 10 keV/nucleon D_2^+ ions (Fig. 12) and 20 keV/nucleon H_2^+ ions (Fig. 13) in collision with Mg vapor. Figure 13 also shows the results of Riviere.[30] His measurements agree reasonably well with the present results.

No H_2^- or D_2^- ions were observed (see Appendix H). The data analysis of the yields allows us to assign an upper bound of 10^{-21} cm^2/atom to the cross section for double electron capture into H_2^- states with lifetimes longer than $\sim 10^{-7}$ sec due to H_2^+ ions in collision with Mg vapor from 7- to 20-keV/nucleon. The H^- yield at 20 keV/nucleon was observed to be less than 1% for $\pi_n \lesssim 10^{15}$ atoms/cm^2. (For the remainder of this section we will not refer to the isotopes of hydrogen. We remind the reader that for E < 20 keV/nucleon D_2^+ was always used as the incident projectile. Also, when the results were compared at equal velocities, no observable differences occurred.)

In going from 20 keV/nucleon (Fig. 13) to 10 keV/nucleon (Fig. 12), we note that the neutral yield of both H and H_2 has increased significantly while the proton yield has decreased. At 10 keV/nucleon with $\pi_n \sim 2 \times 10^{15}$ atoms/cm^2 approximately 90%

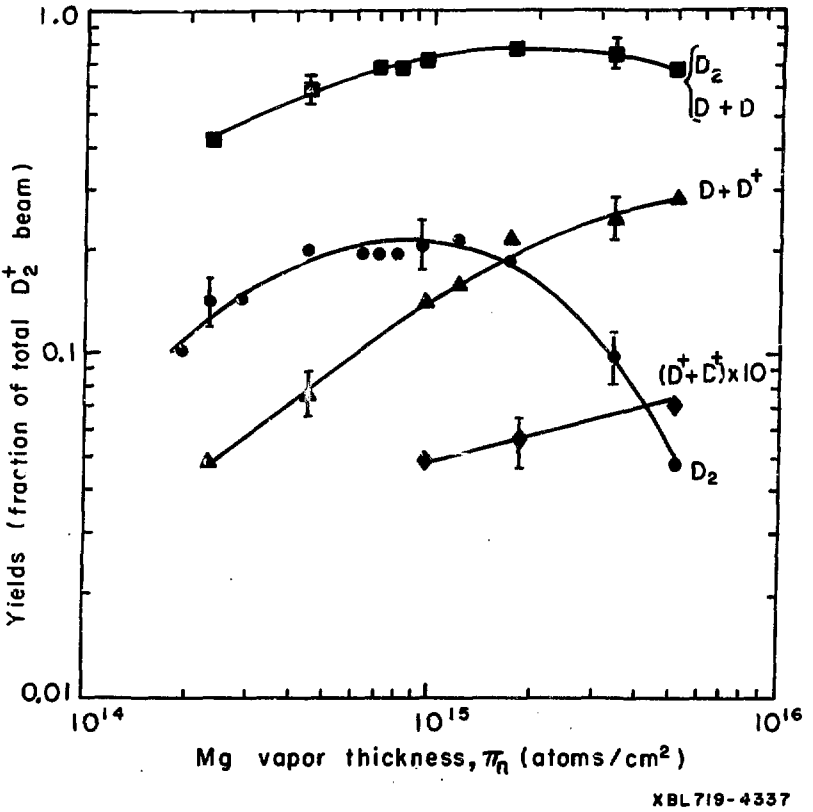

Fig. 12. The observed dependence on the Mg vapor-target thickness π_n of the particle yields from the collisional breakup of D_2^+. The beam energy was 10 keV/nucleon.

■ , $D_2^+ + Mg \rightarrow \begin{cases} D_2 - e + \cdots \\ D + D - e + \cdots \end{cases}$

● , $D_2^+ + Mg \rightarrow D_2 - e + \cdots$

▲ , $D_2^+ + Mg \rightarrow D + D^+ + \cdots$

◆ , $D_2^+ + Mg \rightarrow D^+ + D^+ + e + \cdots$

The lines drawn through our points are to guide the eye and have no other significance.

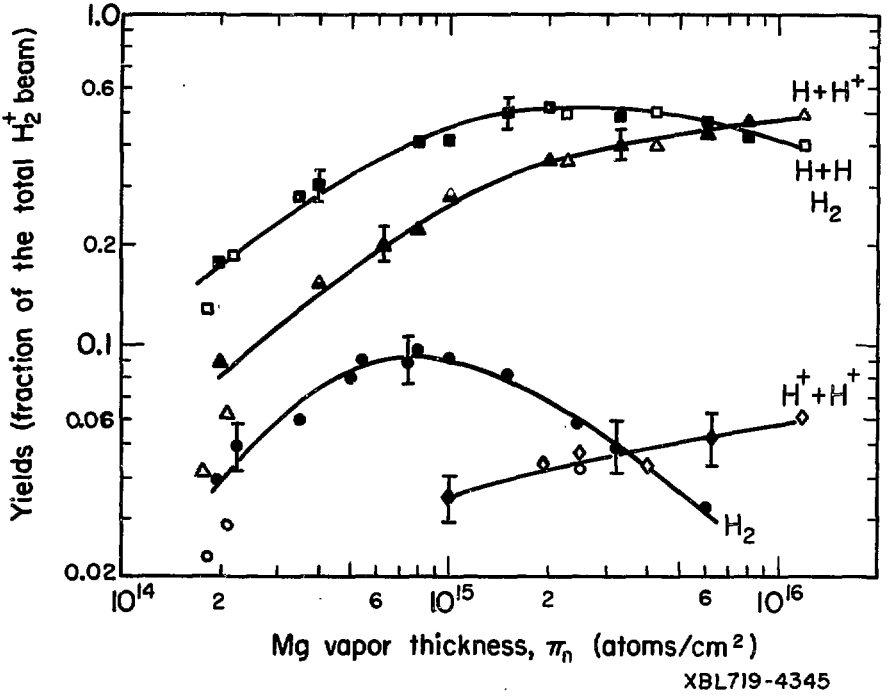

Fig. 13. The observed dependence on the Mg vapor-target thickness π_n of the particle yields from the collisional breakup of H_2^+. The beam energy was 20 keV/nucleon. Solid symbols, present work; open symbols, Ref. 30.

■, □ : $H_2^+ + Mg \rightarrow \begin{cases} H_2 - e + \cdots \\ H + H - e \cdots \end{cases}$

●, ○ : $H_2^+ + Mg \rightarrow H_2 - e + \cdots$

▲, △ : $H_2^+ + Mg \rightarrow H + H^+ + \cdots$

◆, ◇ : $H_2^+ + Mg \rightarrow H^+ + H^+ + e + \cdots$

The lines drawn through our points are to guide the eye and have no other significance.

of the incident H_2^+ ions have been converted to neutrals, but only ∿ 68% at 20 keV/nucleon. Also, at both energies the reaction

$$H_2^+ + Mg \rightarrow H + H - e + \cdots$$

is the dominant inelastic process.

In Fig. 14 we illustrate the variation with Mg vapor thickness and with H_2^+ particle energy of the experimental H_2 yields due to H_2^+ ions in collision with Mg vapor. The maximum H_2 yields occur around 10^{15} atoms/cm^2 for all energies measured and increase with decreasing energy.

2. Yields of $c^3\Pi_u$ Molecules from the Breakup of H_2^+ Ions

The yields of $c^3\Pi_u$ molecules discussed in this section are expressed in two different ways: as a fraction of the H_2 beam (Fig. 15) and as a fraction of the incident H_2^+ beam (Fig. 16).

The results shown in Fig. 15 illustrate the variation with Mg vapor thickness and with H_2^+ particle energy of the measured fraction of the H_2 molecules, formed by electron capture by H_2^+ ions in Mg vapor, that are in the $c^3\Pi_u$ state. We see from Fig. 15 for $\pi_n \lesssim 2 \times 10^{14}$ atoms/cm^2 that the fraction measured is independent of target thickness, i.e., single collision conditions existed. This fraction is a slowly decreasing function of energy, as predicted by Hiskes.[59] As the thickness is increased the fraction decreases as a result of the larger attenuation cross section for $c^3\Pi_u$ molecules than for $X^1\Sigma_g^+$ molecules.

In Fig. 16 we show the variation with Mg vapor thickness

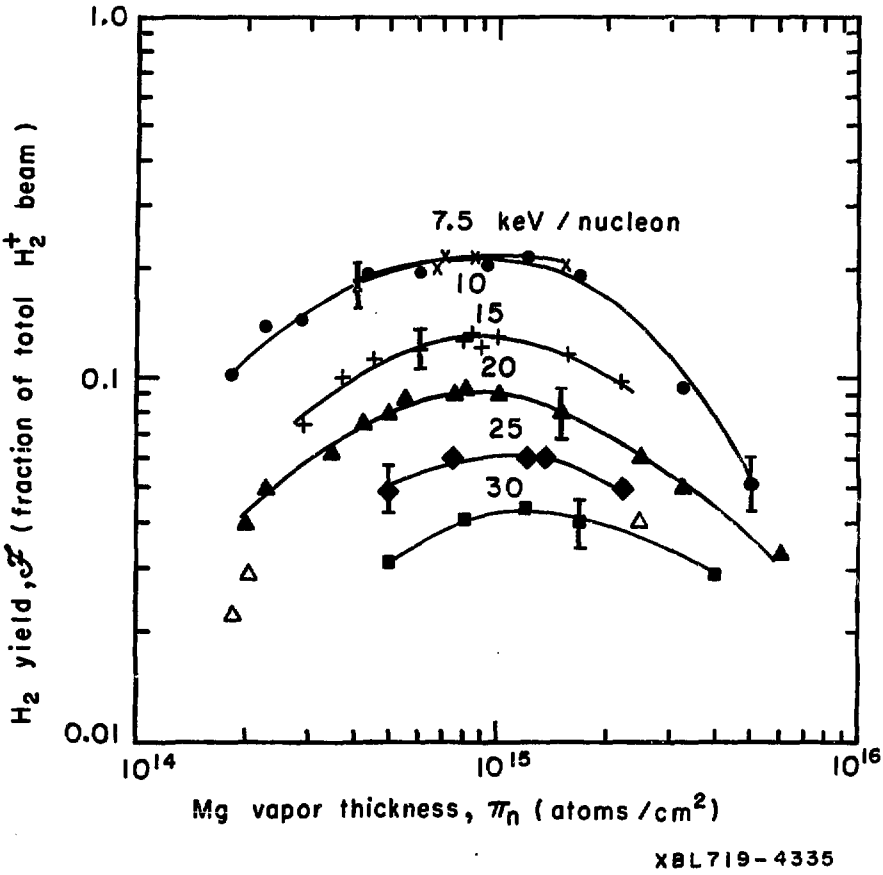

Fig. 14. Fraction of incident H_2^+ ions converted to H_2 molecules versus Mg vapor thickness π_n. Solid symbols, present work; open symbols, Ref. 30. x, 7.5 keV/nucleon; ●, 10 keV/nucleon; +, 15 keV/nucleon; ▲, △, 20 keV/ nucleon; ◆, 25 keV/nucleon; ■, 30 keV/nucleon. (For E < 20 keV/nucleon the incident projectile was D_2^+.) The lines through the points are drawn in to guide the eye and have no other significance.

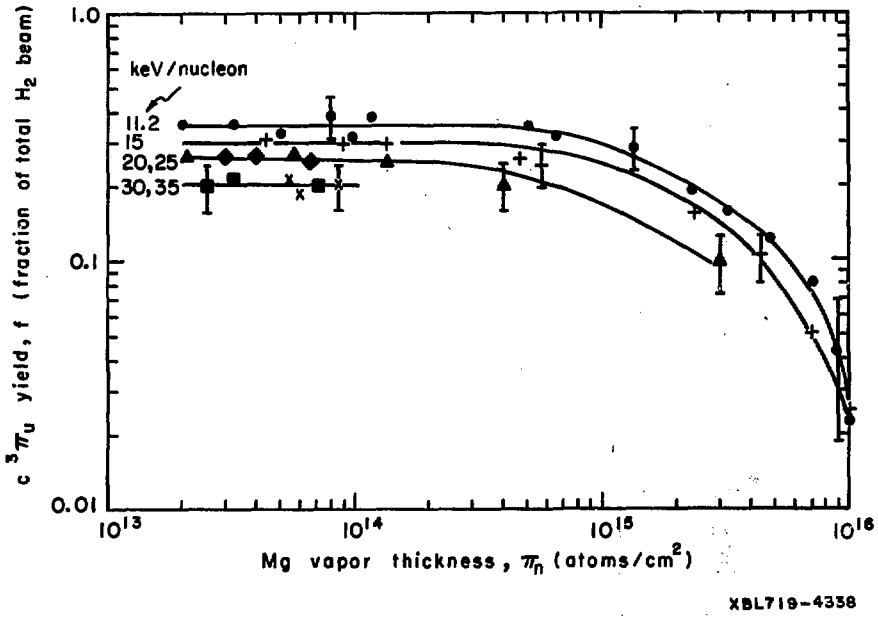

Fig. 15. Fraction of H_2 molecules that are in the $c\,^3\Pi_u$ state versus Mg vapor thickness π_n. ●, 11.2 keV/ nucleon; +, 15 keV/nucleon; ▲, 20 keV/nucleon; ◆, 25 keV/nucleon; ■, 30 keV/nucleon; x, 35 keV/nucleon. (For E < 20 keV/nucleon the incident projectile was D_2^+.) The lines through the points are drawn in to guide the eye and have no other significance.

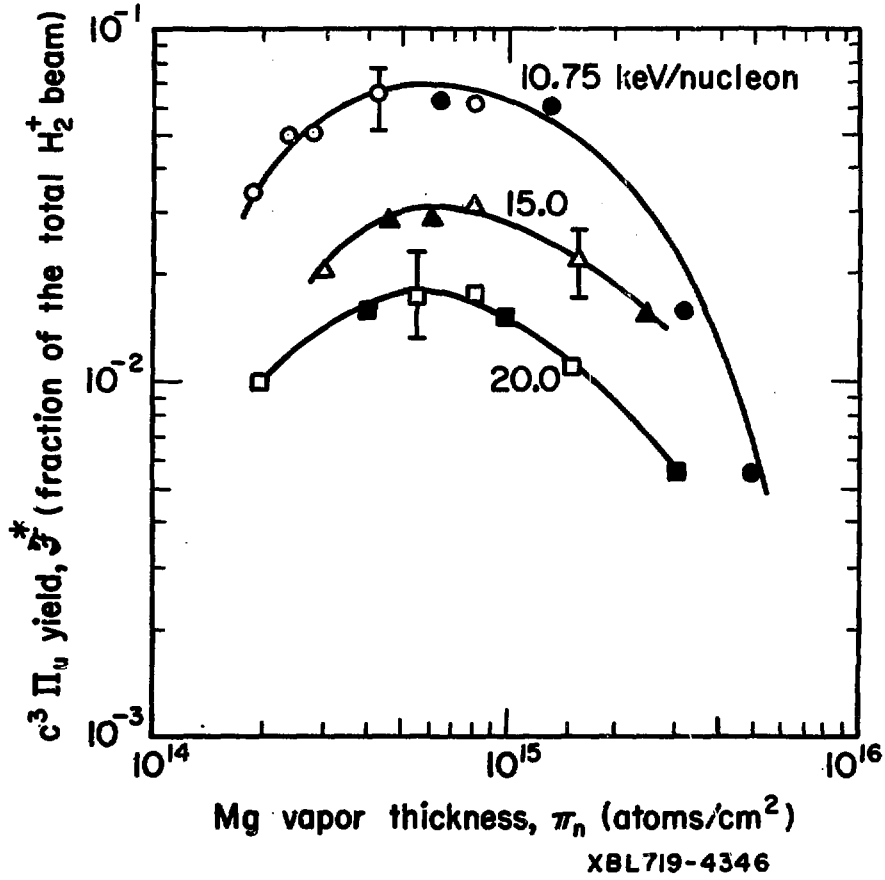

Fig. 16. The fraction of incident H_2^+ ions that are converted to $c^3\Pi_u$ H_2 molecules versus Mg vapor thickness π_n. ●, ○: 10.75 keV/nucleon (see text); ▲, △: 15.0 keV/ nucleon; ■, □: 20.0 keV/nucleon. (For E < 20 keV/nucleon the incident projectile was D_2^+.) The hollow symbols represent interpolated points (see text). The lines through the points are drawn in to guide the eye and have no other significance.

and with H_2^+ particle energy of the fraction of the incident H_2^+ ions than can be converted to $c^3\Pi_u$ H_2 molecules. These curves are generated by multiplying the data of Fig. 14 with the data of Fig. 15. That is, defining

$\mathcal{F}^*(\pi_n) \equiv$ fraction of H_2^+ ions converted to $c^3\Pi_u$ H_2 molecules in a neutralizer of thickness π_n (Fig. 16; $H_2^+ \rightarrow c^3\Pi_u\ H_2$),

$\mathcal{F}(\pi_n) \equiv$ fraction of H_2^+ ions converted to H_2 molecules in a neutralizer of thickness π_n (Fig. 14; $H_2^+ \rightarrow c^3\Pi_u\ H_2 + X^1\Sigma_g^+\ H_2$),

$f(\pi_n) \equiv$ fraction of H_2 molecules in the $c^3\Pi_u$ state after passage of H_2^+ ions through a neutralizer of thickness π_n [Fig. 15; $c^3\Pi_u\ H_2/(c^3\Pi_u H_2 + X^1\Sigma_g^+\ H_2)$],

we have

$$\mathcal{F}^*(\pi_n) = \mathcal{F}(\pi_n) \times f(\pi_n).$$

The hollow symbols in Fig. 16 were obtained by using an experimentally measured value from Fig. 14 and a value taken from the curves drawn through the data in Fig. 15. This was done since the data of the two measurements were in some cases taken at different values of π_n. The curve at 10.7 keV/nucleon is the product of the curve at 10.0 keV/nucleon of Fig. 14 and the curve at 11.2 keV/nucleon of Fig. 15. It is clear that no significant error is introduced by this procedure at this energy.

The maximum values of the results of Figs. 14, 15, and 16 ($\mathcal{F}_M$, f_M, $\mathcal{F}_M^*$) are presented in Table II. These maximum values

Table II. Maximum experimental fractions observed from a Mg vapor neutralizer and a H_2 gas neutralizer. Maximum fraction of H_2 molecules in $c^3\Pi_u$ state, f_M; maximum fraction of H_2^+ ions converted to H_2 molecules, $\mathcal{F}_M$; maximum fraction of H_2^+ ions converted to $c^3\Pi_u$ H_2 molecules, $\mathcal{F}_M^*$.

H_2^+ energy (keV/nucleon)	f_M Mg	f_M H_2	$\mathcal{F}_M$ Mg (±15%)	$\mathcal{F}_M^*$ Mg
7.5			0.220	
10.0			0.210	
11.2	0.36 ±0.06	~ 0 (N_2)[a]		0.065 ±0.014[b]
15.0	0.32 ±0.07	~ 0	0.130	0.031 ±0.008
20.0	$0.28^{+0.06}_{-0.05}$	< 0.05	0.095	0.018 ±0.004
25.0	$0.27^{+0.07}_{-0.05}$	< 0.07	0.063	
30.0	$0.23^{+0.06}_{-0.05}$	< 0.05	0.044	
35.0	$0.23^{+0.06}_{-0.05}$	~ 0		

[a] N_2 neutralizer at 12.5 keV/nucleon.

[b] Value obtained using data for f from Fig. 15 at 11.2 keV/nucleon and for $\mathcal{F}$ from Fig. 14 at 10.0 keV/nucleon. (See Sec. V, A, 2.)

are plotted versus H_2^+ energy in Fig. 17. (We remind the reader that although $\mathcal{F}^*(\pi_n) = \mathcal{F}(\pi_n) \times f(\pi_n)$, $\mathcal{F}^*_M \neq \mathcal{F}_M \times f_M$ since the maximum values do not necessarily occur at the same value of π_n.) The errors assigned reflect our estimate of the absolute reliability of the data based on a 60% confidence level of the random portion of the uncertainty. The assignment of these errors is discussed in Sec. IV, E and Appendix I. Also listed in Table II are our experimentally determined estimates of f_M using a H_2 or N_2 neutralizer. No $c^3\Pi_u$ H_2 molecules were observed due to H_3^+ breakup in Mg vapor.

When the results were compared at equal H_2^+, D_2^+, and HD^+ velocities, no differences, within experimental uncertainties, were observed. Since the nuclear symmetry associated with H_2 and D_2 breaks down for the heteronuclear isotopic molecule HD, the equivalence of the results at equal velocities seems to indicate that the interaction between the electronic and rotational motion is small. In this case the electronic dipole selection rules for homonuclear molecules are very good approximations for heteronuclear molecules.[39]

Finally, Hiskes[32] has predicted, based on his calculations for electron capture of 5- to 100-keV protons incident on ground state atoms, that toward the lower energy range of his calculations up to 50% of the electron capture can be into the $c^3\Pi_u$ state for H_2^+ ions incident on alkali or alkaline-earth vapors. He also estimates,[59] based on an assumed vibrational population

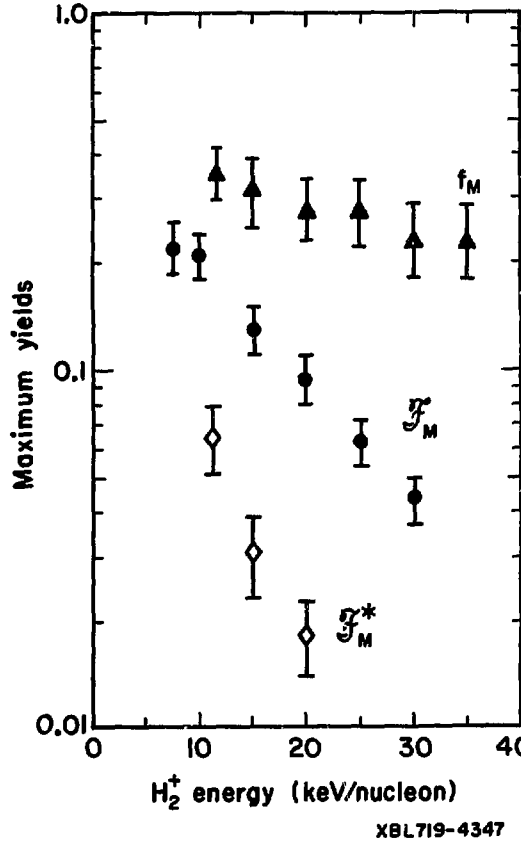

Fig. 17. Maximum experimental fractions from a Mg vapor target: maximum fraction of H_2 molecules in the $c^3\Pi_u$ state, f_M; maximum fraction of H_2^+ ions converted to H_2 molecules, $\mathcal{F}_M$: maximum fraction of H_2^+ ions converted to $c^3\Pi_u$ H_2 molecules, $\mathcal{F}_M^*$. Triangles, f_M; circles, $\mathcal{F}_M$: diamond, $\mathcal{F}_M^*$. (For $E < 20$ keV/nucleon the incident projectile was D_2^+.)

distribution for the H_2^+ ions produced in the ion source, that half of the $c^3\Pi_u$ H_2 molecules formed are capable of pre-dissociation (see Appendix C). Comparison of these theoretical considerations with Fig. 17 (i.e., with f) shows that assuming pre-dissociation of the $c^3\Pi_u$ molecules has occurred before detection in the present experiment, Hiskes' predictions are in excellent agreement at the upper end of the present energy range and are ~ 40% lower than the measurements at the lower end of the present energy range.

B. Cross Sections

1. Total Loss Cross Sections for $X^1\Sigma_g^+$ and $c^3\Pi_u$ H_2 Molecules in Collision with H_2 Gas (σ_t, σ_t^*)

As discussed in Sec. IV, A, while analyzing the excited state population of the H_2 beam by beam attenuation techniques in an H_2 gas target (Method I), we also obtained the total loss cross section for the excited state, σ_t^*, and for the ground state σ_t. The results for σ_t^* and σ_t are given in Table III and in Fig. 18. The results using Method II to determine the cross sections (see Sec. IV, B) are also given. The errors given are our estimates of the absolute reliability of the data based on a ~ 60% confidence level (see Appendix I). McClure[72] has measured the ground state total loss cross section at 5 keV/nulceon by a very different technique. His result is in excellent agreement with the present results (see Fig. 18).

In the course of a measurement to determine the effect of

Table III. Total collisional loss cross sections for $X^1\Sigma_g^+$ H_2 (σ_t) and $c^3\Pi_u$ H_2 (σ_t^*) in H_2 gas. The assigned absolute uncertainties indicated are based on an estimated 60% confidence level (see Appendix I). (For E < 20 keV/nucleon the incident projectile was D_2^+.)

Energy (keV/nucleon)	σ_t (±10%) (10^{-16} cm^2/molecule) Particle counting (Method I)	σ_t (10^{-16} cm^2/molecule) Faraday cup (Method II)	σ_t^* (10^{-16} cm^2/molecule) Particle counting (Method I)	σ_t^* (10^{-16} cm^2/molecule) Faraday cup Method II)
1.0		1.70		
1.7		1.85		
3.0		2.10		
5.0		2.50		$13.3^{+2.6}_{-2.3}$
7.5		2.70		
8.7		2.80		$13.4^{+2.3}_{-2.4}$
11.2		3.10		14.0 ±2.5
12.2	3.25		$13.0^{+2.5}_{-2.3}$	
15.0	3.35	3.20	$12.3^{+2.5}_{-2.1}$	$11.7^{+2.4}_{-2.3}$
20.0	3.52		$13.5^{+2.2}_{-2.6}$	
22.5		3.10		$9.3^{+1.6}_{-1.5}$
22.5		(15.5 ±2.5)	(350 ±90)[a]	
25.0	3.50	3.18	$10.4^{+1.9}_{-1.8}$	
30.0	3.55	3.15	9.0 ±2.2	$8.2^{+1.8}_{-1.4}$
35.0	3.50		$8.1^{+1.8}_{-1.4}$	
42.0	3.50	3.15		$7.6^{+1.8}_{-1.6}$

[a] C_6H_6 target.

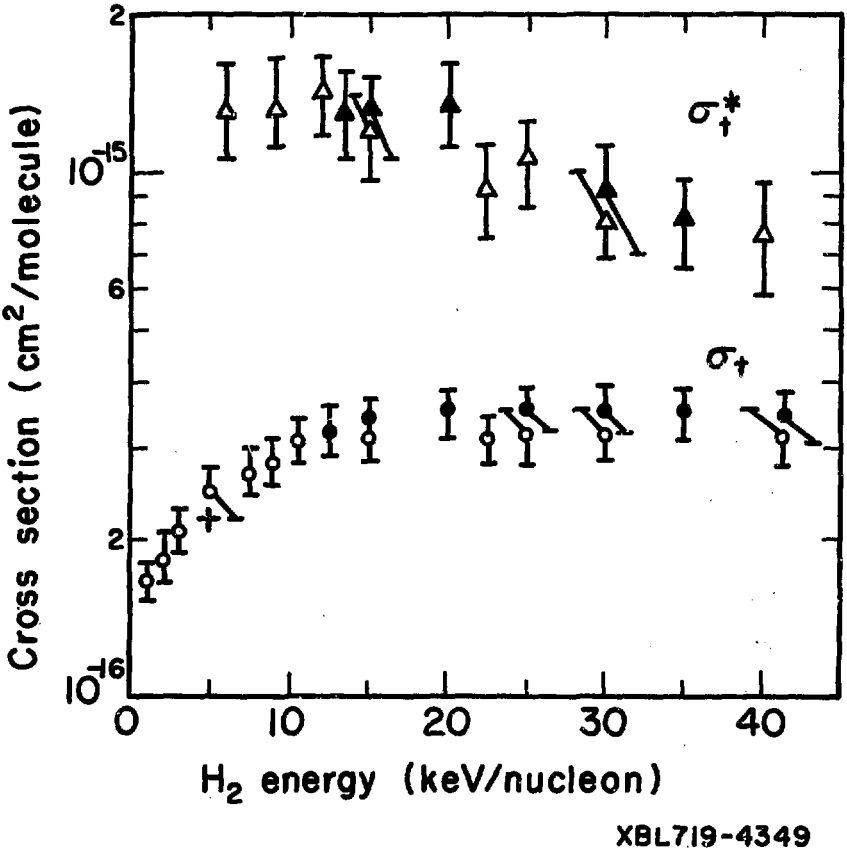

Fig. 18. Total loss cross sections for collisions of energetic $X^1\Sigma_g^+ H_2$, σ_{t^*}, and $c^3\Pi_u H_2$, σ_t^*, with H_2 gas. Present results: triangles, σ_t^*; circles, σ_t. Solid symbols, particle counting techniques (Method I); open symbols, Faraday cup technique (Method II). (For E < 20 keV/ nucleon the incident projectile was D_2^+.) The result of McClure (Ref. 72) at 5 keV/nucleon for σ_t is indicated by + (H_2^+ ion beam).

collisional excitation processes on the present results (see Appendix F), the loss cross sections at 22.5 keV/nucleon using a C_6H_6 target were obtained. These results are also listed in Table III. We are not aware of any theoretical calculations to compared with the present results.

2. Cross Sections for Ionization of $X^1\Sigma_g^+$ and $c^3\Pi_u$ H_2 Molecules in Collision with H_2 Gas ($\sigma_{H_2^+}$, $\sigma^*_{H_2^+}$)

One of the cross sections contributing to the total loss cross section, that for ionization ($H_2 \rightarrow H_2^+$) has also been determined for both the $c^3\Pi_u$ state, $\sigma^*_{H_2^+}$, and $X^1\Sigma_g^+$ state, $\sigma_{H_2^+}$, in H_2 gas. The results are presented in Table IV and in Fig. 19. For the ground state ionization cross section we see from Fig. 19 that the experimental results of McClure[72] agree quite well with the present results over the entire energy range investigated. Again, we know of no theoretical calculations to compare with these results. The errors listed are our estimate of the absolute reliability of the data based on a 60% confidence level (see Appendix I).

3. H Yield Cross Sections Due to the Breakup of H_2 Molecules in H_2 Gas (σ_H)

Defining the yield cross sections in terms of the various reaction cross sections listed in Sec. IV, A, p. 38, we have

$$\sigma_H \equiv \sigma_{HH^+} + 2\sigma_{2H}$$

$$\sigma_{H^+} \equiv \sigma_{HH^+} + 2\sigma_{2H^+}.$$

In terms of these definitions the total loss cross section may

Table IV. Collisional cross sections for the ionization of $X^1\Sigma_g^+$ H_2 ($\sigma_{H_2^+}$) and $c^3\Pi_u$ H_2 ($\sigma^*_{H_2^+}$) in H_2 gas. The assigned absolute uncertainties indicated are based on an estimated 60% confidence level (see Appendix I). (For E < 20 keV/nucleon the incident projectile was D_2^+.)

H_2	$\sigma_{H_2^+}$ (±10%) (10^{-16} cm^2/molecule)	$\sigma^*_{H_2^+}$ (10^{-16} cm^2/molecule)
Energy (keV/nucleon)	Particle counting (Method I)	Particle counting (Method I)
8.7	1.12	
11.2	1.26	
12.2	1.37	$6.2\ ^{+1.2}_{-1.1}$
15.0	1.48	$6.2\ ^{+1.5}_{-1.3}$
20.0	1.70	$6.5\ ^{+1.2}_{-1.5}$
25.0	2.0	$5.5\ ^{+0.9}_{-1.3}$
30.0	2.1	4.8 ±1.2
35.0	2.1	$5.1\ ^{+1.1}_{-1.2}$
42.0	2.0	

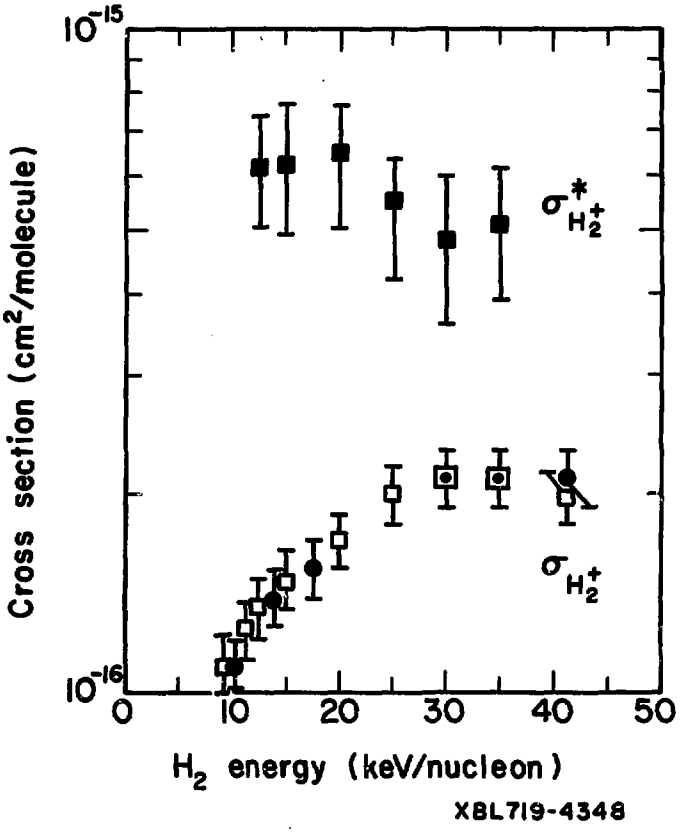

Fig. 19. Cross sections for the ionization of energetic $X^1\Sigma_g^+$ H_2, $\sigma_{H_2^+}$, and $c^3\Pi_u$ H_2, $\sigma^*_{H_2^+}$, in collision with H_2 gas. Present results: solid squares, $\sigma^*_{H_2^+}$; open squares, $\sigma_{H_2^+}$. (For E < 20 keV/nucleon the incident projectile was D_2^+.) The results of McClure (Ref. 72) for $\sigma_{H_2^+}$ are indicated by solid circles (H_2^+ ion beam).

be written as

$$\sigma_t = \sigma_{H_2^+} + \frac{1}{2}(\sigma_H + \sigma_{H^+}).$$

Using the results of McClure[72] for σ_{H^+} and the present measured values for $\sigma_{H_2^+}$ and σ_t, we can calculate σ_H, the cross section for the production of atomic hydrogen due to the breakup of $X^1\Sigma_g^+$ H_2 molecules in H_2 gas. Figure 20 shows the variation of these yield cross sections with H_2 particle energy. For comparison we also show the present measured cross sections for the $c^3\Pi_u$ state, σ_t^* and $\sigma_{H_2^+}^*$. Representative errors are indicated.

4. Electron Capture Cross Sections for H_2^+ Ions in Collision with Mg Vapor

Solov'ev et al.[31] have measured the total neutral yield cross section, the total proton yield cross section, and the electron capture cross section for H_2^+ ions in collision with Mg vapor. As a consequence of the present results (i.e., due to the determination that a large fraction of the H_2 molecules are in the $c^3\Pi_u$ state) a new interpretation must be given to Solov'ev's results for the total electron capture cross section $(\sigma_{10} + \sigma_{10}^*)$, where σ_{10} is the effective cross section for electron capture into the $X^1\Sigma_g^+$ state and σ_{10}^* is the effective cross section for electron capture into the $c^3\Pi_u$ state. Upon examination of the method used in Ref. 31, we conclude that Solov'ev's values for $(\sigma_{10} + \sigma_{10}^*)$ are at best upper bounds to the true value. For a discussion of this point we refer the reader to Appendix J.

We have not performed a study of the yields of particles

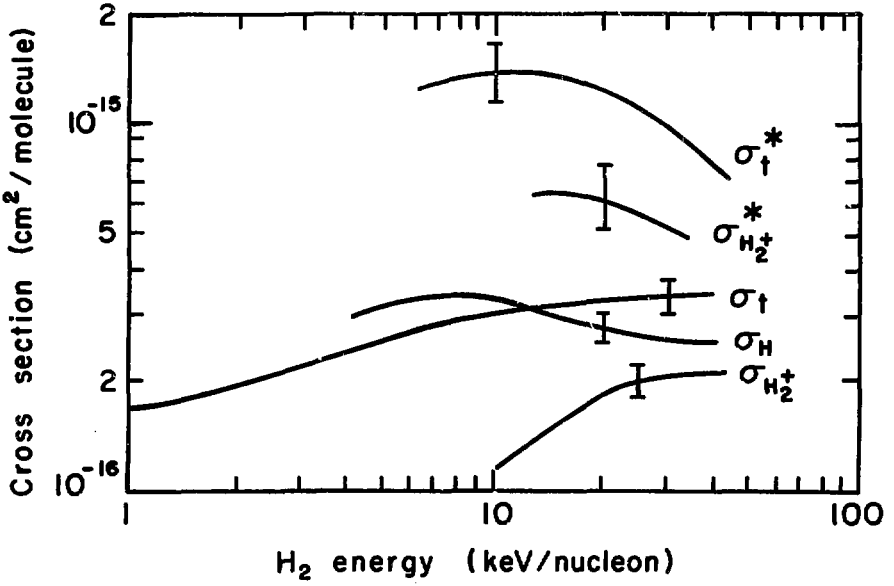

XBL 719-4332

Fig. 20. Collision product yield cross sections for energetic $X^1\Sigma_g^+$ H_2, (σ_H, σ_{H_2}+, σ_t) and $c^3\Pi_u$ H_2, ($\sigma^*_{H_2}$+, σ^*_t) in H_2 gas. Present experimental results: $\sigma^*_{H_2}$+, σ^*_t, σ_t, σ_{H_2}+. σ_H is a calculated cross section (see text). Representative errors are indicated.

from the breakup of H_2^+ ions in Mg vapor for thin target conditions. Therefore we do not present any measured cross sections for H_2^+ ions in collision with Mg vapor. However, it is easy to demonstrate that the fraction of the H_2 molecules emerging from the Mg oven that are in the $c^3\Pi_u$ state, f, for single collision conditions is given by the ratio $\sigma_{10}^*/(\sigma_{10} + \sigma_{10}^*)$. Using Solov'ev's values for $(\sigma_{10} + \sigma_{10}^*)$ and the present results for f, we are able to calculate upper bounds for the cross section σ_{10}^*. (We remind the reader that this cross section is for electron capture into the $c^3\Pi_u$ levels that have lifetimes greater than $\sim 10^{-7}$ sec). Figure 21 shows the variation with H_2^+ energy of upper bounds to the cross sections σ_{10}^* and $(\sigma_{10} + \sigma_{10}^*)$. The reliability of the values given in Ref. 31 is not known since uncertainties were not assigned to the data.

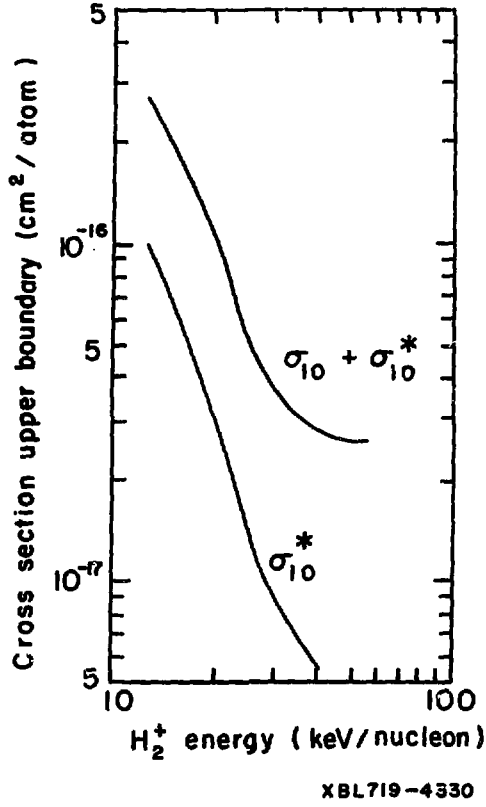

Fig. 21. Upper bounds for effective cross sections for electron capture by energetic H_2^+ into all states of H_2, $(\sigma_{10} + \sigma_{10}^*)$, and into the $c\,^3\Pi_u$ state of H_2, σ_{10}^*, in collision with Mg vapor. $(\sigma_{10} + \sigma_{10}^*)$, the results of Ref. 31; σ_{10}^*, calculated from $\sigma_{10}^* = (\sigma_{10} + \sigma_{10}^*) \times f$ (see text).

VI. APPLICATION OF RESULTS TO CONTROLLED FUSION

In this section we will use the excited state population results of the present experiment to calculate trapping efficiencies for H_2 molecular beams injected into plasma fusion devices. We will also calculate H atom beam trapping efficiencies and compare the two results in order to decide if a H_2 beam could be effectively used to overcome H atom beam asymmetric plasma trapping at intermediate densities, as first suggested by Hiskes (see Sec. I). No instabilities or plasma time dependent processes are considered in the present calculations.

Berkner and Riviere[73] have developed a computer code for H atom trapping. The code includes the collisional processes of ionization, de-excitation, and excitation in the plasma as well as radiative decay of the excited states. There exists no knowledge of the cross sections for the corresponding processes for H_2 molecules. Therefore, in order to get an idea of the H_2 trapping, we assume the H_2 molecule looks like an H atom (i.e., the $c^3\Pi_u$ H_2 state is considered to be the H(n = 2) state except it is taken to be long lived and cannot quench) and use atomic cross sections in the code to calculate H_2 trapping. We include the process of $c^3\Pi_u$ H_2 cascading and treat the highly excited states as hydrogen-like.

The trapping in the H_2 case results mainly in H_2^+ rather than in H^+ ions. The H_2^+ ion will subsequently dissociate and ionize due to collisions with the plasma. We will not consider the details of these processes here.

The model used for the calculation is as follows: The neutral beam is formed in a gas or metal vapor target after which it radiatively decays for 200 cm until it is injected into the plasma. The beam undergoes ionization, de-excitation, and excitation collisions with the ions and electrons of the plasma while still undergoing radiative decay. The calculation is performed by solving the set of coupled-differential equations which describes the population of each excited level in the beam. The parameters of the model used for the calculation are:

(1) The injected H atom beam (produced by charge exchange of H^+) has an excited state population distribution which is governed by the relation[74]

$$N_n = \frac{a}{n^3} \qquad \text{for } n > 1$$

where $N_n \equiv$ the fraction of the beam in th nth level,

$n \equiv$ the principal quantum number, and

$a \equiv$ a constant, characteristic of the target used.

For the present calculation we have used a = 1.0, which roughly corresponds to charge exchange of 15 keV H^+ ions in a thin Cd vapor target.[75] To adjust the result for other targets, all that is required is to multiply by the appropriate "a" value. (For a thin Mg vapor target a ~ 2 for charge exchange of 15 keV H^+.[75])

(2) The injected H_2 beam is produced from charge exchange of H_2^+ ions in a thin Mg vapor target. The initial excited state distribution is assumed to consist of only the ground state and

$c^3\Pi_u$ state. The population of the $c^3\Pi_u$ state is based on the present results.

(3) The cross sections used for the ground and excited states of H_2 are the same as those used for the ground state and n = 2 level of H.

(4) The plasma density distribution is assumed to be uniform over a distance of 10 cm.

(5) The Lorentz force $(e\vec{v} \times \vec{B})$in the trapping region is assumed to ionize all levels with $n \geq 11$.

(6) The excitation cross sections are taken from McCoyd and Milford[76] and the ionization cross sections are taken from Omidvar.[77]

(7) The cross sections used for all collisional processes (both H^+ and e^- impact) are electron cross sections except for ground state ionization by H^+.[78] For electron collisions the cross sections are evaluated at the electron velocity corresponding to the electron temperature. For proton collisions the cross sections are evaluated at the velocity of the incoming neutrals.

From the calculations we obtained the fraction of the beam that is ionized (and hopefully trapped) in the plasma. This trapping fraction has two contributions:

(1) direct collisional ionization of all levels, and

(2) cascade trapping of excited levels which are collisionally excited to n = 11 and then Lorentz ionized.

The calculations were performed for injection particle

energies of 5.0, 11.5, 15.0, 20.0, and 30.0 keV/nucleon. In the case of 5.0 keV/nucleon the value used for the fraction of the H_2 molecules in the $c^3\Pi_u$ state (43%) is obtained by extrapolating the measured values to 5 keV/nucleon (see Fig. 17).

For each injection energy we have calculated the trapping fractions for H atoms and H_2 molecular beams for plasma densities from 10^8 to 10^{14} cm^{-3} and for trapped electron energies of 1.0, 50.0, 200.0, and 1000 eV.

The results are summarized in Tables V through IX, each of which corresponds to a different injection energy. The trapped fractions are presented in three parts: (1) cascade ionization, (2) direct ionization, and (3) total fraction of the beam that is trapped by collisions with the plasma, i.e., (1) + (2).

The following comments are based on an examination of the results of the calculations (see Tables V through IX).

1. Trapping Fraction vs Electron Energy

The total trapping fraction of H or H_2 beams is relatively insensitive to changes in the electron temperature from 1.0 to 1000 eV. The H beam trapping changes by less than a factor of three over this electron energy range while the H_2 trapping fraction changes by less than a factor of two in almost all cases. Also, the trapping fraction is larger for electron energies of 50 and 200 eV than for 1.0 and 1000 eV.

2. Total Trapping Fraction vs Plasma Density

Figure 22 shows the results of the present calculations for the cascade and total trapping fractions of H atom and H_2 molecular

Table V. Collisional trapping fractions for 5.0 keV/nucleon H and H_2 beams. The $c^3\Pi_u$ fraction of the H_2 beam is 43% (extrapolated; see Fig. 17). The negative integers next to the numbers indicate the power of ten by which the numbers should be multiplied.

	Electron energy (eV) →	1				50				200				1000			
	Density (cm^{-3})	H		H_2		H		H_2		H		H_2		H		H_2	
Cascade	↓	1.57	-5	2.0	-22	1.05	-5	6.1	-23	9.3	-6	1.24	-22	8.4	-6	3.1	-23
Direct	10^8	5.38	-7	2.85	- 8	8.4	-7	9.2	- 7	8.0	-7	1.4	- 6	5.7	-7	4.53	- 7
Total		16.2	-6	0.028	- 6	11.3	-6	0.92	- 6	10.1	-6	1.4	- 6	8.97	-6	0.453	- 6
		1.43	-4	2.2	-17	9.9	-5	6.57	-18	8.76	-5	1.35	-17	7.96	-5	3.4	-18
	10^9	5.11	-6	2.85	- 7	8.2	-6	9.22	- 6	7.9	-6	1.43	- 5	5.6	-6	4.5	- 6
		14.3	-5	0.03	- 5	10.7	-5	0.92	- 5	9.5	-5	1.43	- 5	8.5	-5	0.45	- 5
		7.3	-4	3.68	-12	6.0	-4	1.04	-12	5.5	-4	2.23	-12	5.22	-4	5.2	-13
	10^{10}	3.52	-5	2.88	- 6	7.3	-5	9.22	- 5	7.0	-5	1.42	- 4	4.85	-5	4.5	- 5
		7.65	-4	0.029	- 4	6.73	-4	0.92	- 4	6.2	-4	1.42	- 4	5.70	-4	0.45	- 4
		1.24	-3	2.92	- 7	1.19	-3	1.46	- 7	1.16	-3	2.9	- 7	1.14	-3	7.7	- 8
	10^{11}	1.33	-4	3.2	- 5	5.68	-4	9.27	- 4	5.28	-4	1 43	- 3	3.24	-4	4.6	- 4
		1.37	-3	0.032	- 3	1.75	-3	0.927	- 3	1.68	-3	1.43	- 3	1.46	-3	0.46	- 3
		1.33	-3	4.57	- 4	1.33	-3	5.97	- 4	1.31	-3	9.43	- 4	1.3	-3	3.85	- 4
	10^{12}	6.04	-4	7.8	- 4	5.0	-3	1.0	- 2	4.52	-3	1.5	- 2	2.5	-3	5.2	- 3
		0.193	-2	0.124	- 2	0.63	-2	1.06	- 2	0.58	-2	1.59	- 2	0.38	-2	0.56	- 2
		1.34	-3	2.76	- 2	2.6	-3	4.5	- 2	2.18	-3	6.0	- 2	1.81	-3	3.4	- 2
	10^{13}	5.1	-3	2.8	- 2	4.93	-2	1.28	- 1	4.4	-2	1.59	- 1	2.41	-2	8.2	- 2
		0.064	-1	0.26	- 1	0.52	-1	1.73	- 1	0.46	-1	2.19	- 1	0.26	-1	1.16	- 1
				2.0	- 1	4.35	-2	2.02	- 1	3.25	-2	2.22	- 1	2.2	-2	1.96	- 1
	10^{14}			2.1	- 1	4.16	-1	5.18	- 1	3.84	-1	5.26	- 1	2.3	-1	4.13	- 1
				4.1	- 1	4.59	-1	7.2	- 1	4.16	-1	7.48	- 1	2.5	-1	6.09	- 1

Table VI. Collisional trapping fractions for 11.5 keV/nucleon H and H_2 beams. The $c^3\Pi_u$ fraction of the H_2 beam is 36% (see Fig. 17). The negative integers next to the numbers indicate the power of ten by which the numbers should be multiplied.

	Electron energy (eV) →	1				50				200				1000			
	Density (cm^{-3})	H		H_2		H		H_2		H		H_2		H		H_2	
Cascade	↓	9.7	-6	2.8	-23	6.2	-6	1.2	-23	5.33	-6	5.96	-24	4.74	-6	3.0	-24
Direct	10^8	4.3	-7	5.8	- 7	6.0	-7	1.4	- 6	5.83	-7	1.1	- 6	4.27	-7	8.34	- 7
Total		10.13	-6	0.58	- 6	6.80	-6	1.4	- 6	5.91	-6	1.1	- 6	5.16	-6	0.834	- 6
		9.2	-5	3.0	-18	5.97	-5	1.3	-18	5.19	-5	6.25	-19	4.6	-5	3.2	-19
	10^9	4.2	-6	5.8	- 6	6.0	-6	1.4	- 5	5.8	-6	1.1	- 5	4.2	-6	8.3	- 6
		9.62	-5	0.58	- 5	6.57	-5	1.4	- 5	5.77	-5	1.1	- 5	5.02	-5	0.83	- 5
		6.09	-4	4.6	-13	4.48	-4	1.93	-13	4.03	-4	8.85	-14	3.68	-4	4.4	-14
	10^{10}	3.62	-5	5.8	- 5	5.73	-5	1.4	- 4	5.54	-5	1.1	- 4	4.03	-5	8.3	- 5
		6.45	-4	0.58	- 4	5.05	-4	1.4	- 4	4.85	-4	1.1	- 4	4.08	-4	0.83	- 4
		1.49	-3	6.17	- 8	1.35	-3	3.73	- 8	1.28	-3	1.77	- 8	1.24	-3	9.0	- 9
	10^{11}	2.17	-4	5.82	- 4	4.88	-4	1.40	- 3	4.65	-4	1.1	- 3	3.26	-4	8.37	- 4
		1.70	-3	0.582	- 3	1.83	-3	1.40	- 3	1.74	-3	1.1	- 3	1.56	-3	0.837	- 3
		1.8	-3	2.87	- 4	1.79	-3	4.1	- 4	1.76	-3	2.52	- 4	1.75	-3	1.61	- 4
	10^{12}	1.35	-3	6.10	- 3	4.24	-3	1.4	- 2	3.94	-3	1.15	- 2	2.59	-3	8.64	- 3
		0.31	-2	0.64	- 2	0.60	-2	1.44	- 2	0.57	-2	1.15	- 2	0.434	-2	0.870	- 2
		1.82	-3	2.6	- 2	2.71	-3	4.6	- 2	2.4	-3	3.48	- 2	2.14	-3	2.77	- 2
	10^{13}	1.2	-2	7.1	- 2	4.13	-2	1.4	- 1	3.8	-2	1.24	- 1	2.46	-2	9.83	- 2
		0.138	-1	0.97	- 1	0.440	-1	1.86	- 1	0.40	-1	1.58	- 1	0.267	-1	1.26	- 1
		1.83	-3	1.32	- 1	3.55	-2	1.8	- 1	2.7	-2	1.59	- 1	1.83	-2	1.47	- 1
	10^{14}	1.13	-1	2.81	- 1	3.63	-1	4.8	- 1	3.4	-1	4.77	- 1	2.35	-1	4.01	- 1
		1.13	-1	4.13	- 1	3.98	-1	6.6	- 1	3.67	-1	6.36	- 1	2.53	-1	5.48	- 1

Table VII. Collisional trapping fractions for 15.0 keV/nucleon H and H_2 beams. The $c^3\Pi_u$ fraction of the H_2 beam is 32% (see Fig. 17). The negative integers next to the numbers indicate the power of ten by which the numbers should be multiplied.

	Electron energy (eV) →	1				50				200				1000			
	Density (cm^{-3})	H		H_2		H		H_2		H		H_2		H		H_2	
Cascade	↓	8.27	-6	1.3	-23	5.2	-6	5.2	-24	4.45	-6	2.4	-24	3.93	-6	1.23	-24
Direct	10^8	4.12	-7	6.1	- 7	5.5	-7	1.28	- 6	5.36	-7	1.0	- 6	3.97	-7	8.21	- 7
Total		8.68	-6	0.61	- 6	5.75	-6	1.28	- 6	4.98	-6	1.0	- 6	4.32	-6	0.821	- 6
		7.93	-5	1.34	-18	5.05	-5	5.4	-19	4.35	-5	2.5	-19	3.85	-5	1.28	-19
	10^9	4.06	-6	6.1	- 6	5.51	-6	1.28	- 5	5.34	-6	1.05	- 5	3.96	-6	8.2	- 6
		8.33	-5	0.61	- 5	5.60	-5	1.28	- 5	4.88	-5	1.05	- 5	4.24	-5	0.82	- 5
		5.61	-4	1.98	-13	3.99	-4	7.66	-14	3.54	-4	3.45	-14	3.2	-4	1.69	-14
	10^{10}	3.58	-5	6.1	- 5	5.30	-5	1.28	- 4	5.14	-5	1.05	- 4	3.8	-5	8.2	- 5
		5.96	-4	0.61	- 4	4.51	-4	1.28	- 4	4.05	-4	0.105	- 4	3.58	-4	0.82	- 4
		1.56	-3	2.95	- 8	1.37	-3	1.59	- 8	1.29	-3	7.3	- 9	1.24	-3	3.58	- 9
	10^{11}	2.27	-4	6.12	- 4	4.57	-4	1.28	- 3	4.40	-4	1.05	- 3	3.16	-4	8.22	- 4
		1.78	-3	0.612	- 3	1.82	-3	1.28	- 3	1.73	-3	1.05	- 3	1.55	-3	0.822	- 3
		1.99	-3	1.93	- 4	1.96	-3	2.53	- 4	1.92	-3	1.51	- 4	1.91	-3	9.33	- 5
	10^{12}	1.38	-3	6.28	- 3	3.91	-3	1.29	- 2	3.65	-3	1.07	- 2	2.47	-3	8.38	- 3
		0.337	-2	0.62	- 2	0.587	-2	1.31	- 2	0.557	-2	1.07	- 2	0.438	-2	0.838	- 2
		2.12	-3	2.1	- 2	2.88	-3	3.68	- 2	2.58	-3	2.76	- 2	2.35	-3	2.18	- 2
	10^{13}	1.22	-2	6.86	- 2	3.78	-2	1.25	- 1	3.50	-2	1.13	- 1	2.32	-2	9.06	- 2
		0.143	-1	0.89	- 1	0.406	-1	1.61	- 1	0.375	-1	1.40	- 1	0.255	-1	1.12	- 1
		4.90	-3	1.13	- 1	3.49	-2	1.61	- 1	2.68	-2	1.40	- 1	1.9	-2	1.28	- 1
	10^{14}	1.15	-1	2.71	- 1	3.39	-1	4.55	- 1	3.19	-1	4.53	- 1	2.24	-1	3.82	- 1
		1.20	-1	3.84	- 1	3.73	-1	6.16	- 1	3.26	-1	5.93	- 1	2.4	-1	5.10	- 1

Table VIII. Collisional trapping fractions for 20.0 keV/nucleon H and H_2 beams. The $c^3\Pi_u$ fraction of the H_2 beam is 28% (see Fig. 17). The negative integers next to the numbers indicate the power of ten by which the numbers should be multiplied.

	Electron energy (eV) →	1				50				200				1000			
	Density (cm^{-3})	H		H_2		H		H_2		H		H_2		H		H_2	
Cascade	↓	7.0	-6	5.0	-24	4.3	-6	2.0	-24	3.6	-6	8.8	-25	3.2	-6	4.4	-25
Direct	10^8	3.9	-7	5.87	- 7	5.0	-7	1.1	- 6	4.9	-7	9.4	-07	3.7	-7	7.6	- 7
Total		7.39	-6	0.587	- 6	4.80	-6	1.1	- 6	4.09	-6	0.94	- 6	3.57	-6	0.76	- 6
		6.75	-5	5.3	-19	4.2	-5	2.0	-19	3.6	-5	9.1	-20	3.14	-5	4.4	-20
	10^9	3.87	-6	5.87	- 6	5.0	-6	1.1	- 5	4.9	-6	9.5	- 6	3.7	-6	7.6	- 6
		7.13	-5	0.587	- 5	4.70	-5	1.1	- 5	4.09	-5	0.95	- 5	3.51	-5	0.76	- 5
		5.1	-4	7.6	-14	3.5	-4	2.7	-14	3.04	-4	1.2	-14	2.72	-4	5.7	-15
	10^{10}	3.5	-5	5.87	- 5	5.0	-5	1.1	- 4	4.7	-5	9.5	- 5	3.6	-5	7.6	- 5
		5.45	-4	0.587	- 4	4.00	-4	0.11	- 4	3.47	-4	0.95	- 4	3.08	-4	0.76	- 4
		1.6	-3	1.2	- 8	1.37	-3	5.9	- 9	1.28	-3	2.6	- 9	1.2	-3	1.23	- 9
	10^{11}	2.5	-4	5.87	- 4	4.37	-4	1.1	- 3	4.23	-4	9.5	-4	3.1	-4	7.60	- 4
		1.85	-3	0.587	- 3	1.80	-3	1.1	- 3	1.70	-3	0.95	-3	1.51	-3	0.76	- 3
		2.2	-3	1.2	- 4	2.19	-3	1.42	- 4	2.13	-3	8.12	-5	2.1	-3	4.8	- 5
	10^{12}	1.6	-3	5.96	- 3	3.78	-3	1.12	- 2	3.57	-3	9.55	-3	2.5	-3	7.65	- 3
		0.38	-2	0.608	- 2	0.587	-2	1.13	- 2	0.670	-2	0.963	-2	0.46	-2	0.769	- 2
		2.5	-3	1.65	- 2	3.18	-3	2.93	- 2	2.87	-3	2.16	-2	2.65	-3	1.69	- 2
	10^{13}	1.43	-2	6.26	- 2	3.65	-2	1.08	- 1	3.4	-2	9.82	-2	2.4	-2	8.0	- 2
		0.168	-1	0.791	- 1	0.396	-1	1.37	- 1	0.368	-1	0.120	-1	0.266	-1	0.969	- 1
		1.04	-2	1.05	- 1	3.78	-2	1.53	- 1	2.96	-2	1.32	-1	2.25	-2		- 1
	10^{14}	1.38	-1	2.76	- 1	3.30	-1	4.36	- 1	3.12	-1	4.35	-1	2.3	-1	3.71	- 1
		1.48	-1	3.81	- 1	3.67	-1	5.89	- 1	4.41	-1	5.67	-1	2.52	-1	4.91	- 1

Table IX. Collisional trapping fractions for 30.0 keV/nucleon H and H_2 beams. The $c^3\Pi_u$ fraction of the H_2 beams is 23% (see Fig. 17). The negative integers next to the numbers indicate the power of ten by which the numbers should be multiplied.

	Electron energy (eV) →	1				50				200				1000			
	Density (cm^{-3}) ↓	H		H_2		H		H_2		H		H_2		H		H_2	
Cascade		5.5	-5	1.3	-24	3.28	-6	4.6	-25	2.75	-6	2.0	-25	2.38	-6	9.4	-26
Direct	10^8	3.5	-7	4.4	- 7	4.35	-7	8.3	- 7	4.24	-7	7.1	- 7	3.2	-7	5.7	- 7
Total		5.85	-6	0.44	- 6	3.71	-6	0.83	- 6	3.17	-6	0.71	- 6	2 70	-6	0.57	- 6
		5.4	-5	1.3	-19	3.23	-5	4.8	-20	2.72	-5	2.0	-20	2.35	-5	9.6	-21
	10^9	3.5	-6	4.4	- 6	4.34	-6	8.3	- 6	4.23	-6	7.1	- 6	3.2	-6	5.7	- 6
		3.75	-5	0.44	- 5	3.66	-5	0.83	- 5	3.14	-5	0.71	- 5	2.67	-5	0.57	- 5
		4.3	-4	1.8	-14	2.81	-4	6.2	-15	2.42	-4	2.5	-15	2.12	-4	1.2	-15
	10^{10}	3.3	-5	4.4	- 5	4.27	-5	8.3	- 5	4.17	-5	7.1	- 5	3.17	-5	5.7	- 5
		3.63	-4	0.44	- 4	3.23	-4	0.83	- 4	2.83	-4	0.71	- 4	2.43	-4	0.57	- 4
		1.64	-3	3.3	- 9	1.32	-3	1.3	- 9	1.21	-3	5.6	-10	1.12	-3	2.5	-10
	10^{11}	2.52	-4	4.4	- 4	3.92	-4	8.3	- 4	3.81	-4	7.1	- 4	2.9	-4	5.7	- 4
		1.89	-3	.44	- 3	1.71	-3	0.83	- 3	1.59	-3	0.710	- 3	1.41	-3	0.57	- 3
		2.57	-3	5.2	- 5	2.5	-3	5.5	- 5	2.42	-3	2.92	- 5	2.37	-3	1.6	- 5
	10^{12}	1.65	-3	4.5	- 3	3.4	-3	8.3	- 3	3.24	-3	7.18	- 3	2.4	-3	5.76	- 3
		0.422	-2	0.455	- 2	0.59	-2	0.835	- 2	0.566	-2	0.721	- 2	0.477	-2	0.577	- 2
		2.96	-3	1.10	- 2	3.5	-3	1.98	- 2	3.19	-3	1.42	- 2	3.0	-3	1.07	- 2
	10^{13}	1.45	-2	4.72	- 2	3.25	-2	8.22	- 2	3.05	-2	7.45	- 2	2.25	-2	6.02	- 2
		0.174	-1	.582	- 1	0.360	-1	0.841	- 1	0.346	-1	0.887	- 1	0.255	-1	0.707	- 1
		1.60	-2	1.02	- 1	4.11	-2	1.46	- 1	3.25	-2	1.26	- 1	2.59	-2	1.16	- 1
	10^{14}	1.43	-1	2.63	- 1	3.02	-1	4.00	- 1	2.88	-1	4.0	- 1	2.19	-1	3.43	- 1
		1.59	-1	3.65	- 1	3.43	-1	5.46	- 1	3.20	-1	5.26	- 1	2.44	-1	4.59	- 1

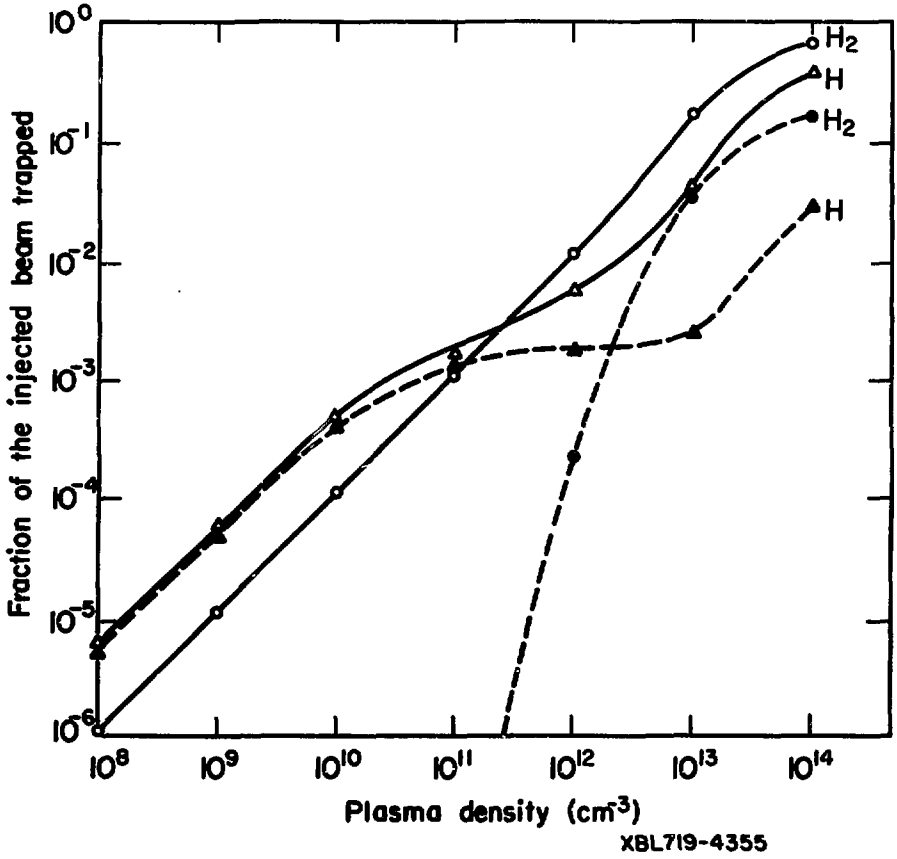

Fig. 22. Fraction of the injected beam that is collisionally trapped versus plasma density for H and H_2 beams. The injection energy is 11.5 keV/nucleon and the electron temperature is 200 eV. The fraction of the H_2 beam in the $c^3\Pi_u$ state is 36%. Solid curves, total trapping; dashed curves, inverted cascade trapping. Triangles, H beam; circles, H_2 beam.

beams with changes in plasma density. The solid curves show the total trapping and the dashed curves show the cascade contribution (cascade ionization + direct ionization = total trapping). The injection energy in Fig. 22 is 11.5 keV/nucleon, the electron temperature is 200 eV, and the $c^3\Pi_u$ fraction in the H_2 beam is 36%. We note the following points from Fig. 22:

(a) At low densities H atom trapping is roughly 6 times greater than H_2 trapping. At about 2×10^{11} cm^{-3}, H_2 trapping becomes larger than H trapping and the cascade contribution to ionization of the H beam has reached a plateau. (This is due to depletion of the excited state atoms from the beam (see Sec. I).)

(b) At high densities, direct ionization of the H beam is the only significant process, whereas almost all of the trapping occurs via an inverted cascade for low densities.

(c) At high densities the cascade ionization of the $c^3\Pi_u$ state contributes about 25% to the total trapping of the H_2 beam.

3. Trapping vs Distance into the Plasma

Fig. 23 illustrates the total collisional trapping for H and H_2 versus distance into the plasma and as a function of plasma density. To illustrate the asymmetry of H trapping at intermediate densities, we have normalized the results of Fig. 23 to the trapping fraction achieved at a distance of 10 cm (the path length through the plasma).

These normalized results are presented in Fig. 24 for densities from 10^{10} to 10^{13} cm^{-3} and for an injection energy of 11.5 keV/nucleon and electron temperature of 200 eV. In this

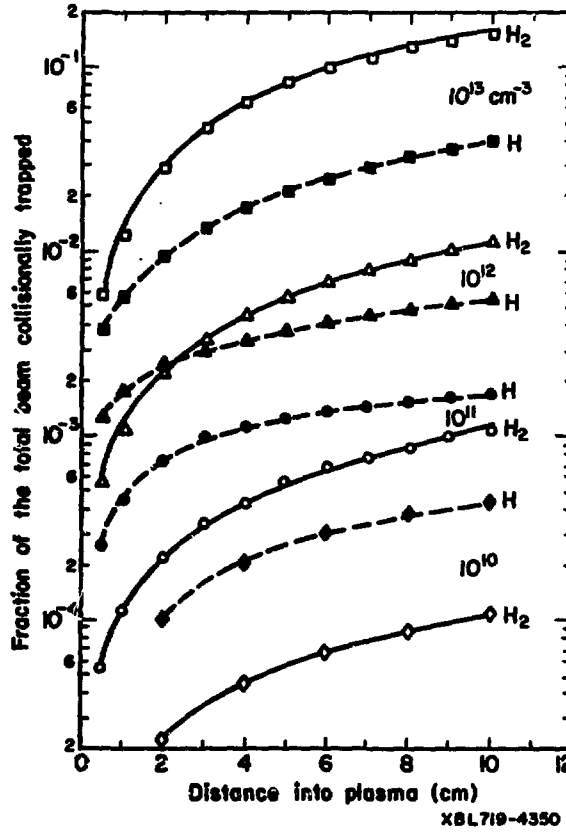

Fig. 23. The trapped fraction of the total injected beam versus distance into the plasma. Open symbols (solid lines), H_2 beam; solid symbols (dashed lines), H beam. Diamonds, 10^{10} cm^{-3}; circles, 10^{11} cm^{-3}; triangles, 10^{12} cm^{-3}; squares, 10^{13} cm^{-3}.

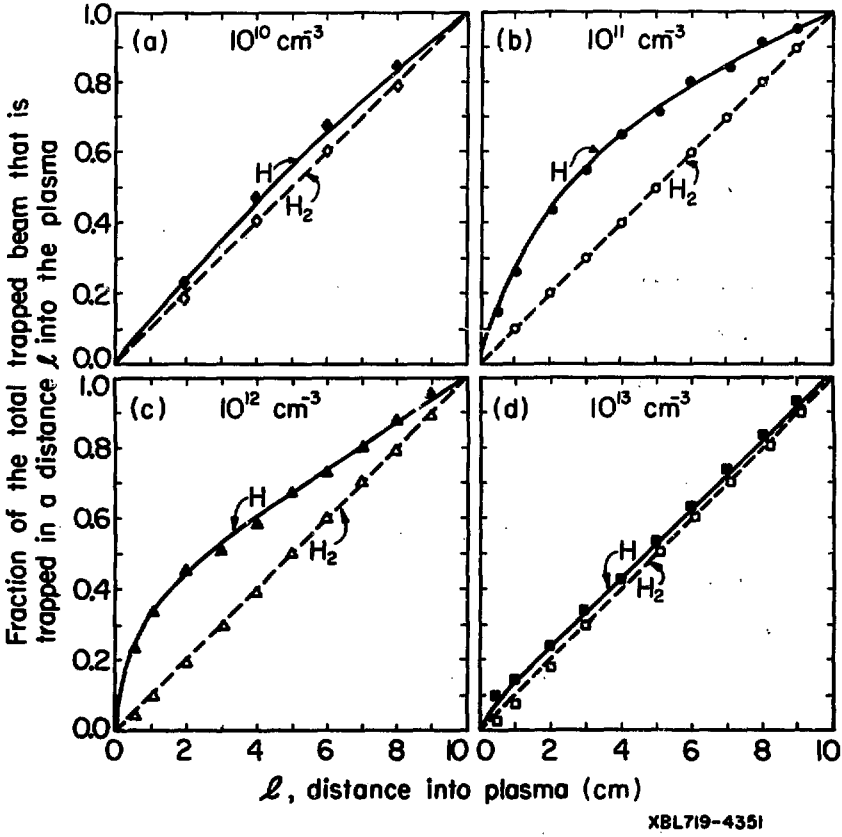

Fig. 24. The fraction of the total trapped beam that is trapped in a distance ℓ into the plasma versus distance ℓ into the plasma. Solid symbols (solid lines), H beam; open symbols (dashed lines), H_2 beam. (a), plasma density of 10^{10} cm^{-3}; (b), 10^{11} cm^{-3}; (c), 10^{12} cm^{-3}; (d), 10^{13} cm^{-3}.

normalized presentation, a 45-deg line indicates uniform trapping over the plasma length. From Fig. 24 we see this is the case for H_2 injection at all densities. For H injection there is significant deviation from uniform trapping at densities of 10^{11} and 10^{12} cm^{-3}. This is due to the cascade depleting the excited states of the beam within the first few centimeters into the plasma. At high densities, i.e., 10^{13} cm^{-3}, the cascade is relatively unimportant compared with direct ionization and the H trapping is again uniform.

From these results we conclude that the total trapping is roughly equal for H and H_2 beams in the density range where the H trapping is asymmetric; the H_2 trapping is greater above this density range, and the H_2 trapping is always uniform. Hence, $H_2(c^3\Pi_u)$ beams are more desirable for neutral injection at densities greater than about 10^{11} cm^{-3} for injection energies from 5.0 keV/nucleon to 30 keV/nucleon. Also, this result is insensitive to changes in electron temperature from 1.0 to 1000 eV.

In the present section we have considered the case of pure H and H_2 beams with the H_2 beam consisting of only two states. More realistically, the H_2 beam will contain significant amounts of atomic hydrogen, as demonstrated in the present yield measurements (see Figs. 12 and 13). This H atom component will increase the total trapping of the H_2 beam. The effect the H atom component has on the uniformity of the trapping depends on the excited state population distribution of these atoms. Solov'ev[31] has measured "a" values (see p. 76) for excited H atoms from the

dissociation of H_2^+ ions in Mg vapor. His results for "a" values from H_2^+ are a factor of about 10 lower than "a" values from H^+ at equal velocities. Therefore, the excited H atoms from H_2 dissociation should not cause asymmetric trapping for densities greater than 10^{10} cm^{-3}.

Furthermore, there exists in the H_2 beam a fraction of highly excited molecules (Rydberg states). Solov'ev[75] has shown in this case that "a" values for H_2 excited molecules are a factor of 10 lower than "a" values for excited H atoms from H^+ and we therefore conclude that the contribution from highly excited molecules will be inconsequential. (Rivere[30] has also found lower "a" values for H_2 excited molecules than for H atoms from H^+, but his values are lower by factors of two rather than 10).

Finally, a relevant question which cannot be presently answered is whether intense H_2^+ beams can be economically produced and converted to H_2 molecules to warrant their use as a more efficient trapping mechanism at intermediate densities. Since the conversion of H_2^+ ions to H_2 and $H_2(c^3\Pi_u)$ molecules is a rapidly decreasing function of energy (as has been shown in the present work, see Fig. 17), we conjecture that the above described trapping process will most likely be desirable only at low energies (i.e., less than ~ 20 keV/nucleon).

VII. SUMMARY AND CONCLUSIONS

The cross sections for the total loss and the ionization of $X^1\Sigma_g^+$ H_2 $\left[1 \leq E \text{ (keV/nucleon)} \leq 42\right]$ and $c^3\Pi_u$ H_2 molecules $\left[5 \leq E \text{ (keV/nucleon)} \leq 42\right]$ in collisions with H_2 gas have been measured. The result of McClure at 5 keV/nucleon for the total loss cross section of the $X^1\Sigma_g^+$ state is in excellent agreement with the present measurements. The data of McClure for the ionization cross section of the $X^1\Sigma_g^+$ state is also in excellent agreement. We have not found any data on collisional cross sections for the $c^3\Pi_u$ state to compare with present results.

The four cross sections measured in the present work ($\sigma_{H_2^+}$, $\sigma^*_{H_2^+}$, σ_t, σ^*_t) are slowly varying over the energy range of the measurements. The excited state cross sections range from two to five times larger than the ground state cross sections. The contribution of the ionization cross section to the total loss cross section, both for the ground and excited states, increases from ~ 30% to ~ 60% as the energy increases over the present range.

The data agreed, within experimental uncertainties, using H_2^+, D_2^+ and HD^+ ions of equal velocity. This suggests that for the $c^3\Pi_u$ molecular state strong coupling between the nuclear rotation and the electronic motion does not exist.

We have measured the $c^3\Pi_u$ H_2 yields due to the breakup of H_2^+ ions in Mg vapor. We find that 6.5% of the incident H_2^+ beam can be converted to $c^3\Pi_u$ H_2 molecules at 11.2 keV/nucleon using an optimized Mg vapor target thickness ~ 7×10^{14} atoms/cm^2. This yield is a steeply decreasing function of energy (decreasing

to 1.8% at 20 keV/nucleon) due to the rapid decrease in the total production of H_2 molecules rather than to a significant change in the fraction of the H_2 molecules in the $c^3\Pi_u$ state. This quantity (the fraction of the H_2 molecules in the $c^3\Pi_u$ state) varies slowly over the present energy range from 36% at 11.2 keV/nucleon to 23% at 35.0 keV/nucleon for Mg vapor thicknesses less than $\sim 1 \times 10^{14}$ atoms/cm^2. We have found no significant $c^3\Pi_u$ yields using H_2 or N_2 targets. The measurements show insignificant yields for Mg vapor target thicknesses greater than $\sim 1 \times 10^{16}$ atoms/cm^2. These results are consistant with estimates by Hiskes.

As shown in the present work, measurements using H_2 beams that have been prepared from H_2^+ collisions in Mg vapor are sensitive to the vapor pressure, i.e., the $c^3\Pi_u$ fraction in the beam. Correspondingly, measurements must be described in terms of a two-state beam. This has been demonstrated in a need to reinterpret the previous measurements of Solov'ev et al.

We expect that H_2 beams, prepared by passage of H_2^+ ions through other low ionization potential vapors, such as Li, Cs, Na, and K, would contain large fractions of $c^3\Pi_u$ H_2 molecules.

The presence of $c^3\Pi_u$ H_2 molecules from the dissociation of H_3^+ ions in Mg vapor has not been observed. Also, no H_2^- ions were observed from the passage of H_2^+ ions through Mg vapor. This observation has allowed us to place an upper bound of 10^{-21} cm^2/atom on the cross section for double electron capture into

H_2^- states with lifetimes longer than $\sim 10^{-7}$ sec by 7- to 20-keV/nucleon H_2^+ ions in collision with Mg vapor.

Using the excited state population results of the present experiment, we have calculated trapping efficiencies for H_2 molecular beams injected into a typical controlled fusion device. We have also calculated H atom trapping. From these calculations asymmetric plasma trapping at intermediate densities in a typical H atom beam neutral injection experiment is analytically demonstrated. Also, for equally intense neutral beams (i.e., projectiles/sec), the total trapping of the molecular beam (containing $c^3\Pi_u$ H_2 molecules) is shown to be from two to five times larger than the total trapping of a H atom beam for plasma densities greater than 10^{11} cm^{-3}, with no significant asymmetric trapping occurring. The total trapping for both H and H_2 beams is shown to be insensitive to changes in the electron temperature of the plasma from 1.0 to 1000 eV. From these calculations we conclude that an H_2 beam, containing $c^3\Pi_u$ excited molecules, is desirable for neutral injection into present day fusion devices at plasma densities greater than $\sim 10^{11}$ cm^{-3} and for injection energies less than $\sim$ 20 keV/nucleon.

In conclusion, we mention a few topics for future experimental investigation:

(1) The present work demonstrates the need for a detailed investigation of the changes in the collisional properties of energetic beams due to changes in source conditions. A study of

the changes in the vibrational population distribution with source conditions would be of interest in attempting to interpret data.

(2) The determination of the predissociation lifetime of the $c^3\Pi_u$ H_2 state is of interest in order to understand experimental measurements involving this state.

(3) Hiskes has conjectured possible factors of two changes in the results, using other low ionization potential neutralizers. Therefore it might prove worthwhile to repeat the present experiment using other metal vapors, such as Cs and Na.

(4) Since such meager information exists on the H_2^- negative ion, we suggest a study of H^- yields at low energies ($E < 5$ keV/nucleon) from H_2^+ breakup in Mg vapor. From measurements of this type cross sections for the formation of H_2^- ions with lifetimes less than $\sim 10^{-7}$ sec could be obtained.

(5) There are a number of cross sections needed in order to perform collision calculations in a plasma. Those for which little information is available are: (a) cross section for the ionization of excited H by proton impact at energies less than $\sim$ 100 keV, and (b) cross sections for dissociation of H_2^+ and H_2 into excited states of H by H^+ and e^- impact.

ACKNOWLEDGEMENTS

I am indebted to Dr. Robert V. Pyle for his continuous interest and active supervision during the course of this work. My sincere thanks to Dr. Klaus H. Berkner for his guidance and encouragement and for his help in solving many of the problems encountered during the course of this work. I am grateful to Dr. John R. Hiskes for suggesting this problem and for many useful and stimulating theoretical discussions. Also: John W. Stearns for his skillful experimental assistance; Vincent J. Honey for maintaining the electronic equipment; and Margaret R. Thomas for her patience and aptitude in typing this manuscript.

I would like to acknowledge with extra special thanks my wife Janet and two-year-old son Brian for their important part in the overall effort.

This work was performed under the auspices of the U. S. Atomic Energy Commission and, in part, under the tenure of a Nuclear Science and Engineering Fellowship awarded by the U. S. AEC.

APPENDICES

A. Motivation for Using the Attenuation Rather Than the Electric-Gap or Optical Technique in the Present Experiment

Since the binding energy of the ground state of H_2^+ and the $c^3\Pi_u$ state of H_2 is ~ 2.7 eV, we may apply the calculations of Hiskes[79] for electric field ionization of the ground state of the H_2^+ ion in order to get a feeling for the feasibility of using the electric-gap technique for the $c^3\Pi_u$ state of H_2. We conclude that it would require on the order of 10^8 V/cm to ionize all vibrational levels of the $c^3\Pi_u$ state in 10^{-8} sec. Experiments in this laboratory, using the electric-gap field ionization technique,[63] employing regular application of 3×10^5 V/cm, have yielded enough experience to conclude that electric fields greater than 3×10^5 V/cm prove experimentally difficult and unfeasible to work with.

The use of optical techniques to study populations, absolute production cross sections, and quenching cross sections requires a knowledge of the overall absolute optical efficiency of the photon detector and its associated electronics. Systematic errors associated with calibration procedures usually range from ±20 to ±50%. Also, calculations by Freis and Hiskes[35] have shown that to reduce the radiative lifetime of the first four vibrational levels of $c^3\Pi_u$ state to less than 10^{-6} sec by the application of a static electric field (the optical approach used in metastable H(2s) experiments) would require an electric field of 10^6 V/cm. Even with the application of such an experimentally difficult

field, a significant correction for insufficient quenching would have to be made, based on an assumed vibrational population distribution. Optical techniques could perhaps be used if one employed a resonant cavity and applied an electric field of enough intensity and of the proper frequency to induce transitions of the $c^3\Pi_u$ state to its neighboring $a^3\Sigma_g^+$ state which radiatively decays to the $b^3\Sigma_u^+$ state in $\sim 10^{-8}$ sec.

But, based on predictions by Hiskes[32] that charge-transfer collisions of H_2^+ ions with alkali or alkaline-earth targets are expected to lead to relatively large populations (up to 50%) of the $c^3\Pi_u$ state, the beam-attenuation method was chosen, since, if large fractional yields do exist, it offers a significantly more direct approach to the determination of the quantities of interest.

B. A Survey of the Recent Theoretical Efforts on Electron Capture into, and Loss from, the n = 2 Excited State of H and He

In this appendix we relate the recent advances in excited state theoretical studies of the n = 2 state of H and He. The main objective of this discussion is to indicate to the reader the present theoretical efforts in the field. We choose here to refer only to the n = 2 excited state of H and He since the present work deals with the n = 2 equivalent state of H_2 (no direct calculations on the collision properties of this state exist).

For a detailed and comprehensive study of this topic, the

reader is referred to one of the standard general references.[80-82]

Since the collision problem cannot be solved exactly, a number of approximations exist. The most often used approximations for obtaining information about excited state inelastic collisions are (1) classical and semi-classical impulse approximation and (2) Born approximation.

Classical and semi-classical methods have received considerable attention since 1960 due to the work of Gryzinski.[83,84] Recently, Bates and Kingston[85] have assessed the worth of classical calculations by comparing calculated and measured cross sections. We refer the reader to Ref. 85 for a list of references on this topic. As noted in Ref. 85, in order for the classical or semi-classical impulse approximation to be valid, the relative velocity of the colliding particles must be larger than the velocity of the active orbital electron. In both methods the incident particle is described by a classical trajectory. The difference between the methods lies in the manner of describing the active electron's part in the collision, i.e., by classical or quantum mechanics.

The Born approximation is a completely quantum mechanical approach which requires the interaction between the incident particle and the target to be small so that the incident particle can be described as a plane wave which is only slightly diffracted by the target. This formalism has been used extensively to obtain inelastic collision cross sections.

There are a large number of other approximations less frequently used for excited state calculations, such as the Oppenheimer-Brinkman-Kramers approximation (OBK), the distorted wave approximation, and the quantal and classical coupled-state approximations. Again, we refer the reader to the literature for a discussion of these methods.[80-82]

Below in Table X we list some of the recent theoretical calculations on H and He in the n = 2 level in collisions with heavy particles. We have been able to find calculations for the formation and loss of H(2s,2p), but only for the loss of $He(2^3S)$. Although there exists work on symmetrical resonance exchange of $He(2^3S)$, we are not aware of any calculations on electron capture into the $He(2^3S)$ state by He^+ ions in collisions with gases. (Most references cited also contain information on excited states in addition to n = 2.)

A comparison of these theoretical calculations with experimental results, in general, shows rather good agreement.

C. Pertinent Molecular Electronic Transitions

Independent of external influence, electronic transitions in molecules can be classified into two general categories: spontaneous radiative transitions and transitions induced by the coupling of different momenta. The $c^3\Pi_u$ H_2 molecule should follow Hund's b coupling[94] quite closely. Hund's coupling cases differ according to the strength of the interaction between different momenta of the molecule. The important features of case b are a strong coupling of the electronic orbital angular momentum

Table X. Recent theoretical calculations on electron loss and electron capture in collisions involving H and He in the n = 2 level

Particle	Approximation	Energy (keV)	Reaction	Reference
		Electron Loss		
H	Born	1-1000	$H(2s,2p) + H(1s) \rightarrow \begin{cases} H^+ + H(1s) + e \\ H^+ + H(n) + e \\ H^+ + H^+ + 2e \end{cases}$	Omidvar and Kyle (Ref. 86)
H	Born	20-150	$H(2s) + \begin{Bmatrix} H \\ Na \\ Li \end{Bmatrix} \rightarrow H^+ + \cdots$	Lodge (Ref. 87)
H	Born	10-30	$H(2s) + \begin{Bmatrix} H(1s) \\ He(1s^2) \end{Bmatrix} \rightarrow H^+ + \cdots$	Bell and Kingston (Ref. 88)
H	Classical	1-500	$H(2s) + \begin{Bmatrix} He \\ Ar \\ N_2 \end{Bmatrix} \rightarrow H^+ + \cdots$	Bates and Walker (Ref. 89)
He	Classical	10-1000	$He(2s) + \begin{Bmatrix} Kr, He \\ Ar, He \\ N_2, H_2 \end{Bmatrix} \rightarrow He^+ + \cdots$	Bates et al. (Ref. 90)
		Electron Capture		
H	OBK	5-140	$H^+ + \begin{Bmatrix} \text{ground} \\ \text{state} \\ \text{atoms} \end{Bmatrix} \rightarrow H(2s) + \cdots$	Hiskes (Ref. 91)
H	Impact	1-1000	$H^+ + He(1s^2) \rightarrow H(2s) + \cdots$	Sin Fai Lam (Ref. 92)
H	Coupled-state	5-100	$H^+ + H(1s) \rightarrow H(2s,2p) + H^+$	Wilets and Gallaher (Ref. 93)

to the internuclear axis and the lack of strong interaction between the electronic spin angular momentum and the electronic orbital angular momentum. Figure 25 shows the coupling of the momenta of a diatomic molecule in case b. The notation is as follows:

- A the electronic orbital angular momentum in the direction of the internuclear axis
- O the rotational angular momentum
- S electron spin
- I nuclear spin
- N total orbital angular momentum
- J total angular momentum exclusive of nuclear spin
- F total angular momentum of molecule.

1. Spontaneous Radiative Transitions

From the quantum theory of radiation, we know that the probability per unit time for a particle to undergo a spontaneous transition from state n to state m is proportional to the matrix element:[95]

$$R_{nm} = \int \psi_n^* \sum_{\ell} e^{i\vec{k}\cdot\vec{r}_\ell} \frac{\partial}{\partial x_\ell} \psi_m \, d\tau$$

where ψ_n^* is the complex conjugate of the wave function of state n,

ψ_m is the wave function of state m,

$\vec{k}$ is the propagation vector of the emitted photon,

$\vec{r}_\ell$ is the position of the ℓth electron,

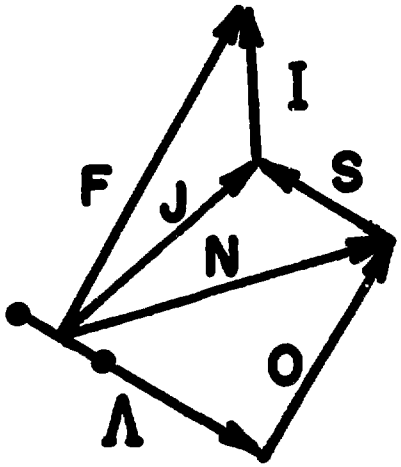

XBL719-4328

Fig. 25. Angular momenta in case b coupling for a diatomic molecule (from Ref. 41). The symbols used in the figure are described in the text.

x is the polarization direction of the ℓth electron,

τ is the configuration space variable.

Assuming for a moment that the important electron distance from the nucleus is that of the excited electron, we may write

$$R_{nm} = \int \psi_n^* \, e^{i\vec{k}\cdot\vec{r}} \frac{\partial}{\partial x} \psi_m \, d\tau.$$

Expanding the exponential, we have

$$R_{nm} = \int \psi_n^* \left[1 + i(\vec{k}\cdot\vec{r}) - \left(\frac{\vec{k}\cdot\vec{r}}{2}\right)^2 + \cdots \right] \frac{\partial}{\partial x} \psi_m \, d\tau.$$

The first term is the electric dipole contribution, the second term is the sum of the magnetic dipole and the electric quadrupole contributions, and the higher order terms are somewhat analogous to higher order multipole radiation.[95] Calculations show that magnetic dipole transition probabilities are only 10^{-5} and quadrupole transition probabilities only 10^{-8} of dipole transition probabilities.[96] Therefore the higher-moment terms only take on importance if

$$\int \psi_n^* \frac{\partial}{\partial x} \psi_m \, d\tau = 0.$$

In the case of the $c^3\Pi_u$ state of H_2 it can be shown (see selection rules below) that this integral vanishes except for the transition $c^3\Pi_u - a^3\Sigma_g^+$ (see Fig. 2). Due to the proximity of these two states, which causes a destructive interference of $\psi_{c^3\Pi_u}$ and

$\psi_{a^3\Sigma_g^+}$, the value of the integral is small and the corresponding transition probability is much smaller than usual electric dipole transition probabilities.[35]

Listed below are the electric dipole, magnetic dipole, and electric quadrupole selection rules for diatomic homonuclear molecules.

	Electric dipole	Magnetic dipole	Electric quadrupole
1)	$\Delta J = 0, \pm 1$	$\Delta J = 0, \pm 1$	$\Delta J = 0, \pm 1, \pm 2$
	$(0 \not\leftrightarrow 0)$	$(0 \not\leftrightarrow 0)$	$(0 \not\leftrightarrow 0,\ 0 \not\leftrightarrow 1,\ \frac{1}{2} \not\leftrightarrow \frac{1}{2})$
2)	$- \longleftrightarrow +$	$- \not\leftrightarrow +$	$- \not\leftrightarrow +$
3)	$s \not\leftrightarrow a$	$s \not\leftrightarrow a$	$s \not\leftrightarrow a$
4)	$g \longleftrightarrow u$	$g \not\leftrightarrow u$	$g \not\leftrightarrow u$
5)	$\Delta S = 0$	$\Delta S = 0$	$\Delta S = 0$
6)	$\Delta \Lambda = 0, \pm 1$	$\Delta \Lambda = 0, \pm 1$	$\Delta \Lambda = 0, \pm 1, \pm 2$
7)	$\Delta I = 0$	$\Delta I = 0$	$\Delta I = 0$

where +, - refer to the parity of the total eigenfunction of the molecule with respect to reflection through the origin,

s, a refer to the symmetry based on the exchange of nuclei,

g, u refer to the parity of the electronic wave function upon reflection through the origin.

2. Transition Induced by Momenta Coupling--Predissociation

Chiu[47] has shown that radiationless perturbations between the $c^3\Pi_u$ and $b^3\Sigma_u^+$ states of H_2 are the major mechanism for the decay of the metastable $c^3\Pi_u$ state, i.e., allowed predissociation

induced by the interaction of rotational and electronic momenta. Indeed, Herzberg[49] has experimentally verified that predissociation takes place in the case of the $c^3\Pi_u$ state. Predissociation is the process whereby a bound state interacts with a level of the same energy of the continuum of a repulsive state, thus causing the radiationless decomposition of the bound state. Physically it can be thought of as the states mixing together due to their proximity and each state assuming properties of the other. The fact that the states must be spatially close together is a consequence of the Franck-Condon principle, although it can also be shown to be true by the use of wave mechanics. Chiu also concluded that spin-spin interaction is probably much larger than spin-orbit interaction between these states but still much smaller than allowed predissociation.

It is a well-known fact that based on perturbation theory the effect one state has on another, i.e., the amount of interaction between two states, is dependent on the amount of overlapping of the eigenfunction of the states.

Fig. 26 shows in detail the relevant portion of Fig. 2. The $b^3\Sigma_u^+$ curve is based on the theoretical calculations of Kolos and Wolniewicz.[97] The $c^3\Pi_u$ state is based on calculations of Herzberg.[49] The eigenfunctions of the $c^3\Pi_u$ state overlap those of the $b^3\Sigma_u^+$ state such that the interaction integral

$$\int \Psi_{b^3\Sigma_u^+} M \Psi_{c^3\Pi_u} \, d\tau$$

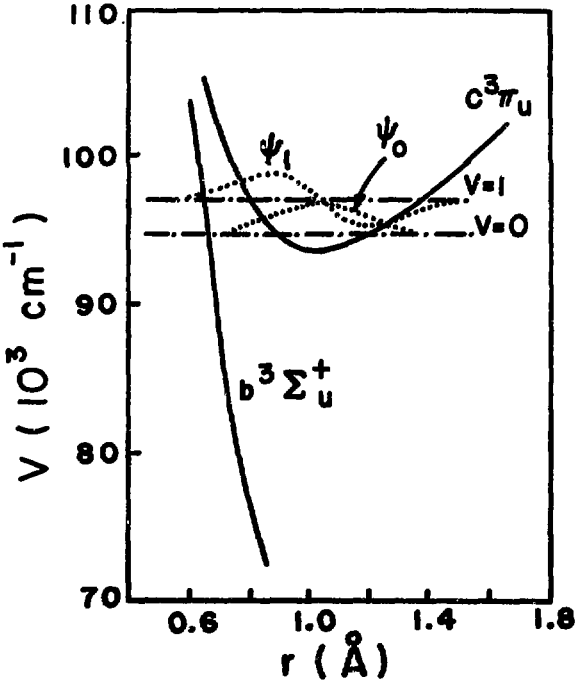

XBL719-4329

Fig. 26. The potential nuclear separation curves of the $c^3\Pi_u$ and $b^3\Sigma_u^+$ states of H_2. The $b^3\Sigma_u^+$ curve is based on the theoretical calculations of Kolos and Wolniewicz (Ref. 97). The $c^3\Pi_u$ curve is a Morse function with the correct dissociation energy and equilibrium internuclear distance. The first two vibrational levels of the $c^3\Pi_u$ state are indicated by dot-dash lines; the corresponding vibrational wave functions, shown by dotted lines, are approximated by harmonic oscillator functions (from Ref. 49).

(where M ≡ the predissociation operator) is nonvanishing.

For reference, the selection rulse for allowed predissociation for Hund's case b coupling are listed below.

1) $\Delta J = 0$

2) $- \not\leftrightarrow +$

3) $s \not\leftrightarrow a$

4) $g \not\leftrightarrow u$

5) $\Delta S = 0$

6) $\Delta \Lambda = 0, \pm 1$.

Examination of these selection rules shows that the $c^3\Pi_u$ state is capable of predissociation to the $b^3\Sigma_u^+$ state.

D. The Population of the Excited States of H_2 in the Present Experiment

The time of flight of the H_2 molecules in the present experiment ranged from 0.286 to 0.527 x 10^{-6} sec. Therefore, based on the discussion in Sec. II, B, we conclude that, while in flight, decay of all excited states, except the hydrogen-like states with $n \gtrsim 8$, the $F^1\Sigma_g^+$ state, and the $c^3\Pi_u$ state, has taken place. First, we consider the population of the $F^1\Sigma_g^+$ state in the present experiment. The population distribution of the vibrational levels of the H_2^+ ion is determined by the vibrational distribution of the H_2 gas and by the energy of the electrons in the source area. Since the energy spacing of the first vibrational level of H_2 is ~ 0.4 eV, essentially all of the H_2 gas molecules were in the lowest vibrational level. Based on the Franck-Condon principle (i.e., the time required for an electronic

transition is small compared with the nuclear motion so that the initial and final states have almost the same internuclear separation), the H_2^+ ions formed by electron ionization in the source will almost exclusively be in levels $v \leq 5$ (see Fig. 2). Again employing the Franck-Condon principle, we see that the capture of an electron to form H_2 in the $F^1\Sigma_g^+$ state is only possible for the very highest vibrational levels of H_2^+ (see Fig. 2). We therefore exclude the possibility of a significant population of the H_2 beam being in the $F^1\Sigma_g^+$ state.

We now direct our remarks to the hydrogen-like Rydberg states with $n \gtrsim 8$. From measurements by Kingdon et al.[98] and Solov'ev et al.[31] we conclude that less than 2% of the H_2 formed by electron capture by H_2^+ in Mg at 40 keV is in hydrogen-like states with $n \gtrsim 8$. We observed excited state fractions of 28% at this energy. We therefore attribute the experimental observations to the presence of the $c^3\Pi_u$ excited state and the $X^1\Sigma_g^+$ ground state only.

Unfortunately, there exists, as discussed in Sec. II, B, the nonradiative loss mechanism of predissociation in the case of the $c^3\Pi_u$ state. Hiskes[59] has estimated, based on typical source conditions, the population of the $c^3\Pi_u$ levels that are susceptible to predissociation after charge exchange of keV H_2^+ ions in Mg vapor. He has concluded that approximately half the $c^3\Pi_u$ state population will be in allowable predissociation levels. Therefore, based on the bounds we are able to assign the predissociation lifetime (see Sec. II, B), we infer that predissociation

will have taken place in approximately half of the $c^3\Pi_u$ molecules before detection.

E. The H_2 Excited State Production Medium

According to the Massey hypothesis[99] the maximum cross section for charge exchange is large when the energy defect is small. (The energy defect is the difference between the internal energy of the initial and final states of the collision particles.) In the case of the charge-exchange process of interest in the present experiment, i.e.,

$$H_2^+ + X \rightarrow H_2 + \cdots,$$

the energy defect for electron capture into n = 2 stable states of H_2 is about 4 eV for a Mg vapor target and about 12 eV for a H_2 or N_2 gas target. Therefore, at low energies where the Massey criterion is valid, we expect Mg vapor to be a more effective charge-exchange medium for capture int excited states than H_2 or N_2 gas.

The desirability of metal vapors as charge-exchange media for the formation of excited atoms has been experimentally verified for hydrogen by Futch and Damm[27] (lithium vapor) and Il'in et al.[100] (magnesium vapor), among others,[16,29] and for helium by Donnally and Thoeming (cesium vapor).

A theoretical survey of electron capture into excited states of atomic hydrogen by ground state elements has been performed by Hiskes.[91] Figure 27 demonstrates the significant differences between Mg vapor and Ne gas for use as a medium for producing excited states of atomic hydrogen. Using these results, Hiskes

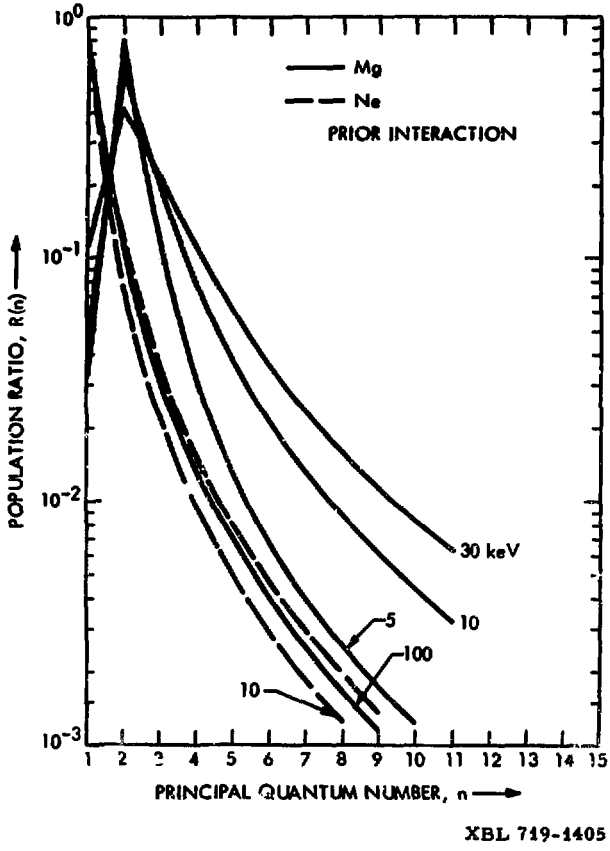

Fig. 27. Population ratio, R(n), versus principal quantum number for protons incident upon the $2s^2\ 2p^6\ 3s^2$ configuration of Mg for proton energies of 5, 10, 30, and 100 keV. Dashed curves: ratios for 10 and 100 keV protons incident upon $2s^2\ 2p^6$ Ne (from Ref. 91).

has estimated up to 50% electron capture into the $c^3\Pi_u$ state of H_2 by passage of H_2^+ through Mg vapor.

Based on the above considerations, Mg vapor was used to attempt to enhance the $c^3\Pi_u$ excited state population of H_2 beams. In order to compare the metal vapor results with common gases we also used H_2 and N_2 targets. The results of the present experiment (see Sec. V) show conclusively the desirability of using Mg vapor rather than H_2 or N_2 gas as a medium for producing $c^3\Pi_u$ H_2 molecules.

F. A Discussion of the Effects of Collisional Excitation and De-Excitation on the Present Measurements

The analysis of the H_2 attenuation data discussed in Sec. IV, A is based on the assumption that the processes of collisional excitation and de-excitation of the $c^3\Pi_u$ and $X^1\Sigma_g^+$ states in collision with H_2 gas are negligible. If we assume that these processes occur in the case of $c^3\Pi_u$ H_2 with cross sections similar to those of atomic hydrogen,[20] our results for the $c^3\Pi_u$ fraction in the beam could be as much as a factor of two too small. But as we will see below this assumption is not true.

We have found no information available for these processes for H_2; however, collisional quenching has been looked at for H(2s) and He(2^3S) in collision with gaseous targets. We will describe these investigations and use the results to argue that quenching for H_2 is negligible. In this appendix we will also describe a measurement performed to note changes in the results

due to possible collisional excitation or de-excitation.

Gilbody et al.[7] have considered this subject in relation to measurements on metastable helium beams. Since the effect of the above processes should be a function of the type of target gas used, the measured value of the excited state population should also depend on the target. Gilbody used a wide variety of gases with no observable change in the metastable excited state population. He concludes that over his energy range (7.5 to 87.5 keV/nucleon) collisional de-excitation of $He(2^3S)$ is not important.

Also, Gilbody et al.[20] have measured the cross section for the following two quenching reactions of H(2s) from 10 to 30 keV:

$$(1)\quad H(2s) + Z \rightarrow H^+ + X\left[\Sigma(n,\ell)\right] + e,$$

$$(2)\quad H(2s) + X \rightarrow H(1s) + X\left[\Sigma(n,\ell)\right] .$$

They find that in this case the de-excitation process (2) is of the same order or larger than the ionization process (1) in a variety of gases.

The reason for the difference in the importance of collisional de-excitation in He and H is easily explained. The conservation of spin in nonexchange collisions is a well-established fact. Therefore the only allowable mechanism for a triplet excited-state projectile to convert to a singlet excited-state projectile is by electron loss with subsequent capture of an electron of different spin. But this is a two-step process which is therefore relatively unlikely and in any case will not be detected owing to the presence of an externally applied electric field in the target to sweep fast charged particles aside immediately upon

formation. Now, since there exists in the $He(2^3S)$ case no lower state of the same multiplicity, collisional de-excitation processes in general must be very small in all but the most violent collisions. But, in the case of atomic hydrogen all states have a spin multiplet of 2 and only one spectrum exists. Furthermore, since the 2p state lies only 4×10^{-6} eV below the 2s state (the Lamb shift), collisional mixing of these states with subsequent decay to the 1s state is expected to be large.

(Mention should be made here of the special case of resonant electron exchange between like targets and projectiles formed via the creation of an intermediate pseudo-molecular state. The reaction

$$He(2^3S) + He(1^1S) \rightarrow He_2^* \rightarrow He(1^1S) + He(2^3S)$$

has been studied by Holstein et al.[101] up to 0.55 keV/nucleon. Although the cross section is large at low energies ($\sigma \approx 9.0 \times 10^{-16}$ at 0.05 keV/nucleon), extrapolation of their results using the general velocity dependence of the cross section,

$$\sigma^{1/2} = a - b \ln v,$$

as first suggested by Bates,[102] yields at 10 keV/nucleon

$$\sigma \approx 1.6 \times 10^{-17} \text{ cm}^2,$$

which is a factor of 20 smaller than the measured metastable helium electron-loss cross section.[7])

For the H_2 molecule there exists again, as in the case for

He, two electrons which produce two distinct term schemes, depending on the orientation of the electron spins. Therefore the $c^3\Pi_u$ state cannot quench to the $X^1\Sigma_g^+$ ground state and vice versa in simple collisions. Other possibilities for collisional de-excitation are: collisional mixing of the $c^3\Pi_u$ state and its neighboring state the $a^3\Sigma_g^+$ with subsequent decay in $\sim 10^{-8}$ sec to the $b^3\Sigma_u$ state,[54] or collisional mixing causing the transition $c^3\Pi_u$ - $b^3\Sigma_u$ directly. But the $b^3\Sigma_u$ state is repulsive and dissociates to two ground state atoms in $\sim 10^{-14}$ sec,[41] thereby causing the loss of the H_2 molecule from the beam.

In summary, collisional de-excitation of the $c^3\Pi_u$ state to the stable ground state cannot occur while de-excitation to the repulsive ground state with subsequent observable loss of the H_2 molecule can occur. However, this loss process is included in the total loss cross section that is measured from the attenuation data, so that the analysis of Sec. IV, A is correct.

Although a systematic study of the $c^3\Pi_u$ fraction in the H_2 beam as a function of target gas was not carried out, one other target was used so as to experimentally convince ourselves of the above arguments. The vapor of C_6H_6 was chosen as the target. The choice was based on its properties being quite different from H_2. Since the ionization potential of C_6H_6 is less than the excitation energy of the $c^3\Pi_u$ state (9.6 and 11.9 ev, respectively) this target vapor permits Penning ionization to occur. That is, the reaction $H_2(c^3\Pi_u) + C_6H_6 \rightarrow H_2 + (C_6H_6)^+ + e$ is energetically possible, which greatly increases the available final-state phase

space and so enhances the de-excitation probability.

If we were unable to observe a change in the measured value of the $c^3\Pi_u$ fraction by using C_6H_6, we may assume that within the accuracy of the measurements there are no effects occurring which our detectors are not capable of "seeing." No change in the $c^3\Pi_u$ fraction was observed at 22.5 keV/nucleon.

As part of this investigation we have also measured the total-loss cross sections in C_6H_6. We obtained

$$\sigma_t^* = 3.50 \pm 0.90 \times 10^{-14},$$
$$\sigma_t = 1.55 \pm 0.25 \times 10^{-15}.$$

G. The Least Squares Fit (LSF)

The LSF routine used was an adaptation of a technique used by Halbach[103] for the design of magnets. The main reason for the use of this routine (PISA) is its applicability for use on a limited storage teletype on-line computer system. The program is specific and therefore kept relatively small in statement size. The computer results of PISA were checked by using a more sophisticated LSF program (VARMIT) available in the library of the Lawrence Berkeley Laboratory Computer Center. With the use of PISA all the experimental data could be reduced by use of a teletype which was located in the experimental area. The teletype was connected to a CDC 6600 computer housed in the Computer Center.

Typically, the fit minimized the sum of the squares of the difference between the data and the function, i.e.,

$$\sum_j \left[y_j - f(x_j)\right]^2 \equiv \sum_j \delta y_j^2$$

where y_j is the jth data point and $f(x_j)$ is the function evaluated at x_j corresponding to y_j.

The error associated with the fit of each parameter was also calculated, based on the well-known statistical formula for the root mean square error, i.e.,

$$\text{error in } p_k \equiv \sqrt{\overline{\delta p_k^2}} = \left[\overline{\sum_j \left(\frac{\partial p_k}{\partial y_j}\right)^2 \overline{\delta y_j^2}}\right]^{1/2}.$$

H. The H_2^- Negative Ion

Dalgarno and McDowell[104] in 1956 calculated the potential energy curve for the ground state of $H_2^-(X^2\Sigma_g^+)$ and showed it to contain a minimum at ~ 3 Å, which is 0.9 eV below the $X^1\Sigma_g^+$ ground state of H_2, thus indicating that the ion should be stable against both radiative decay and autoionization. Since then a number of theoretical and experimental studies have been conducted on the H_2^- ion.

Chen and Peacher[105] have calculated a minimum in the ground state potential energy curve of the $H + H^-$ system at ~ 0.53 Å. Fischer-Hjalmars[106] theoretically investigated the H_2^- ion and found a minimum point in the potential to exist between 0.53 and 1.06 Å for the $^2\Sigma_u^+$, $^2\Pi_u$, $^2\Sigma_g^+$, and $^4\Sigma_u$ states but found these states to all possess vertical detachment energies that were negative, i.e., the potential energy of these states is larger

than that of the $X^1\Sigma_g^+$ state, thereby allowing autoionization of these states to occur. However, from her work she did conclude the possibility of the $^2\Sigma_g^+$ and $^4\Sigma_u^+$ states of H_2^- to be metastable.

Experimentally, Khvostenko and Dukel'ski[107] observed the existence of H_2^- by use of an ion source mass spectrometer unit using a mixture of H_2O and Sb bombarded by 80-eV electrons. The ions were observed by use of electron multipliers. The maximum H_2^- ion current they were able to observe was $\sim 5 \times 10^{-15}$ A.

Carter and Davis[108] have reported finding the H_2^- ion by extracting positive ions from a duoplasmatron ion source, accelerating them to 40 keV and converting them to negative ions by passage through a gas cell. The ions were detected by a Faraday cup after being momentum-analyzed. Main et al.[109] performed the same experiment as Carter and Davis but with the inclusion of particle-counting detectors, which act as energy analyzers. Their results indicated that no H_2^- was present, in contrast to the interpretation of Carter and Davis.

Devienne[110] has reported observing fast H_2^- created by 3-keV H_3 breakup in a gas cell. In this case the target gas was deuterium. Based on experience at this laboratory, contamination of an ion source area by the migration of target gas can be a serious problem. Specifically, Stearns[111] has found that a mixture of He^3 and D_2 as a source gas, while using H_2 as a target gas can yield 20% D_2H in a beam of He^3D. The migration length

in these studies was ~ 500 cm, with target gas pressures on the order of 1 mtorr. Since Devienne does not mention investigating this possibility and his path length was only ~ 40 cm, with a target pressure of 10 mtorr, we conclude that contamination of the beam by HD was a possibility. The presence of HD, from which D^- could be formed, could explain the observations of Devienne. Therefore, based on these experiments, we feel that the observation of energetic H_2^- produced by collision of a neutral or charged parent has not been firmly established.

Hence, we have attempted to observe the D_2^- ion by pasage of D_2^+ through Mg vapor. Based on the work of Donnaly and Sawyer,[112] who found that H^- production by passage of H^+ through Ar arose almost exclusively from the reaction

$$H^+ \rightarrow H(2s) \rightarrow H^-,$$

and based on the observations of Donnally and Thoeming,[12] concerning the enhancement of He^- yields, by use of a Cs metal vapor target, via the reaction

$$He^+ \rightarrow He(1s\ 2s) \rightarrow He^-(1s\ 2s\ 2p),$$

we felt that the use of Mg metal vapor, which produces metastable H_2, was an excellent approach to producing H_2^- via the reaction

$$H_2^+ \rightarrow c^3\Pi_u\ H_2(1s\ 2p) \rightarrow {}^4\Sigma_u^+\ H_2^-(1s\ 2s\ 2p).$$

(As mentioned earlier in this appendix, the ${}^4\Sigma_u^+\ H_2^-$ state is possibly metastable and has an equilibrium internuclear separation

which, based on the Franck-Condon principle, permits population via the reaction $c^3\Pi_u - {}^4\Sigma_u^+$.) As mentioned in Sec. IV, D, no H_2^- was observed.

From this study we are able to assign an upper bound to the cross section for double electron capture into H_2^- states with lifetimes longer than $\sim 10^{-7}$ sec by H_2^+ ions in collision with Mg vapor from 7- to 20-keV/nucleon. We obtain

$$\sigma_{H_2^-} < 10^{-21} \text{ (cm}^2\text{/atom)}.$$

I. Error Discussion

In this appendix the following topics are presented:

(1) A summary of all sources of error discussed in the text.

(2) A discussion of the possiblity of target gas impurities, source gas impurities, and modulated background signals.

(3) A discussion of the method in which the excited state uncertainties are generated from the ground state uncertainties.

(4) A discussion of the assignment of a confidence level to the data.

(5) A discussion of uncertainties generated by a lack of knowledge of the vibrational distribution of the molecules.

1. Error Summary

Mg vapor pressure, standard deviation, ±10%

Target pressure, possible correction factor, ±5%

Target length, possible correction factor, ±5%

Particle energy, possible correction factor, ±3% (almost always)

Counting statistics, standard deviation, ±1% (almost always)

Ground state data, long term reproducibility, ±5%

Ground state data, least-squares-fit standard deviation, ±3%

Excited state data, long term reproduciblity, ±17%

Excited state data, least-squares-fit standard deviation, ±5 to ±20%

Target gas impurities, possible correction factor, inconsequential

Source gas impurities, possible correction factor, inconsequential

Modulated background signals, possible correction factor, inconsequential.

2. Impurities and Background

(a) Target. Although mass spectrometry of the target gas was not performed, we assume negligible gas-bottle contamination (fresh commercial gas bottles were used) and since, with the system open to the bottle neck, the pressure in the target cell was typically 1×10^{-6} torr, we conclude that no other significant sources of contamination existed.

(b) Source. Since the final total kinetic energy (E) attained by an ion in the accelerator is proportional to its charge (e), and since the momentum analysis of the bending magnet requires the charge of the accepted particle to be proportional to $(Em)^{1/2}$, where m ≡ mass of the particle, the fast projectiles reaching the experimental region are governed by the relation m/e = constant. Therefore the following projectiles could be

obtained when accelerating D_2^+ (m/e = 4) and H_2^+ (m/e = 2).

m/e = 4	m/e = 2
	D^+
He^+	He^{++}

This is, of course, just a partial list of possibilities, but the most likely candidates.

Let us first consider in detail the D^+ contamination of H_2^+. If when switching from D_2 source gas to H_2 source gas precautions are not taken to purge the system of D_2, a contamination of a few percent D^+ in an H_2^+ beam can easily exist. (This is based on experimental evidence of the reverse situation, i.e., switching from H_2 gas to D_2 gas. In this case, after flushing the source area once with D_2 gas, we have experimentally obtained H_2^+ signals up to 3% of the D^+ signal. But with several D_2 gas flushes of the system, combined with a few days of pumping, the H_2^+ signal decreased to < 0.1% of the D^+ signal.) Contamination of the H_2^+ signal by 3% D^+ would have an observable effect on the results, since the ratio of the electron capture cross section by 50-keV D^+ to that by 25 keV/nucleon H_2^+ in Mg is 7.88 (based on data for D^+ from Ref. 64 and data for H_2^+ from Ref. 31), thereby producing an effective neutral D contamination of the H_2 beam of 24%. Hence, strict precautions were taken when switching between H_2 and D_2 source gases. Under these conditions the contamination was shown to be negligible since measurements, using a thick Mg vapor target, showed no indication of the existence of a signifi-

cant full energy neutral particle equilibrium value.

The only other likely contamination is from He. It is well known that He possesses a metastable state that would produce a bend in an attenuation curve which could introduce error in the interpretation of the results.[4] But He has not been used as a source gas in the accelerator for a number of years and we therefore rule out this contamination possibility.

Hence, we conclude that the fast projectiles were essentially all H_2^+ or D_2^+ ions.

(c) Background. A constant background of unknown origin was accounted for by modulating the beam. In most cases this background was small and of no consequence. But if there existed a constant background signal which was modulated with the beam, it could produce a large nonlinear effect in the attenuation curves. An example of this type of background is electrical noise generated by the modulator power supply. Effects of this type were experimentally investigated in situ by interrupting the beam at the entrance to the target and noting the beam-on, beam-off counts. This was done for a variety of target thicknesses with the counts always agreeing within the statistics of the measurements. Also, the attenuation data was fit to the sum of two exponential functions plus a constant, i.e.,

$$y(\pi_t) = Ae^{-\sigma_t^* \pi_t} + Be^{-\sigma_t \pi_t} + C.$$

Typically, the constant, C, was ~ 0.1% of the sum of A and B and

therefore this type of background is considered inconsequential.

3. Excited State Uncertainties

As mentioned in Sec. IV, A, the ground state total-loss cross section was obtained by using a hydrogen neutralizer to produce a H_2 beam by electron capture by H_2^+ ions. A semilogarithmic plot of the transmission of this H_2 beam versus target thickness yielded a straight line reproducible to ±5%, indicating that significant amounts of $c^3\Pi_u$ H_2 molecules were not present. The transmission data of the H_2 beam produced by using Mg vapor as a neutralizer was then analyzed by a 3-parameter least-squares fit to the sum of two exponential functions, one exponent of which is known, i.e., the total-loss cross section of the ground state. The transmission data using a Mg vapor neutralizer was least-squares fit 3 times; once using, for the total-loss cross section of the ground state, the most probable value (the mean of the repeated data), and twice again using ±5% of this value, i.e., the limits of the reproducibility of the values. This procedure was used on several repeated experimental runs using a Mg vapor neutralizer. We then took the mean of the data that used the most probably value for the total-loss cross section as the experimental result and assigned the bounds of the uncertainty as the mean value of the data, using ±5% of the most probable value. This method of assigning the excited-state uncertainties reflects the experimental uncertainty in the known quantity needed for the analysis.

4. Confidence Level

The least-squares fit standard deviation of the ground-state measurements was ~ ±3%. We therefore assigned an uncertainty to the random portion of the ground-state results of ±3%. But since the results are reproducible to within ±5%, we cannot assign a confidence level of one standard deviation (i.e., ~ 67%). We therefore estimate a confidence level of ~ 60%. A similar argument holds for the excited state measurements.

5. Vibrational Population Distribution

Theoretical treatments[113,114] of inelastic scattering of H_2^+ molecules in collisions with electrons, protons, and hydrogen atoms have demonstrated the importance of including the vibrational distribution of the H_2^+ ion in determining cross sections for collisional processes. McClure[71] has experimentally verified changes of as much as 20% in the yields of dissociation fragments of 10- to 100-keV H_2^+ and H_3^+ ions in collision with H_2 gas with changes in ion-source pressure. Williams and Dunbar[115] have found changes of as much as 30% for the dissociation cross sections of H_2^+ and H_3^+ from 2-to 50-keV for changes in operating conditions of their ion source.

The present experiment cannot differentiate between vibrational levels so that the results fall prey to this uncertainty. No attempt was made to systematically study the results as a function of source conditions. We were able to run the source in two very different modes, i.e., as a high-pressure PIG discharge and as a low-pressure electron gun. (Although we did not monitor the

source pressure directly, based on the pressure measured by an ion gauge outside the source region, we estimate the PIG mode source pressure to have been 5 to 10 times larger than the electron gun mode source pressure.) Unfortunately both modes could not easily be used for the same detection method, so a comparison of results as a function of source condition is not available. For particle counting techniques (Method I), where low beam intensities are required (incident H_2^+ beam intensities required for this method were $< 10^{-11}$ A), the PIG source mode could not be operated without considerable fluctuations. To run this mode quietly at these intensities proved difficult. The reproducibility of the data was poor under these conditions and accurate measurements could not be obtained. For the Faraday cup method of detection (Method II) the electron gun mode was not capable of producing high enough beam intensities (incident H_2^+ beam intensities required for this method were $> 10^{-10}$ A).

For $E \geq 20$ keV/nucleon the results for the $X^1\Sigma_g^+$ ground state total-loss cross section, using the PIG source mode with Faraday cup particle detection (Method II), were ~ 9 % lower than the results using the electron gun source mode with particle detection techniques (Method I). The results seem to converge for $E < 20$ keV/nucleon (see Fig. 18). Based on the results of McClure[71] and of Williams and Dunbar[115] and a comparison of the H_2^+ breakup cross sections of several investigators,[116] we conclude that the effect we observe is most likely due to differences in the population of the vibrational energy states of the ions,

depending of whether the ions are produced in the electron gun or PIG source mode. The apparent energy dependence of the difference in the results is most likely due to differences in the energy dependence of individual vibrational states.

There does not exist enough experimental data to quantitatively predict variations in measurements under different source conditions. We cannot even, in the present case, predict conclusively whether the result of a measurement should increase or decrease with source condition changes.

J. A Discussion of the Results of Solov'ev et al. for Electron Capture by H_2^+ Ions in Mg Vapor

In the method used in Ref. 31 to obtain the total cross section for electron capture ($\sigma_{10} + \sigma_{10}^*$) by H_2^+ ions in Mg vapor, the emerging H_2 beam was passed through a He target and the resulting H_2^+ signal measured. In order to relate this signal to the H_2 beam a knowledge of the ionization cross section of fast H_2 molecules in He gas ($\sigma_{H_2^+}$) is required (see analysis below). This value is obtained by an independent experiment. Fast He was passed through a H_2 gas target and $\sigma_{H_2^+}$ determined by an e/m analysis of the slow charged particles. This measured $\sigma_{H_2^+}$ reflects only the $X^1\Sigma_g^+$ state of H_2 since the target gas is at room temperature. But the H_2 beam from the Mg oven contains large amounts of $c^3\Pi_u$ H_2 whose ionization cross section, $\sigma_{H_2^+}^*$, is larger than $\sigma_{H_2^+}$. Therefore, using a value for $\sigma_{H_2^+}$ obtained from a fast He experiment to analyze the fast H_2 beam emerging from the oven results in a value for the electron capture cross

section that is too large. This is easy to see if we consider the following: The current of H_2^+ ($i_{H_2^+}$) emerging from the He target is proportional to the incident equivalent current of H_2 (i_{H_2}), i.e.,

$$i_{H_2^+} = i_{H_2} \sigma_{H_2^+} \pi_{He}$$

where $\pi_{He} \equiv$ the He target thickness (atoms/cm^2). But

$$i_{H_2} \propto (\sigma_{10} + \sigma_{10}^*)\pi_{Mg}$$

where $\pi_{Mg} \equiv$ the Mg vapor target thickness (atoms/cm^2)

so $$i_{H_2^+} \propto (\sigma_{10} + \sigma_{10}^*)\sigma_{H_2^+} \pi_{He} \pi_{Mg}.$$

Analogously, the H^+ current detected (i_{H^+}) is proportional to $\sigma_{10}^H \sigma_{01}^H \pi_{He} \pi_{Mg}$

where σ_{10}^H is the electron capture cross section for the process $H^+ + Mg \rightarrow H - e + \cdots$

and σ_{01}^H is the electron loss cross section for the process $H + He \rightarrow H^+ + e + \cdots$.

Therefore,

$$(\sigma_{10} + \sigma_{10}^*) = \sigma_{10}^H \left(\frac{\sigma_{01}^H}{\sigma_{H_2^+}} \right) \left(\frac{i_{H_2^+}}{i_{H^+}} \right).$$

The ratio ($i_{H_2^+}/i_{H^+}$), σ_{10}^H, σ_{01}^H, and $\sigma_{H_2^+}$ are measured in independent experiments so that ($\sigma_{10} + \sigma_{10}^*$) can be determined.

Estimates based on the results of the present experiment show that the $\sigma_{H_2^+}$ value used in Ref. 31 could results in values

of ($\sigma_{10} + \sigma^{*}_{10}$) that are too large by as much as a factor of two. (There will also be a larger than anticipated H^{+} signal due to the $c^{3}\Pi_{u}$ breakup, but this effect should be much smaller than the error introduced by neglecting the $c^{3}\Pi_{u}$ H_2 contribution to the value of $\sigma_{H_2^{+}}$.)

REFERENCES

1. C. F. Barnett and P. M. Stier, Charge Exchange Cross Section for Helium Ions in Gases, Phys. Rev. 109, 385 (1958).

2. S. K. Allison, Electron Loss Cross Sections for Helium Atoms in the Kinetic Energy Range 100-450 keV, Phys. Rev. 110, 670 (1958).

3. A. B. Wittkower, G. Levy, and H. B. Gilbody, Charge-Changing Collisions Involving Fast Helium Beams--The Effect of a Metastable Atom Component, Proc. Phys. Soc. (London) 91, 862 (1967).

4. H. B. Gilbody, R. Browning, and G. Levy, A Quantitative Analysis of Fast Metastable Helium Atoms in Collisions Involving Electron Loss, J. Phys. B 1, 230 (1968).

5. H. B. Gilbody, R. Browning, G. Levy, A. I. McIntosh, and K. F. Dunn, Formation and Destruction of Fast Metastable Helium Atoms in Charge-Changing Collisions, J. Phys. B 1, 863 (1968).

6. H. B. Gilbody, R. Browning, K. F. Dunn, and A. I. McIntosh, Formation of He^- Ions in Charge-Changing Collisions During Passage of Fast Helium Beams Through Hydrogen, J. Phys. B 2, 465 (1969).

7. H. B. Gilbody, K. F. Dunn, R. Browning, and C. J. Latimer, Electron Loss of Fast Metastable and Ground State Helium Atoms in Passage Through Gaseous Targets, J. Phys. B 3, 1105 (1970).

8. Francois Bastien, Elaine Depuydt, and Annie Sinturel, Measurements of the Cross Section for Electron Loss of the Ground and Metastable States of Helium in Hydrogen and Neon from 10 to 50 keV, Comptes Rendus B, Series 269, 459 (1969).

9. R. E. Miers, A. S. Schlachter, and L. W. Anderson, Production and Loss of Fast Metastable Helium Atoms in Collisions with Xe, H_2, Ar, and He, Phys. Rev. 183, 213 (1969).

10. R. E. Miers and L. W. Anderson, Production and Loss of Fast Metastable Helium Atoms in Collisions with Permanent Gases, Phys. Rev.A 1, 534 (1970).

11. R. E. Miers and L. W. Anderson, Ionization of Fast H^0 in the Metastable State, Phys. Rev.A 1, 819 (1970).

12. Bailey L. Donnally and Theorge Thoeming, Helium Negative Ions from Metastable Helium Atoms, Phys. Rev. 159, 87 (1967).

13. A. S. Schlachter, D. H. Coyd, P. J. Bjorkholm, L. W. Anderson, and W. Haeberli, Charge-Exchange Collisions Between Helium Ions and Cesium Vapor in the Energy Range 15-25 keV, Phys. Rev. 174, 201 (1968).

14. E. P. Andreev, V. A. Ankudinov, S. V. Bobashev, and V. B. Matveev, Effect of Electric Fields on Intensity of Hydrogen L_β Line Excited in Proton Charge Exchange with Inert Gases, Zh. Eksperim. i Teor. Fiz. 48, 40 (1965) English Transl.: Soviet Phys.-JETP 25, 232 (1967) .

15. J. E. Bayfield, Measurements of the Total Cross Section for Charge Transfer into the Metastable State H(2s) for Protons Incident on H_2 and Ar Gases, Phys. Rev. 182, 115 (1969).

16. K. H. Berkner, W. S. Cooper III, S. N. Kaplan, and R. V. Pyle, Cross Sections for Electron Capture into the Excited Level n = 6 of Hydrogen by 5- to 70-keV Protons in Mg Vapor and in Neon, Phys. Rev. 182, 103 (1969).

17. V. Dose, V. Meyer, and M. Solzmann, Collisional Quenching of Metastable Hydrogen, J. Phys. B 2, 1357 (1969).

18. J. L. Edwards and E. W. Thomas, Formation and Destruction of Excited Hydrogen Atoms at High Impact Velocities, Phys. Rev. A 2, 2346 (1970).

19. T. D. Gaily, D. H. Jaecks, and R. Geballe, Polarization of Lyman-Alpha Radiation from H^+- and D^+-Rare-Gas Charge-Transfer Collisions, Phys. Rev. 167, 81 (1968).

20. H. B. Gilbody, R. Browning, R. M. Reynolds, and G. I. Riddle, Collisional Destruction of Fast Metastable Hydrogen Atoms, J. Phys. B 4, 94 (1971).

21. R. H. Hughes, C. A. Stigers, B. M. Doughty, and E. D. Stokes, Electron Capture into the n = 3 States of H by Fast H^+ Impact on Gases, Phys. Rev. A 1, 1424 (1970).

22. G. Ryding, A. B. Whittkower, and H. B. Gilbody, A Study of Lyman-α Emission in Charge Transfer Collisions Involving 40-200 keV Protons, Proc. Phys. Soc. (London) 89, 547 (1966).

23. C. E. Head and R. H. Hughes, Electron Capture into Excited Helium by Fast He^+ Impact on the He, N_2, and O_2, Phys. Rev. 139, A1392 (1965).

24. L. Wolterbeek Muller and F. J. DeHeer, Electron Capture into Excited States by Helium Ions Incident on Noble Gases,

Physica 48, 345 (1970)

25. C. F. Barnett and J. A. Ray, Highly Excited States of H_2, IV ICPEAC (Quebec), Abstracts, 250 (1965).

26. R. Le Doucen, J. M. Lenormand, and J. Guidini, A Study of the Charge Exchange of Protons with the Formation of Excited States, Comptes Rendus B, No. 271, 437 (1970).

27. A. H. Futch and C. C. Damm, Enhancement of the Excited-State Populations in a Hydrogen Atom Beam, Nucl. Fusion 3, 124 (1963).

28. Robert H. McFarland and Arthur H. Futch, Jr., Measurements of Excited-State Population Ratios of Atomic Hydrogen Produced by Charge-Exchange Neutralization of Energetic Proton Beams, Phys. Rev. A 2, 1795 (1970).

29. V. A. Oparin, R. N. Il'in, and E. S. Solov'ev, Production of Highly Excited Hydrogen Atoms by Charge Exchange of Protons in Metal Vapors, J. Exptl. Theoret. Phys. (USSR) 52, 369 (1967).

30. A. C. Riviere, The Yield of Excited Atoms and Molecules from the Break-up of H_2^+ ions in Magnesium Vapour, V ICPEAC (Leningrad), Abstracts, 12 (1967).

31. E. S. Solov'ev, R. N. Il'in, V. A. Oparin, and N. V. Fedorenko, Production of Highly Excited Hydrogen Molecules and Atoms by Fast H_2^+ and H_3^+ Ions Passing Through H_2, N_e, and Mg and Na Vapors, Zh. Eksperim. i Teor. Fiz. 53, 1933 (1967) English Transl.: Soviet Phys. JETP 26, 1097 (1968).

32. J. R. Hiskes, Ionization Processes in the Intermediate Density Range, Bull. Am. Phys. Soc. 13, 308 (1968).

33. J. R. Hiskes, Electric and Magnetic Dissociation and Ionization of Molecular Ions and Neutral Atoms, Nucl. Fusion 2, 38 (1962).

34. J. R. Hiskes, Inverted Cascade in Energetic Neutral Hydrogen Beams, Phys. Rev. Letters 10, 102 (1963).

35. R. P. Fries and J. R. Hiskes, Radiative Lifetimes for the $2p\pi\,^3\Pi_u$ State of the Hydrogen Molecule, Phys. Rev. A 2, 573 (1970).

36. G. Herzberg, Spectra of Diatomic Molecules (D. Van Nostrand Company, Inc., New York, 1950), pp. 530-31.

37. Ibid., p. 501.

38. Ibid., pp. 146-212.

39. R. H. Garstang, in Atomic and Molecular Processes, D. R. Bates, ed. (Academic Press, Inc., New York, 1962), pp. 19-32.

40. J. R. Hiskes and C. B. Tarter, Radiative Transition Probabilities in Hydrogen, Lawrence Radiation Laboratory Report UCRL-7088, Rev. I, 1964 (unpublished).

41. W. Lichten, Metastable Hydrogen Molecules, Phys. Rev. 120, 848 (1960).

42. P. R. Brooks, W. Lichten, and R. Reno, Metastable Hydrogen Molecules III: Hyperfine Structure of Ortho H_2, to be published in The Physical Review A, in December 1971.

43. William Lichten, Metastable Hydrogen Molecules II: Fine Structure of Parahydrogen, Phys. Rev. 126, 1020 (1962).

44. D. A. Frey and Masataka Mizushima, Hyperfine Structure of

the Hydrogen Molecule in Its Metastable $^3\Pi_u$ State, Phys. Rev. 128, 2683 (1962).

45. W. Lichten, Measurements of Lifetimes of Metastable Hydrogen Molecules: A Forbidden Predissociation in H_2, Bull. Am. Phys. Soc. 7, 43 (1963).

46. J. C. Browne, Some Excited States of the Hydrogen Molecule I. $^1\Pi_u(1s2p\pi)$ and $^3\Pi_u$ $(1s2p\pi)$, J. Chem. Phys. 40, 43 (1964).

47. Lue-Yung Chow Chiu, Electron Magnetic Perturbations in Diatomic Molecules of Hund's Case b, J. Chem Phys. 40, 2276 (1964).

48. John Olmsted III, Amos S. Newton, and K. Street, Jr., Determination of the Excitation Functions for Formation of Metastable States of Some Rare Gases and Diatomic Molecules by Electron Impact, J. Chem. Phys. 42, 2321 (1965).

49. G. Herzberg, A New Predissociation of the H_2 Molecule, Science of Light 16, 14 (1967).

50. J. T. Dowell and T. E. Sharp, Electron Impact Excitation of the $^3\Pi_u$ States of H_2 and D_2 by a Trapped-Electron Method, J. Chem. Phys. 47, 5068 (1967).

51. A. Hotop, F. W. Lampe, and A. Niehaus, Collision Reactions of Electronically Excited Hydrogen Molecules, J. Chem. Phys. 51, 593 (1969).

52. C. Bottcher, Calculations on the Small Term in the Hamiltonian of a Diatomic Molecule, Ph.D. Thesis, Queens University of Belfast, 1968 (unpublished).

53. C. E. Johnson, Lifetime of the $c^3\Pi_u$ Metastable State of H_2, D_2, and HD, Lawrence Berkeley Laboratory Report LBL-328, 1971, submitted to The Physical Review A.

54. H. M. James and A. S. Coolidge, Continuous Spectra of H_2 and D_2, Phys. Rev. 55, 184 (1939).

55. G. Herzberg, Spectra of Diatomic Molecules (D. Van Nostrand Company, Inc., New York, 1950), pp. 405-434.

56. G. H. Dieke, A Class of Perturbations of Molecular Levels, Phys. Rev. 47, 870 (1935).

57. G. H. Dieke, Intensities in Perturbations, Phys. Rev. 60, 523 (1941).

58. G. Herzberg, Spectra of Diatomic Molecules (D. Van Nostrand Company, Inc., New York, 1950), p. 410.

59. John R. Hiskes, Lawrence Livermore Laboratory, private communication.

60. James E. Hesser, Absolute Transition Probabilities in Ultra Violet Molecular Spectra, J. Chem. Phys. 48, 2518 (1968).

61. Ernest R. Davidson, First Excited $^1\Sigma_g^+$ State of the Hydrogen Molecule, J. Chem. Phys. 35, 1189 (1961).

62. L. Wolniewicz, Theoretical Investigation of the Transition Probabilities in the Hydrogen Molecule, J. Chem. Phys. 51, 5002 (1969).

63. W. D. Wilson, Investigation of the Helium Hydride Molecular Ion for Injection into Thermonuclear Plasmas (Ph. D. Thesis), Lawrence Radiation Laboratory Report UCRL-16308, September 27, 1965 (unpublished).

64. Klaus H. Berkner, Robert V. Pyle, and J. Warren Stearns, Electron Transfer Cross Sections of 5- to 70-keV Hydrogen Atoms and Ions in Magnesium Vapor, Phys. Rev. 178, 248 (1969).

65. Ralph R. Hultgren, Raymond L. Orr, Philip D. Anderson, and Kenneth K. Kelly, Selected Values of Thermodynamic Properties of Metals and Alloys (John Wiley and Sons, Inc., New York, 1963).

66. L. Kay, Criteria for the Production of Excited Atom Beams by Photo-excitation, UKAEA Culham Laboratory Report CLM-M54, 1965 (unpublished).

67. Prudencio Martinez and Frank E. Senftle, Effect of Crystal Thickness and Geometry on the Alpha-Particle Resolution of CsI(Tl), Rev. Sci. Instr. 31, 974 (1960).

68. A. C. Riviere and D. R. Sweetman, Energy Resolution of CsI(Tl) Scintillation Counter for 12.5- to 100-keV Protons, Rev. Sci. Instr. 34, 1286 (1963).

69. A good discussion of photomultiplier tubes and scintillation detectors can be found in William J. Price, Nuclear Radiation Detection (McGraw-Hill Book Company, New York, second edition, 1964), Ch. 7, pp. 159-212.

70. P. M. Stier and C. F. Barnett, Charge Exchange Cross Sections of Hydrogen Ions in Gases, Phys. Rev. 103, 896 (1956).

71. G. W. McClure, Charge Exchange and Dissociation of H^+, H_2^+, and H_3^+ Ions Incident on H_2 Gas, Phys. Rev. 130, 1852 (1963).

72. G. W. McClure, Ionization and Dissociation of Fast H_2 Molecules Incident on H_2 Gas, Phys. Rev. 134, A1226 (1964).

73. K. H. Berkner and A. C. Riviere, Fraction of Atom Beam Trapped as a Function of Central Density in Phoenix II, UKAEA Culham Laboratory Phoenix Memo No. 7, May 20, 1966.

74. J. D. Jackson and H. Schiff, Electron Capture by Protons Passing through Hydrogen, Phys. Rev. 89, 359 (1953).

75. E. S. Solov'ev, R. N. Il'in, V. A. Oparin, and N. V. Fedorenko, The Formation of Highly Excited Hydrogen Molecules and Atoms in the Passage of Fast H^+, H_2^+, and H_3^+ Ions through Gases and Metal Vapors, V ICPEAC (Leningrad), Abstracts, 16 (1967).

76. G. C. McCoyd and S. N. Milford, Born Cross Sections for Inelastic Scattering of Electrons by Hydrogen Atoms. IV. Approximate Values for Allowed Transitions up to n = 10, Phys. Rev. 130, 206 (1963).

77. K. Omidvar, Ionization of Excited Atomic Hydrogen by Electron Collisions, Phys. Rev. 140, A26 (1965).

78. W. L. Fite, R. F. Stebbings, D. G. Hummer, and R. T. Brackmann, Ionization and Charge Transfer in Proton-Hydrogen Atom Collisions, Phys. Rev. 119, 663 (1960).

79. J. R. Hiskes, Dissociation of Molecular Ions by Electric Fields (Ph. D. Thesis), Lawrence Radiation Laboratory Report UCRL-9182, May 4, 1960 (unpublished).

80. N. Mott and H. S. W. Massey, The Theory of Atomic Collisions third edition (Oxford University Press, Oxford, 1965).

81. E. H. S. Burhop, "Theory of Collisions" in Quantum Theory, Vol. I (edited by D. R. Bates), Academic Press, New York, 1961.

Momentum GeV/c R	.75	1.0	1.25	1.5	1.75	2.0	Avg
$d + C \rightarrow \pi^{\pm}$	.966	1.03	1.02	.974	1.04	1.07	1.02 ± .03
$\alpha + C \rightarrow \pi^{\pm}$	.993	1.05	---	1.01	1.08	1.03	1.02 ± .04

Table 15. Ratio R for π^+/π^- production by 2.1 GeV/nucleon beams

93. L. Wilets, D. Gallaher, Coupled - State Calculations of H^{+-} H Scattering, Phys. Rev. 147, 13 (1966).

94. G. Herzberg, Spectra of Diatomic Molecules (d. Van Nostrand Company, Inc., New York, 1950), p. 221.

95. Hans A. Bethe and Edwin E. Salpeter, Quantum Mechanics of One and Two Electron Atoms, Springer - Verlag OHG, Berlin (1957), p. 248.

96. G. Herzberg, Spectra of Diatomic Molecules (D. Van Nostrand Company, Inc., New York, 1950), p. 19.

97. W. Kolos, L. Wolniewicz, Potential-Energy Curves for the $X^1\Sigma_g^+$, $b^3\Sigma_u^+$, and $C^1\Pi_u$ States of the Hydrogen Molecule, J. Chem. Phys. 43, 2429 (1965).

98. J. Kingdon, M. Payne and A. C. Riviere, UKAEA Culham Laboratory Progress Report CLM-PR11, p. B.23, 1968 (unpublished).

99. H. S. W. Massey and E. H. S. Burhop, Electronic and Ionic Impact Phenomena, Oxford University Press, Oxford, 1956, Chapter VII, p. 441.

100. R. N. Il'in, V. A. Oparin, E. S. Solov'ev, N. V. Fedorenko, Charge Exchange of Protons in Alkali Metal Vapors Involving Highly Excited Hydrogen-Atom Formation, IV ICPEAC, Quebec, Canada, 315 (1965).

101. M. Hollstein, J. R. Sheridan, J. R. Peterson and D. C. Lorents, De-excitation of Helium 2^1S and 2^3S Atoms in Fast Collisions with Normal Helium Atoms, Phys. Rev. 187, 118 (1969).

102. D. R. Bates, Resonance Effects in Atom-Atom Collisions, Discussions of Faraday Soc. 33, 7 (1962).

103. Klaus Halbach, A Program for Inversion of System Analysis and Its Application to the Design of Magnets, UCRL #17436, 1967, (unpublished).

104. A. Dalgarno and M. R. C. McDowell, Charge Transfer and the Mobility of H^- Ions in Atomic Hydrogen, Proc. Phys. Soc. (London) A-69, 615 (1956).

105. Joseph C. Y. Chen and Jerry L. Peacher, Interaction Potential Between the Ground States of H and H^-, Phys. Rev. 167, 30 (1968).

106. Inga Fischer-Hjalmars, Note on Some Possible Metastable States of H_2^-, Arkiv Fys. 20, 461 (1961).

107. V. I. Khvostenko and V. M. Dukel'ski, The Negative Ion H_2^-, J. Exptl. Theoretical Phys. (USSR) 34, 1026-1027 (1958).

108. E. B. Carter and R. H. Davis, He^-, H_2^- and Other Negative Ion Beams Available from a Duoplasmatron Ion Source with Gas Charge Exchange, Rev. Sci. Instr. 34, 93 (1963).

109. I. G. Main, J. L. Durell and R. A. Sareen, Search for the Formation of H_2^- Ions from 40 keV H_2^+ Ions in Hydrogen, J. Phys. B 1, 755 (1968).

110. M. F. Marcel Devienne, Ionization by Inelastic Collisions of a High Energy Beam of Triatomic Molecular Hydrogen on a Target of Deuterium, Comptes Rendus, 268, serie B, 1969, p. 1303.

111. J. W. Stearns, K. H. Berkner, R. V. Pyle, B. P. Buiegleb, M. L. Warren, Dissociation Cross Sections for 0.5- to 1- MeV HeH^+ Ions in H_2, He, N_2, and Ne Gases, to be published in the Phys. Rev. A, November, 1971 and UCRL report #20817 (1971).

B. Apparatus

1. The Ion Source and Electrostatic Accelerator

The ion source and accelerator used in the present work have been described in detail elsewhere.[3] Here we will mention only the main features of the apparatus, noting any changes necessary for the present application.

The source was a typical PIG discharge which could also be operated as an electron-gun source. The electron gun was a 0.256-mm-diam tungsten filament operating at a current of from 4 to 6 A. The source area was surrounded by an electromagnet which was used to produce an electron-confining axial magnetic field of from 0 to 400 gauss in the source.[63] The ions were extracted through a 0.916-mm hole in the cathode, after which they passed through an accel-decel potential focusing lens (einzel lens) and were accelerated by use of four rings to which a total of from 1 to 90 kV was applied. The desired ions were then selected by a 90-deg analyzing magnet which was monitored by a Hall probe and traveled 120 cm through a drift tube where they entered the experimental region. Just in front of the experimental region is an electromagnet that is used to produce a transverse magnetic field in order to sweep the primary H_2^+ ions out of the beam path but still allow the H_2 molecules, produced by electron capture by H_2^+ in the drift tube, to pass. This contribution is detected and subtracted as background. Under typical single collision conditions in the neutralizer the background neutral production was $\lesssim 10\%$. The beam, before the experimental